Addis Ababa University
አዲስ አበባ ዩኒቨርሲቲ
Seek Wisdom, Elevate your Intellect and Serve Humanity

COLLEGE OF NATURAL AND COMPUTATIONAL SCIENCES

SCHOOL OF EARTH SCIENCES

INTEGRATED GEOPHYSICAL INVESTIGATION FOR MAPPING GROUNDWATER POTENTIAL ZONES OF THE MERSA-GIRANA SUB BASIN, NORTH WOLLO ZONE, ETHIOPIA

A Thesis Submitted to the School of Earth Sciences, Addis Ababa University in Partial Fulfillment of the Requirements for the Degree of Masters of Science in Geophysics

(Applied Geophysics)

By:
MEHARI SISAY

June, 2024

Addis Ababa, Ethiopia

DECLARATION

I, the undersigned, hereby state that the thesis allowed "Integrated geophysical investigation for mapping groundwater potential zones of the Mersa - Girana sub basin, north wollo zone, Ethiopia" is my unique work approved under the supervision of Dr. Mebatseyon Shawl. The thesis has not been offered to any university or institution for the award of any degree or diploma and all sources of materials used for the thesis are duly acknowledged.

Name of the Candidate	Signature	Date
Mehari Sisay	______________________	___________

SIGNATURE PAGE

This is to certify that the thesis prepared by Mehari Sisay, entitled: "Integrated geophysical investigation for mapping groundwater potential zones of the Mersa-Girana sub basin, north wollo zone, Ethiopia" and submitted in partial fulfillment of the requirements for the degree of Master of science in applied geophysics complies with the regulations of the university and meets the accepted standards for originality and quality.

Approved by examining committee:	Signature	Date
____________________	________	_______
(Chairperson)		
Dr. Mebatseyon Shawel	__________	________
(Advisor)		
Dr. Behailu Birhanu	__________	________
(Co-Advisor)		
D.r Abera Alemu	__________	________
(Internal examiner)		
Dr Dessie Nedaw	__________	________
(External examiner)		

ABSTRACT

This study was conducted in the Mersa-Girana sub basin in north wollo zone, Ethiopia. It aims to map the groundwater potential zones in the area. VES and magnetic geophysical methods were employed to achieve this objective. As part of the geophysical survey, 293 magnetic data were collected at 100 meter intervals along east-west profiles and 10 VES points were acquired along four east –west profiles with an interval of 500 meter between the VES points. In addition to the primary VES data, ten (10) VES data were collected from secondary sources. The VES data were acquired using a Schlumberger array and a maximum current electrode spacing of 1000 m. The results reveal the main aquifer depth is between 43 and 351 meters in the area. Furthermore, the analysis of Dar- Zarrouk parameters in the research area shows that 35% of the aquifers exhibit high productivity, while 65% of the aquifers demonstrate moderate productivity. The estimated hydraulic conductivity and transmissivity values are high in the central and eastern region of the research area. The results of electrical resistivity and magnetic measurements also demonstrates the region is strongly affected by faulting, which is believed to regulate the groundwater movement in the underlying volcanic series.

Keywords: groundwater, aquifer, magnetic survey, vertical electrical sounding.

ACKNOWLEDGEMENT

I extend my sincere gratitude to the numerous individuals and organizations whose invaluable contributions facilitated the completion of this dissertation. Foremost, I express my heartfelt appreciation to my advisors, Dr. Mebatseyon S. and Dr. Behailu B., whose unwavering guidance, support, and insightful feedback were pivotal at every stage of my research journey, from fieldwork to the culmination of the study. Their mentorship has profoundly shaped my academic and professional growth. I am also indebted to my esteemed lecturers, Professor Tilahun Mammo, Professor Tigistu Haile, and Dr. Abera Alemu, whose wealth of knowledge and invaluable insights enriched my learning experience in geophysics.

Special gratitude is extended to my dear friends Alemu Mola, Akililu Hailu, Halie Alemu, and AWOL Muhamad for their constant support and encouragement throughout my academic pursuits. Their unwavering belief in my capabilities served as a source of motivation.

I extend thanks to the Kobo-Girana Valley Pressure Irrigation Project and for generously providing essential resources, including the high-quality PASI Mod. 16GL-N earth resistivity meter, secondary VES data, and lithological log data, which significantly contributed to my thesis.

Lastly, I am deeply appreciative of my friend Samuel Abenew for her steadfast support, encouragement, and understanding throughout my academic journey. Her patience and encouragement were invaluable sources of strength. Additionally, I express gratitude to my wife, Desta Aleble, for her unwavering support from the inception to the completion of my studies. Their collective support and encouragement have been instrumental in the successful culmination of this thesis.

LIST OF ACRONYMS

2D	Two Dimensional
BH	Borehole
CMER	Central Main Ethiopian Rift
EIGS	Ethiopian Institute of Geological Survey
GPS	Global Position System
IGRF	International Geomagnetic Reference Field
MER	Main Ethiopian Rift
m	Meter
NS	North-South
NW	Northwest
nT	Nano tesla
SE	Southeast
NE	Northeast
SI	Structural Index
TMI	Total magnetic intensity
TMA	Total magnetic anomaly
Ω-m	Ohm meter
VES	Vertical electrical sounding
MVES	measure vertical electrical sounding
^{o}C	Degree centigrade
MN	potential electrodes
AB	current electrode

Table of contents

LIST OF FIGURES

LIST OF TABLE

CHAPTER I
INTRODUCTION

1.1 Background of the Study

Water is vital and essential for food security, economic growth and energy production (Ayenew et al. 2008). However, due to population growth and increasing irrigation, water resources are becoming scarce (Ali et al., 2015). Therefore, it is crucial to effectively locate, develop and sustainably use water resources to ensure sufficient water supplies and protect the environment, including groundwater availability.

Groundwater is one of the prime necessities of life next to air in the order of importance for the survival of man and a host of other living things. It is available in oceans, ice caps and glaciers, seas, lakes and in the subsurface. In many developing countries, groundwater is a lifeline, providing clean drinking water. The minimum exposure of groundwater to pollutants makes it the ideal source of clean drinking water (Igor et al., 2004). Groundwater plays an important role in Ethiopia as a major source of water for domestic, industries and livestock uses.

The occurrence and flow of groundwater are significantly influenced by a variety of factors, including topography, geology, and climate (Doris et al., 2011).Therefore, a multidisciplinary approach that includes geological, hydrological and geophysical studies are required for groundwater potential studies. Hydrogeological studies are conducted for a detailed understanding of groundwater flow dynamics, recharge mechanisms, and aquifer properties in the study area. Whereas geological and geophysical studies are carried out to delineate subsurface lithological variations, to identify geological structures and assess the hydrogeological potential of various geological formations (Moussa, et al., 2021).

The most commonly employed geophysical methods in groundwater studies are the vertical electrical soundings (VES) and magnetic methods. These methods provide an acceptable image of the shallow subsurface layers (Ayenew et al., 2008). The VES method provides insight into the number and type subsurface layers and their appropriate depths based on the electrical resistivity of the layers (Ali et al., 2015). The magnetic method is sensitive to the presence of magnetic minerals, which are more abundant in igneous and metamorphic rocks compared to sedimentary rocks. The changes in magnetic susceptibilities of rocks result in magnetic anomalies that are utilized, among other purposes, for mapping geological structures.

In this research geophysical studies were conducted using VES and magnetic methods to assess the potential of groundwater in the Mersa-Girana sub basin, north wollo zone, Ethiopia through the mapping of lithological variations. The aim of the research is to identify the presence of aquifers, their depths, thicknesses and the analysis of aquifer parameters such as hydraulic conductivities, transmissivities as well as the mapping of geological structures that control the flow of groundwater. The study contributes to society water needs by providing valuable information about the groundwater potential in the study area.

1.2 Description of study area

1.2.1 Location

The study area is situated in the Amhara regional state of North Wollo zone, which is 491 km from Addis Ababa through the main asphalt road. The area is geographically bounded between 555000 and 591000 meter longitude and 1272000 to 1296000 meter latitude covers the area of 503.852 km^2 and geophysical data was collected in 40 km^2 (Fig 1.1).The area is accessed via gravel and all weathered roads during the actual field investigation.

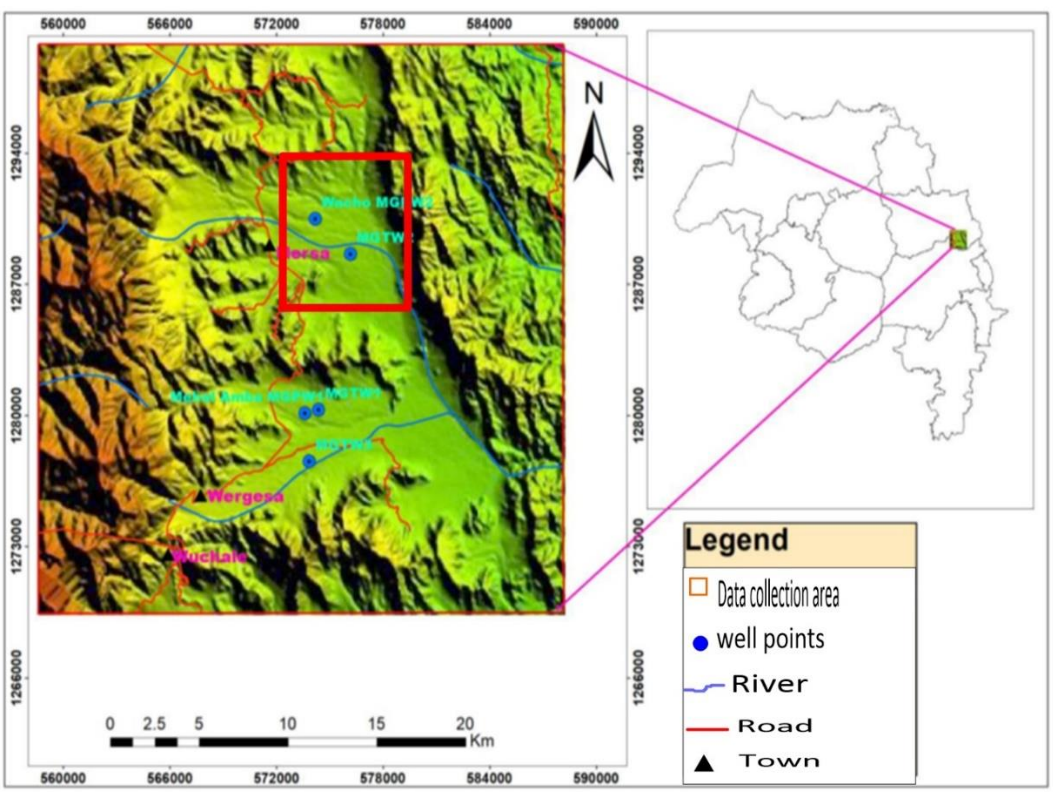

Figure 1.1: Location map of the study area

1.2.2 Topography and drainage pattern of the research area

The study area includes the western edge of the Mersa and Girana marginal basins and is situated in near the waste Afar rift margin. The topography of the research area characterized undulating and steep mountains from the western parts of 3500 meters elevation, flatlands are the central parts of the research area is evaluated elevation of 1200 meters (Fig 1.2).

The drainage network of the studied sub-basin is parallel and dendritic, structurally controlled from different sources to the Mille River, the area with many smaller streams joining the main river's branches and the main body of the Mille River. The gradient of the terrain is followed towards the mille river channels (Fig 1.3).

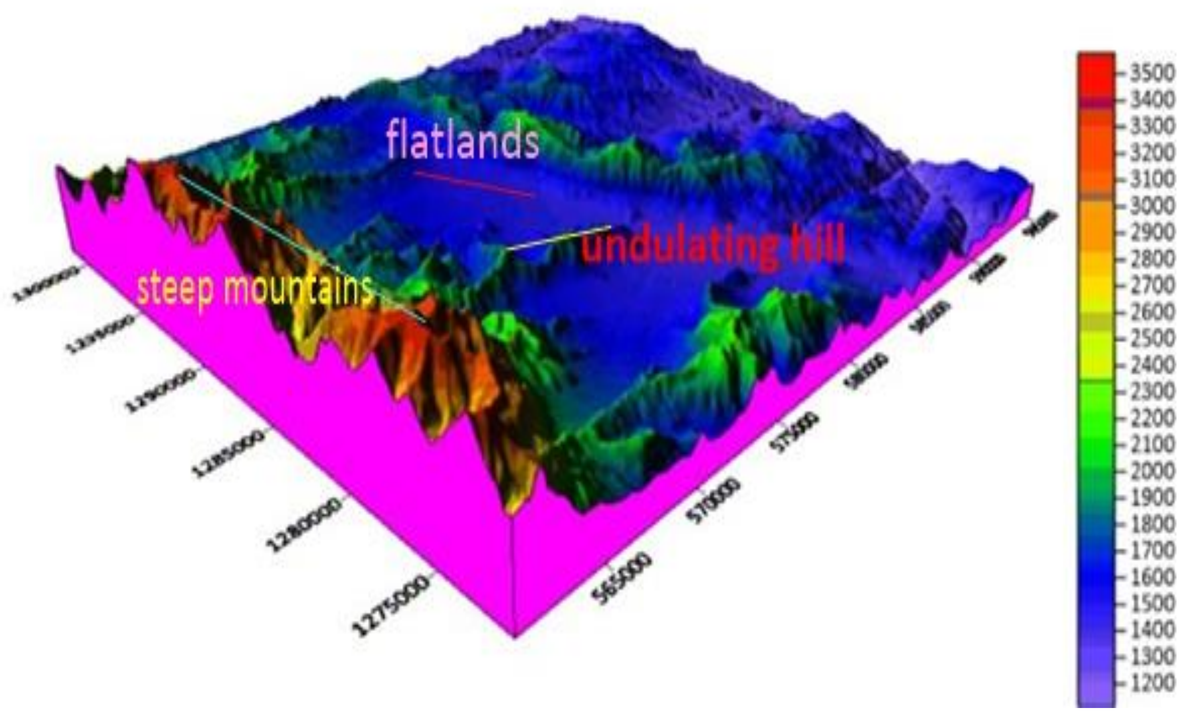

Figure 1.2: Physiography map

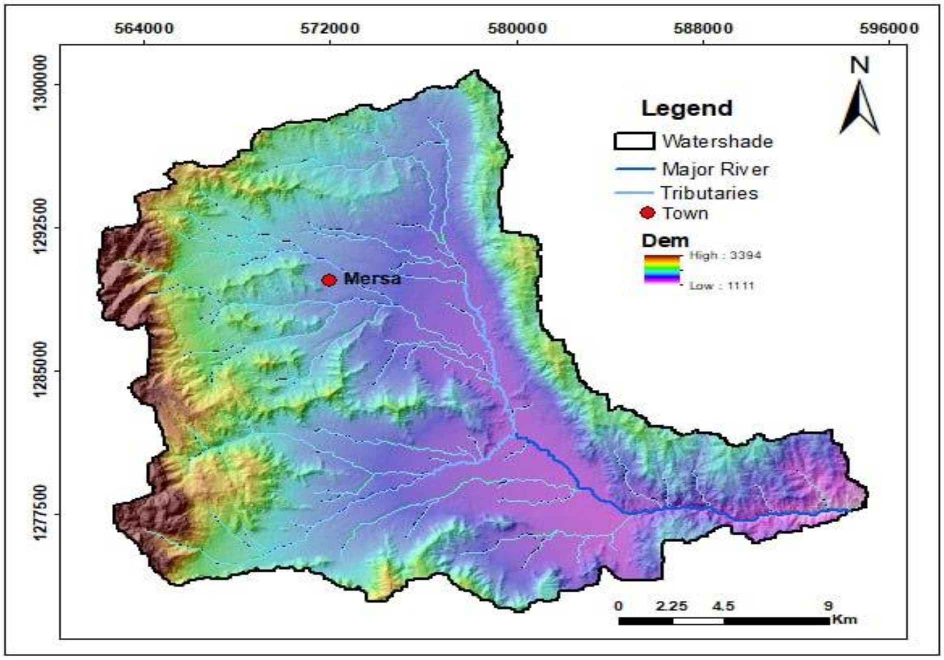

Figure1.3: Drainage map

1.2.3 Climate

1.2.3.1 Temperature

Due to the lower altitude of the study area compared to the Mersa meteorological station, which is located Mersa town, the temperature data of Mersa were reported in degrees Celsius. The maximum temperature recorded in Mersa area are 32°C in June and the minimum temperature was 7°C in December.

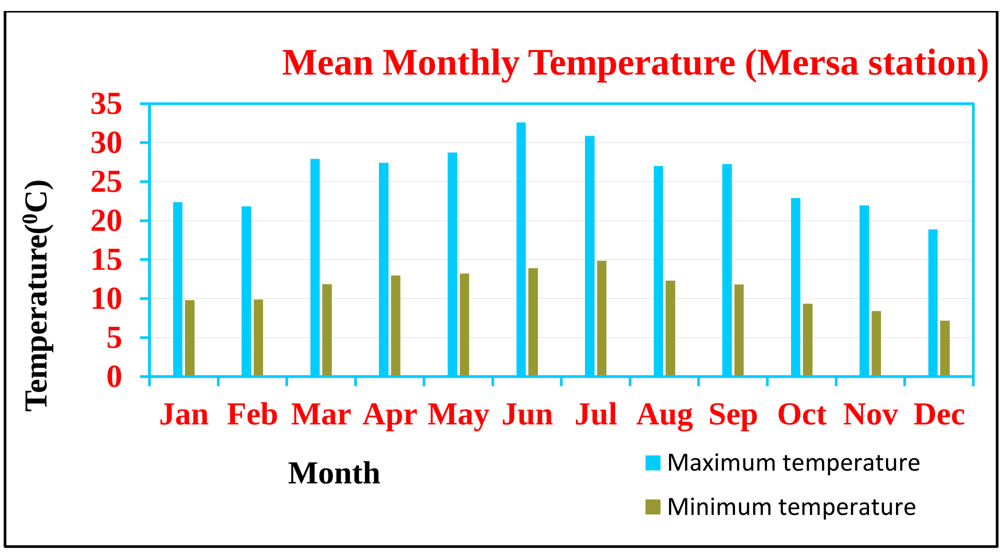

Figure 1.4: Mean monthly Temperature (Mersa station)

1.2.3.2 Rainfall

The area receives a maximum annual rainfall of 1352.8 mm in the year 2018 and a minimum annual rainfall of 249.9 in the year 2015. The mean monthly precipitation of the area gets higher value during august 245 mm and a minimum value were recorded in February 15 mm.

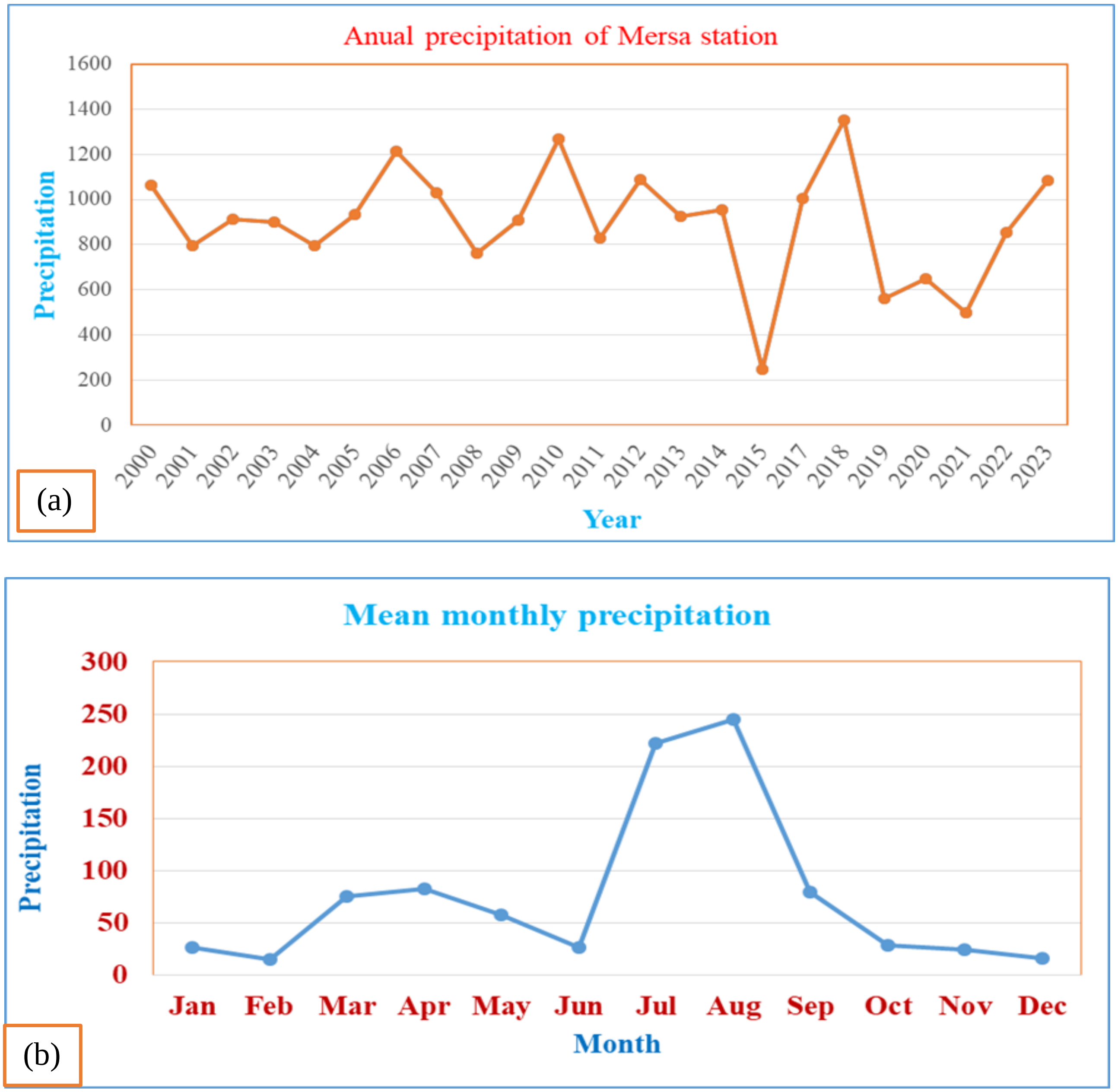

Figure 1.5: Annual precipitation of the Mersa station from the year 20000-2023 (a), and mean monthly precipitation of Mersa station (b).

1.3 Statement of the Problem

Geophysical investigation to assess the groundwater potential of the Mersa - Girana sub basin, north Wollo zone, has not yet been carried out to date. Furthermore, the mapping of geological structures and their role in groundwater flow in the study area remains unknown. Previous studies have not studied subsurface geological structures which are critical for groundwater availability and flow, the thickness of alluvial sediment that is important as a reservoir, and the estimation of aquifer parameters using geophysical data. This study aims to address these issues using VES and magnetic methods. The present work includes assessing groundwater potential zones by determining the subsurface geological structures, determining the thickness of sediment, and estimating aquifer parameters.

1.4 Research motivation

Although there are many detailed geophysical studies of groundwater systems in the Ethiopian context, there is no detailed study on groundwater investigations in the study area. In this study, the possible potential groundwater area is investigated using geophysical methods by correlating existing drill hall data. Reports conducted in the region using vertical electrical resistivity surveys (VES) found that the area's geological strata did not identify the geological structure and fault lines. So my interest lies in delineating geological structures, determining sediment thickness and evaluating the most important potential groundwater zones.

1.5 Objectives of the study

1.5.1 General objective

The main objective of this geophysical investigation is to map the groundwater potential zones of the Mersa-Girana sub basin by utilizing geophysical (VES and magnetic) methods.

1.5.2 Specific objectives

The specific objectives of the study are:

- To investigate subsurface geological structural and lithological units.
- To delineate the thickness of aquifers.
- To characterize the aquifer parameters
- To delineate the main potential groundwater zones in the study area.

1.6 Basic research questions and hypothesis

1.6.1 Basic research questions

The proposed research question is formulated as follows:

- What are the orientation of lineaments (fault and fractures) in the study area?
- What are the subsurface geological units in the study area?
- How deep is the water table?
- Where are the potential zones (drilling points) for abstraction?

1.6.2 Research hypothesis

Proposed predictions of geophysical phenomena studied using magnetic and electrical resistivity methods are called geophysical hypotheses. These predictions are put to the test by collecting and analyzing data, and the conclusions are then used to confirm or refute the theory. The following hypothesis is formulated: The hypothesis could be that variations in magnetic susceptibility and electrical resistivity are correlated with subsurface geological features such as faults, fractures and lithological boundaries. The hypothesis could suggest that variations in magnetic susceptibility and electrical resistivity reflect the spatial heterogeneity of aquifer properties such as porosity, permeability and hydraulic conductivity, and influence groundwater storage and flow behavior.

1.7 Significance of the study

Urbanization and population are progressively increasing. As the population increases, the need for water will also increase and therefore to solve the scarcity of water, investigation of groundwater potential using geophysical methods is required. This study is addressed to investigate the groundwater potential in the study area. It has the following significance:

- Since the community requires more potable water, this research will assist in developing sustainable water sources.
- It enhances the theoretical concepts and instrumental and software usages for the applicability of geophysical methods while developing the research ability.
- Able to bridge the current knowledge gap and comprehend the region's geological structure.
- The information emanating from this research will be used as a data management tool for students, researchers and any scientific community in the region.

1.8 Research outcomes

Understanding Earth's underlying characteristics is better through the study of magnetic and electrical techniques in geophysics. This research attempts to:

- Determine the thickness and unit of the aquifer in the research area

- Identify groundwater potential zones
- Map geological structures

1.9 Limitations of the research

This study has some limitations such as: limited borehole data. Due to the small number of drill holes and VES locations, the results may not be representative of the entire region and the data may not adequately reflect the complexity of the geological formations in the region.

1.10 Previous works

Although there are no detailed geophysical studies of groundwater in the research area, there are numerous detailed geophysical studies of groundwater systems worldwide and in the Ethiopian context. However, some regional studies have been conducted by various organizations and authors. (Getachew, 2018) The assessment and evaluation of the groundwater potential zones of Mechare Meda and Woldia University. Groundwater surveys using magnetic and vertical electrical surveys (VES) were conducted to investigate possible groundwater bodies and geological features are the main objective of the study. According to the interpretation, there were two aquifer zones in the area. This is the upper basalt aquifer, which is found between alluvial deposits and slightly fractured basalt. The second is the lower basalt aquifer, which is comprised by the moderately fractured basalts, namely the lower basalt aquifer. The lower aquifer is 180 meters deep, whereas the top aquifer is between 20 and 60 meters deep. Another author conducted, Tewodros (2017) "Application of Integrated Geophysical Techniques for Mapping Groundwater Resources in Tisabalima Sub basin, East Amhara Regional State, Ethiopia" with the aim of determining possible locations for test drilling and production wells as well as the sub basin expected groundwater zone. The area has high groundwater potential due to the prevailing restricted aquifer, as shown by the results of the electrical study, which mapped the potential geo electric/geological units and aquifers in the area and allowed drilling sites to be selected for each diagonal. The area contains gravel, sand and clay sedimentary formations with a maximum thickness of two hundred and five meters. The magnetic data suggests that the tectonic setting of the region, particularly the northeast and southwest oriented faults, has a significant influence on this area and may be the main factor regulating the groundwater source In addition, the assessment and drilling of the test wells of the groundwater resources of Kobo Chefa was carried out by (Teshome et al., 2018). Data integration and in-depth geological mapping of the entire region making up the study area are two of the techniques used in the report. The Mersa-Girana alluvial aquifers can provide an annual yield of approximately 87 MCM, 78 MCM, 31 MCM and 27 MCM based on the expected annual dynamic recharge and static groundwater storage

1.11 Material and Methods

To fulfill the study objectives, various materials were utilized. Geophysical equipment such as the Pasi Resistivity meter and Proton Precession Magnetometer were employed for data collection. To accomplish the stated objective in section 1.5 the following primary and secondary data collection and procedures were employed.

1.12 Materials

Magnetic and electrical techniques for groundwater investigation often use specialized sensors, connections, and data acquisition devices. These techniques discover and map groundwater resources by determining the properties of the electrical and magnetic subsurface. When electrical currents are passed through the earth, sensors, usually mounted on the earth's surface or below, collect data. By analyzing the resulting data, comprehensive maps of groundwater resources can be created. The following materials were used to achieve the objectives of the study. I, Geophysical Device: Pasi Resistivity Meter Proton Precession Magnetometer. Software packages Geosoft (v-8.4), Arc GLS 10.4, Global Mapper, WINRSIST, ipi2win, Surfer 20 and Microsoft Excel are is a software component. Supplementary materials: 1:50,000 scale topographic map, aerial photographs, geological map of the research area and field equipment including a digital camera and GPS.

1.13 Methods

In geophysics, “research method” refers to the methodical process of studying the physical properties and functioning of the Earth's interior and its surroundings. Various methods can be used here. As part of the methodology, the groundwater potential and structural components of the study area were investigated using magnetic and VES methods. After processing and analysis, the collected data provided insightful information about the potential groundwater supply of the research area as well as underground geological structures. In order to achieve the objective of the study, several measures were taken, including the evaluation of various previous works on geology, hydrogeology and geophysical works of the field (related to groundwater investigation and identification of geological structures). Finally, the research area would employ two geophysical methods: magnetic and VES methods. To collect data across the study area, both methods would be applied to separation profiles. To obtain integrated results, the research methodology consists of three main phases: pre-fieldwork, fieldwork and post-fieldwork.

A. Per-field work

The study project's surveying and analysis stages will draw on previously collected information and materials from a range of sources. These include:

- Hydrogeological logs and maps are essential for interpreting geophysical data.
- VES data from earlier reports conducted in the study region.
- Borehole information (coordinates, depth, and drilling year).

B. Actual field investigation

In geophysics, field investigation includes gathering information and samples from the study site to examine geological and geophysical properties, as well as modeling and mapping subsurface structure and possible resources using methods such as magnetic, and electrical surveys.

During the fieldwork, the following activities where conducted.

- Identified the station and the travel line where geophysical data would be collected.
- Measuring the vertical electrical sounding (VES) data to travel lines
- Measuring the magnetic data by using a proton precision magnetometer with x, y, and z coordinates.

C. Post-fieldwork (reporting and data analysis)

In geophysics, post-fieldwork reporting and data analysis are crucial to process and interpret field data to make conclusions regarding subsurface factors and geological structures. As such, integrated the field-collected primary data and the secondary data obtained from various stakeholders.

- Processed and analyzed the collected geophysical row data.
- Integrated each resistivity stratification based on geological and hydrological logs.
- Complied and reported written documents based on geophysical information.

The following flowcharts of the research methods that would be implemented are shown in (Fig 1.6).

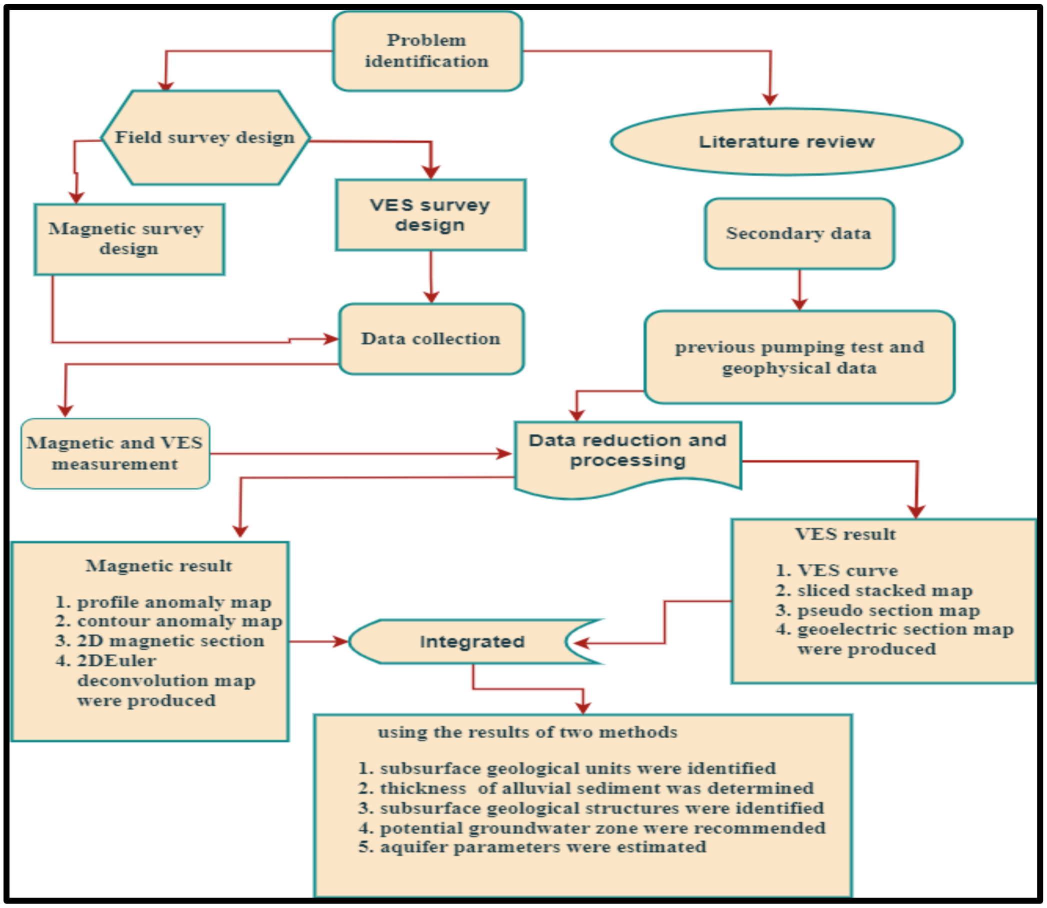

Figure 1.6: Methodology of flow chart

1.14 Organization of the work

This thesis is divided into six chapters. The introduction, problem statement, research motivation, study objectives and relevance, research methodology, fundamental research question and hypothesis, and anticipated study outcomes, previse geophysical research, limitations of the study's, location of the study area, topography and drainage pattern, temperature and weather, precipitation are all covered in the first chapter. Geology and hydrogeology are also included in second Chapter. The third Chapter covers the theoretical underpinnings of the geophysical approaches which are resistivity and magnetic techniques applied in this thesis organized from many different sources. The fourth chapter covers field data acquisition and processing. The analysis has been processed data are the main topics of the fifth chapter. Ultimately, the sixth chapter contains the research work's conclusions as well as recommendation derived from the finding.

CHAPTER II

2. GEOLOGY AND HYDROGEOLOGY

2.1 Regional geology

Tertiary volcanoes dominate the Ethiopian highlands, which are often depicted and described as floodplain basalt provinces (Ukstins et al., 2002). Due to tectonic processes, the Ethiopian Plateau (Central Highlands) is generally a large mountain range facing north, extending from its eastern border (3,000 to 4,000 m above sea level) to the border and western border (1,000 to 1,500 m above the sea level) is slightly inclined m above sea level) (Kieffer et al., 2004). Based on previous research studies (Zanettin et al., 1975), the Tertiary volcanism of northwestern Ethiopian volcanoes is divided into three main stages and their corresponding subdivision. These phases were separated by rest phases. Each stage has been divided into one or more volcanic formations by Belay (2020), and other authors have included additional volcanic phases, including the Tana Graben Lake region and the Oligocene Wegel Tana rhyolitic ignimbrite ,Pliocene eruptions were the main source of Quaternary volcanic eruptions (Ayalew et al., 2002).

A. Ashangai formation

It represents the earliest Tertiary volcanic deposits discovered in northern Ethiopia. Situated above Mesozoic formations within the Mekele basin, this sequence is characterized by the presence of phenocrysts, which crystallized before the magma's ascent to the surface. Thesis formation in question represents one of the pre-Oligocene stages and is recognized as the oldest basalt volcanism on the northwest Ethiopian plateau. This volcanism, which occurred about 54 million years ago, was fed by fissures and resulted in extensive basalt flows (Kazmin, 1979; Zanettin, 1975). The structure of these trap lava flows is characterized by faulting, tilting, crushing, and weathering, and is largely believed to have occurred prior to the main Oligocene period. The flow-over thickness of these basalts varies between 200 and 1200 meters, with the thickest exposures located near the rift escarpment. This suggests a connection between the rift fault and the primary volcanic sources (Visentin, 1975; Kazmin, 1979). Notably, the ashangai basalts, which outcrop above the upper sandstone, are only found in the north-central region of Ethiopia's plateau (Kazmin, 1979).

B. Aiba basalt

The Aibas basalt formation is characterized by extensive basalt layers alternating with agglomeratic beds, reaching a maximum thickness of approximately 1 kilometer (Mohr & Zanettin, 1988). These Aiba basalts extensively fracture and flood the Ashangi flows plain, exhibiting characteristics that fall between the tholeiitic and slightly alkaline range (Mohr & Zanettin, 1988). The Aiba basalt is closely interbedded with conglomerate layers and features massive, well-developed columnar joints, both vertical and sub-vertical, resulting from temporary overflow basalt movements. The formation's age ranges from 34 to 28 million years, situating it within the Oligocene stage (Zanettin, 1978). The Aiba basalt is divided into units that constitute the second major volcanic cycle, formed through fissure eruptions, with an overall thickness ranging from 200 to 600 meters. These basalts are generally compact aphyric rocks, displaying distinct layering in some areas. As cited by Hoffmann, Kazmin (1979) suggested that the age of the Aiba basalts might be around 30 million years, further confirming their placement in the Oligocene.

C. Termaber-Guassa basalt

The formation consists of zeolitized basalt and scoraceous basalt, with a notable presence of tuff. It is primarily exposed along the escarpments of the northwest Ethiopian plateau and the westernedge of Afar, indicating the presence of a shield volcano the age of the Termaber formationspans from 23 to 11ma.

Termaber Megezez formation

The Termaber megezez formation is located in the Oligo-Miocene stage and is also described as dark gray, coarse-grained, vesicular, smooth and dome-shaped forming phyric pyroxene-plagioclase basalt. The earlier fission volcanism terminated in a central alkaline volcanic zone between 15 and 7 Ma in age, compositionally extremely similar to the termber-guassa formation) (Zanettin & Visentin., 1975). As well Kieffer et al (2004) also recorded the volcanic centers of the Guna Shield's age (around 10.7 million years) during this Miocene period. These are shield volcanoes with low-angle fissures and fissures eruption that form the basalt layers of the formation that have a total thickness of 100 meters.

D. Wegel Tena rhyolitic-ignimbrite

Rhyolitic-ignimbrite investigated by Ayalew et al (2002) with respective series approximations of 30.2 and 31.104. This felsic unit is located in the northwestern Ethiopia continental shelf provinces (CFB) and was formed the following impacts beneath the Ethiopian lithosphere of the Afar mantle plume. Furthermore Ayalew et al (2002) reported in the upper reaches of northwest Ethiopia's flood basalts and Jimma rhyolite layers estimated at 43,1o4km3 were transformed by the wegel tena rhyolite mass and other rhyolite outbreaks (Lima Limo area) of the total 20% of this episode. Basalt traps ignimbrite from very high plateau terrain, evidently seen in the areas of Wadla, Dawunt, and Wegel tena (Delanta). The thick blocks are primarily exposed in the town of Wegel Tena's northern regions. Then the profound ravines of the Jita and Bashilo streams have significantly eroded and sliced through the blocks, creating cliffs on both sides in the regions mentioned (Ayalew et al., 2002).The extreme thickness of this unit is approximately 500 meters The layered and the thickness of the individual and stratified flows ranges from 3 to 15 meters.

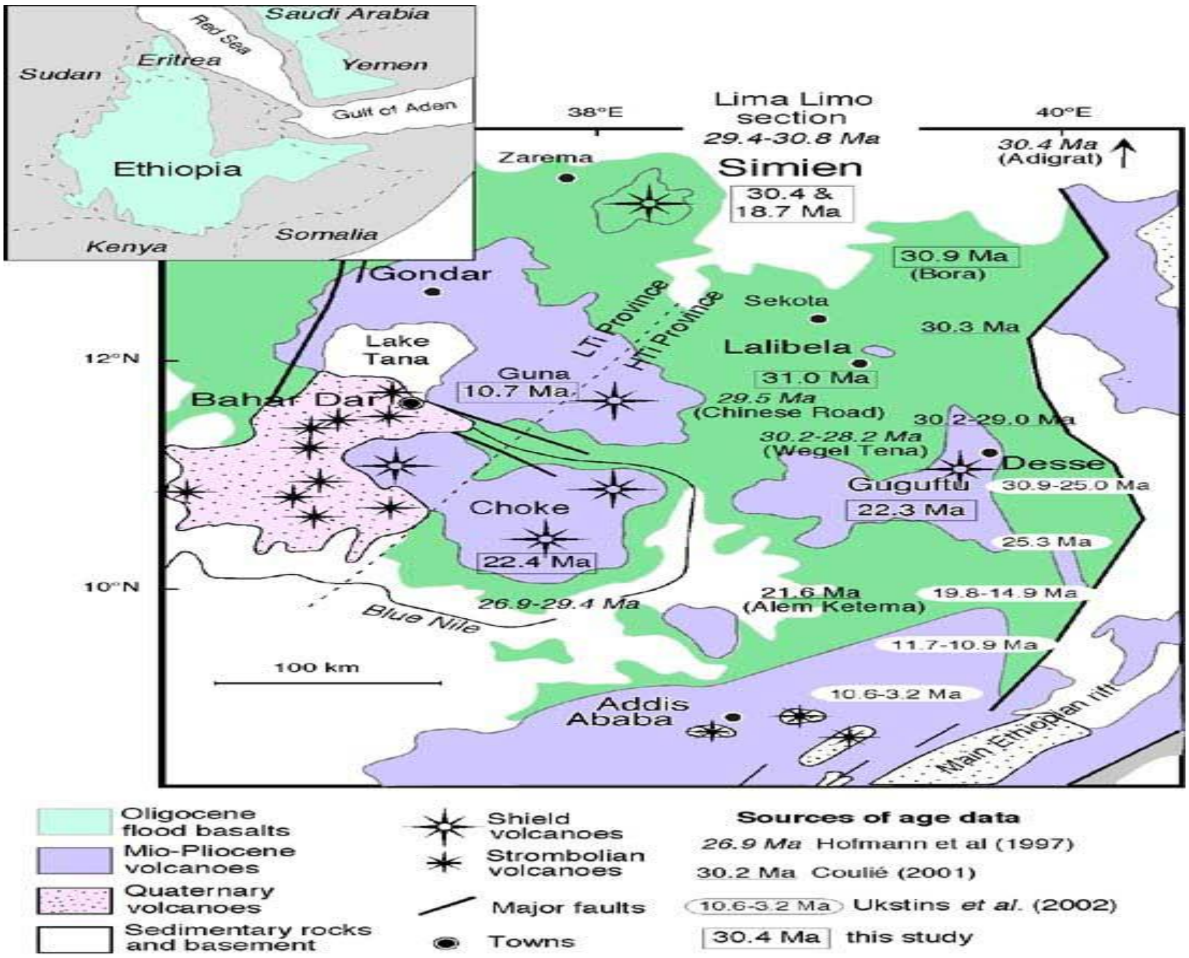

Figure 2.1: The geological map of the Northern Ethiopian plateau (Keiffer et al., **2004**)

2.2 Local geology

Around the research area, there are four distinct geological units: Rhyolite, Basalt, Trachyte, and Alluvial/Colluvial sediments. The Mersa-Girana Basin, located in northern Ethiopia within the broader Ethiopian Main Rift System and extending into the Afar Region, is predominantly comprised of volcanic rocks. This area forms part of the western escarpment of the Main Ethiopian Rift. The geological formations around Mersa and Girana towns are mainly volcanic rocks that create mountainous terrain, integral to the western escarpment of the Main Ethiopian Rift Valley. Research indicates that this volcanic rock unit includes the Alage rhyolites, composed of rhyolites and basalts associated with graben structures, and the Ashangai basalt at the valley bottom, which covers the upper sandstone unit (Kobo-Girana., 2009).Basalt Unit: Found in the northeastern, northwestern, and northern regions, particularly covering the western and northeastern mountainous areas. This unit exhibits high levels of fracturing.

2.2.1 Volcanic unit

This unit is exposed along roads and rivers and is highly fractured and weathered. The volcanic formations include various types of deposits such as tuff, ignimbrite, and ash. The western and northern parts of the study area are dominated by fractured basalt (Fig 2.2a), which is also highly weathered (Fig 2.2b). The tuff unit is found in the southeastern and southwestern parts of the research area.

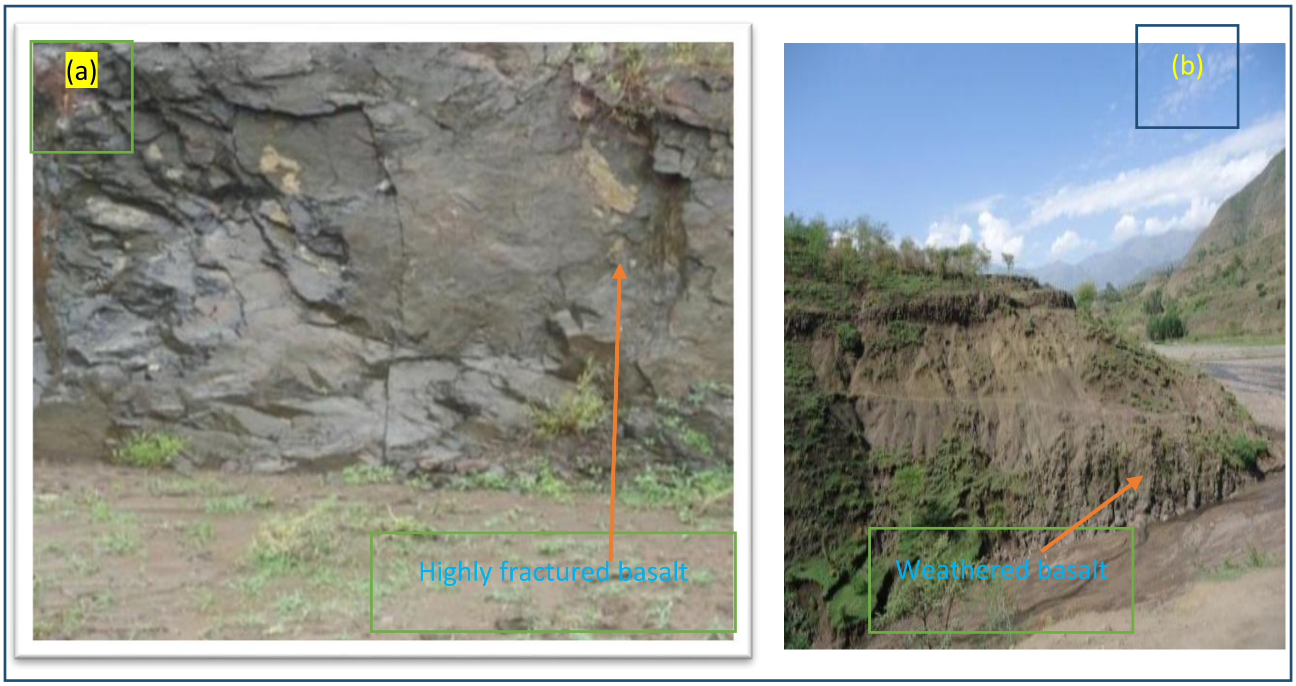

Figure 2.2: The volcanic units in the Mersa-Girana basin

2.2.2 Alluvial deposits

This unit is found in the central part of the study area and consists of a mixture of silt, sand, gravel, and clay particles that are transported and deposited by rivers and streams. These alluvial deposits are characterized by their relatively loose and unconsolidated nature, which makes them significant sources of groundwater due to their high porosity and permeability. In hydrogeology, alluvial deposits often serve as important aquifers, storing and transmitting groundwater (Fig 2.3) depicts these sedimentary deposits along the river course, showing soil, clay, and gravel rocks.

Figure 2.3: The Alluvial units in the Mersa-Girana Basin

2.2.3 Local geological structure

The major geological structures in the basin are northwest-southeast and northeast-southwest oriented fractures. The presence of different layers such as topsoil, sand-gravel layers, clayey sediments, weathered volcanic rock, and bedrock, which contribute to the overall hydrogeological setting of the area (Kobo-Girana ., 2009). Fracturing and Weathering: The volcanic units in the Mersa-Girana Basin are highly fractured and weathered, especially the basalts in the western and northern regions. This fracturing enhances the permeability of the rocks, contributing to the basin's potential as a groundwater reservoir. Escarpment and Graben Structures: The presence of graben structures and the western escarpment of the Main Ethiopian Rift indicates significant tectonic activity, which has influenced the deposition and current structure of the volcanic and sedimentary units.

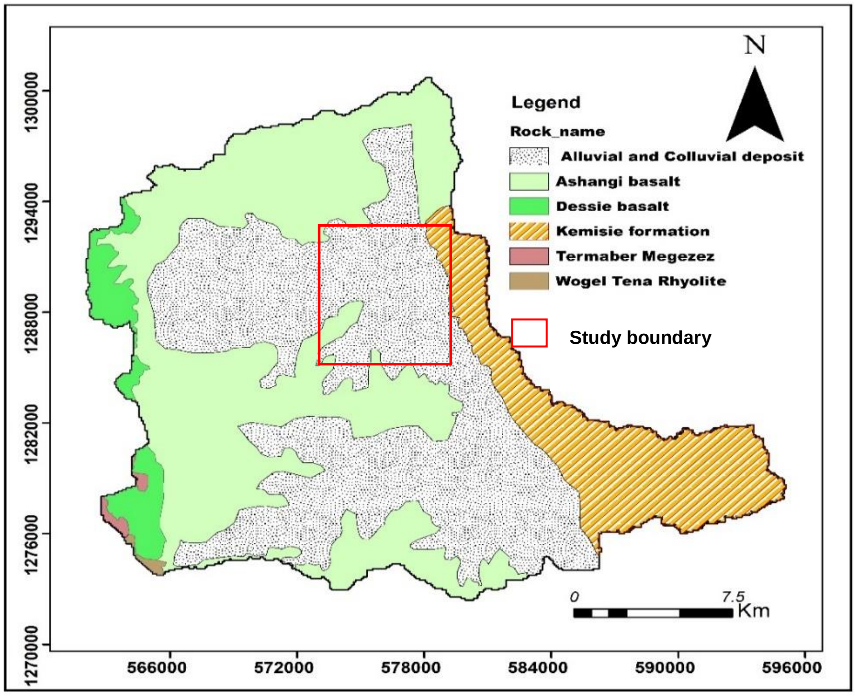

Figure 2.3: Geology map of the study area

2.3 Hydrogeology of the study area

Hydrogeological studies have been conducted to comprehensively understand groundwater dynamics, recharge mechanisms, and aquifer characteristics within the Mersa-Girana sub-basin, situated in the Ethiopian Highlands. This sub-basin features prominent geographical elements such as Ambassel Mountain, Lideta Mountain, and Bukero Mountain. It encompasses a diverse hydrogeological landscape comprising interrelated aquifers, fractured and weathered bedrock formations, and alluvial deposits.

The Mille River intersects both the western and eastern escarpments that delineate the alluvial sediments in the area. Groundwater flows originate from high mountainous regions towards Mersa and Girana within the Mille Catchment, influenced significantly by elevation gradients and geological structures. The elevated western and eastern parts of the study area consist of highly fractured and weathered volcanic rocks, which play a crucial role in groundwater recharge.

Conversely, the lower elevation areas of the Mersa-Girana marginal graben function as the primary discharge zones for groundwater. These areas include springs, wells, and various outlets where groundwater emerges naturally.

CHAPTER III

THEORTICAL BACKGROUND OF GEOPHYSICAL METHODS

3.1 Introduction

Geophysical methods are broadly classified as either using Earth's natural fields or requiring the Injection of artificial fields into the ground. These techniques can be categorized into two sizable categories. Those are active and passive methods (Gibson & George., 2013). Passive methods are those that monitor changes in natural fields, such as gravitational and magnetic fields, about the Earth. Active methods that employ artificially generated sources like seismic and electrical tools and others (Kearey et al., 2002). This study intends to carry out a comprehensive geophysical study by using techniques for electrical resistivity gravity method and magnetic perspective. Among these, mapping is done using the magnetic approach to map large-scale lithological units and geological structures and the electrical resistivity method also map local structure and establish vertical stratification of geo-electric layers (Telford et al., 1990).

3.2 Electrical resistivity method

The resistivity method is one of the geophysical methods that use electrical sources to the variation of resistivity of underground soil and rock formation (Kearey et al., 2002). Through the resistivity method, two electrodes are used to apply a direct cumulative or low-frequency alternating current to the soil. Additionally, another pair of two-point electrodes known as the potential electrodes assess the voltage between two spots on the ground (Telford et al., 1990). The distribution of surface rock resistivity variation and surface potential distribution are also impacted by the resistivity variation of subterranean rock, which influences of current. The potential difference pattern of uniform soil provides information about the shape of underground irregular soil mass called resistivity anomaly (Holden et al., 2002). The resistivity of the ground between the measuring terminals is measured by the potential difference of the unit current transferred to the ground. This resistivity is dependent on the electrical characteristics of the ground as well as the geometric configuration of the electrodes (Raymond., 1947).

3.2.1 Major principle of vertical electrical sound (VES)

Values of resistivity distributed vertically in a geological unit are reflected in the observed value of vertical electrical sound (VES), which is the electrode position that fluctuates concerning a fixed point (Kearey et al., 2002). And also the technique of studying the apparatus resistivity variation of the rocks by regularly increasing the current electrode spacing. The producer is employed, together with electrodrilling or convectional vertical electrometric (VES), to measure changes in resistivity in a vertical direction. The matching probe curve is obtained by equally increasing the spacing in the current electrodes' vicinity around a point known as the probe point while maintaining the location of MN potential electrodes (Raymond., 1947). As the depth of the investigation increases and the space between the current electrodes increases, so ensures the corresponding apparatus resistivity (Lillie., 1999). The Schlumberger and Wenner's displays remain the two networks used for the electrical survey. But mostly my study uses the Schlumberger electrode array technique. The potential electrodes' distance from one-tenth of the current electrodes is the maximum when utilizing the Schlumberger array. And choose a cylindrical coordinate system whose origin is the source point of the direct current located on the earth's surface (Raymond., 1947). The subsurface is made up of an unlimited number of layers, $h_i = h_1, h_2, h_3 \dots \dots h_n$with the lowest layer, which is infinitely deep, and the remaining levels having a finite thickness. The layers are divided by a horizontal boundary plane. In addition, resistivity $\rho_i = \rho_1, \rho_2, \rho_3 \dots . \rho_n$ of each layer is isotropic and electrically homogenous (Kearey et al., 2002). The potential's derivative based on the conduction mentioned above is because the electric field V of the direct current satisfying the Laplace differential equation is given by:

$$\frac{\partial^2 \mathrm{v}}{\partial \mathrm{x}^2} + \frac{\partial^2 \mathrm{v}}{\partial \mathrm{y}^2} + \frac{\partial^2 \mathrm{v}}{\partial \mathrm{z}^2} = 0 \qquad (3.1)$$

The potential field exhibits a distinct vertical axis that passes through the current sources, giving a cylindrical symmetry. The solution can be given a symmetric vertical axis by using the Laplace equation in cylindrical coordinates

$$\frac{\partial v}{\partial \theta} = \frac{\partial^2}{\partial \theta^2} = 0 \text{ Then}$$

$$\frac{\partial^2 \mathrm{v}}{\partial \mathrm{x}^2} + \frac{1}{\mathrm{r}}\frac{\partial \mathrm{v}}{\partial \mathrm{r}} + \frac{\partial^2 \mathrm{v}}{\partial \mathrm{z}^2} = 0 \qquad (3.2)$$

Using a separation of variables method, then a specific solution to Eq (3.2) can be determined and accepted as the form

$$\mathrm{V}(\mathrm{r}, \mathrm{z}) = \mathrm{U}(\mathrm{r})\mathrm{W}(\mathrm{z}) \qquad (3.3)$$

From Eq (3.3) is replaced with Eq (3.2), and the entire calculation is divided by the product *which* is given as

$$\frac{1}{U(R)}\frac{\partial^2 U(r)}{\partial r^2}+\frac{1}{rU(r)}\frac{\partial U(r)}{\partial r}+\frac{1}{W(z)}\frac{\partial^2 W(z)}{\partial z^2}=0 \quad (3.4)$$

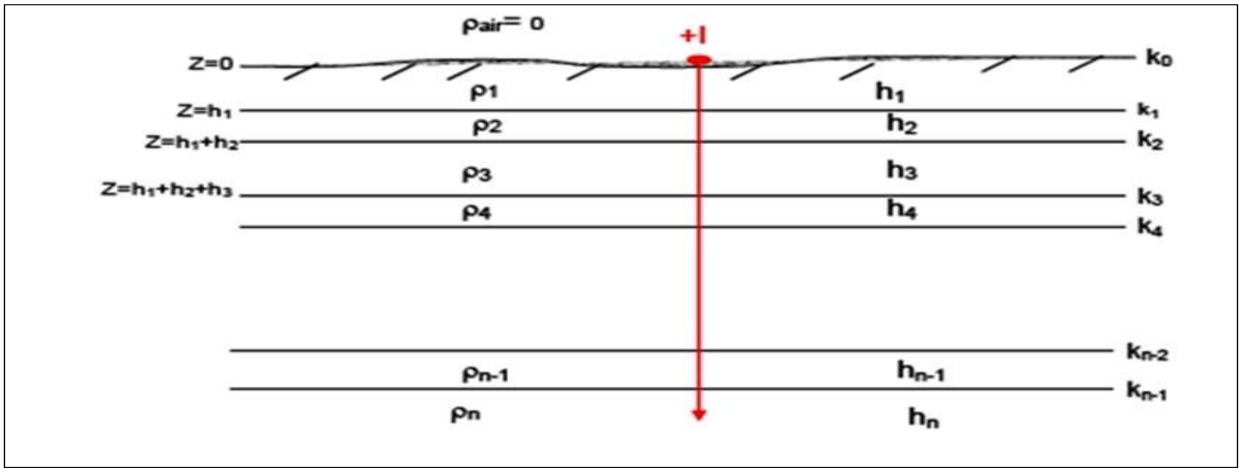

Figure 3.1: Problem presentation for solution of potential in multi-layer earth

.Then the equation is met only if

$$\frac{1}{u(r)}\frac{\partial^2 u(r)}{\partial r^2}+\frac{1}{ru(r)}\frac{\partial\, u(r)}{\partial r}=\lambda^2 \quad (3.5)$$

$$\text{And } \frac{1}{\mathrm{w(r)}}\frac{\partial^2 \mathrm{w(r)}}{\partial \mathrm{z}^2}=-\lambda^2 \quad (3.6)$$

Where λ is a constant that is chosen at random. One possible interpretation of equation (3.6) is:

$$W(\mathrm{Z})=C_1e^{-\lambda Z} and\ W(Z)=C_2\ e^{+\lambda Z} \quad (3.7)$$

From the above equation (3.5) is specified as

$$\mathrm{U(r)}=C_3J_0(\lambda\mathrm{r}) \quad (3.8)$$

Then Jo is the order of zero Bessel function. Then the differential problem provided by equation (3.9) can be specifically solved by arranging equations (3.7) and (3.8), which are as follows:

$$\mathrm{V(r,z)}=\ \mathrm{C4e^{+\lambda Z}J_O(\lambda r) and\ V(r,z)=C4e^{-\lambda z}\ J_0(\lambda r)} \quad (3.9)$$

Given that C and λ are constants and since each linear arrangement of a specific solution is a key solution. According to differential equation theory, one can set λ to roughly represent all possible values ranging from zero to infinity and allow the constant "c" to be very independent of λ. One can obtain the overall answer to equation (3.2) as

$$\mathrm{V(r,z)}=\int_0^\infty[\,\phi(\lambda)\mathrm{e}^{+\lambda z}+\psi(\lambda)\mathrm{e}^{-\lambda z}]\ \phi(\lambda)\mathrm{e}^{+\lambda z}\ ]J_0(\lambda\mathrm{r})\mathrm{d}\lambda \quad (3.10)$$

The special form of these equations is determined by the boundary conditions, as ϕ (λ), and are arbitrary functions. When On the surface of an electrically homogeneous earth, there is a single point source of current intensity, denoted by "I", the potential it generates can be calculated using a simple theory as follows:

$$V = \frac{I\rho}{2\pi} \frac{1}{\sqrt{r^2 + z^2}} \qquad (3.11) \text{ And}$$

$$\int_{0}^{\infty} e^{-\lambda z} J_{0}(\lambda r) d\lambda = \frac{1}{\sqrt{r^2 + z^2}} \qquad (3.12)$$

So equation (3.12) related as $V = \frac{I\rho}{2\pi} e^{-\lambda z} J_0(\lambda r) d\lambda$ (3.13) and the combination solution of the two equations can be given by:

$$V(r,z) = \frac{I\rho}{2\pi} \int_{0}^{\infty} [\, e^{-\lambda Z} + X(\lambda) e^{+\lambda z} + \theta(\lambda) e^{+\lambda z}] J_0(\lambda r) d\lambda \qquad (3.14)$$

Where Θ (λ) and ̨ (λ) are functions. All subsurface layers have effective solutions for equation (3.14). Even though, it must be comparable in various underlying layers. Then layer is content it needs to contain the potential at the surface of a conductive point source are parallel stratified earth.

$$V_1 = \frac{I\rho}{2\pi} \int_{0}^{\infty} [\, e^{-\lambda Z} + Xi(\lambda) e^{+\lambda z} + \theta i(\lambda) e^{+\lambda z}] J_0(\lambda r) d\lambda \qquad (3.15)$$

The Stefanescu Integral is the name given to this equation, where "i" stands for the several subsurface layers.

Boundary conduction

The following boundary conduction criteria are met by the potential function identified by a single current source on the horizontally stratified earth surface. The potential essential equal to

$$Vi = V \ at \ z = \ hi \qquad (3.16)$$

$$(J_0)N = (J_{1+1})N, \frac{1}{\rho i} \frac{\partial V_i}{\partial z} = \frac{1}{\rho i+1} \frac{\partial V_{i+1}}{\partial z} \qquad (3.17)$$

According to the formal (3.17), as the source of current in the air is J air is zero, the current density at depth zero must be zero. The potential is effectively not line infinity when the current source is closed, and it must stay finite.

$$V = \frac{I\rho}{2\pi} \frac{1}{\sqrt{r^2 + z^2}} \qquad (3.18)$$

3.2.2 Electrode configuration

The configuration of the electrodes for potential and current is known as electron configuration (Kearey et al., 2002). The resistivity approaches may generally be used for a wide variety of electrode array configurations. The electrode array consists of gradients, squares, Wenner, Schlumberger, Lee partitions, pole-pole, pole-dipole, and diagonal square arrays, among other configurations. Resistivity assessments typically use two potential electrodes and two current electrodes (Raymond., 1947).

3.2.3 Schlumberger electrodes array

A current electrode was methodically advanced outward in AB>5 MN steps, but the potential electrodes were only occasionally moved (Kearey et al., 2002). The electrodes in this system are arranged

symmetrically around the array's center point.the configractation as show in (Fig 3.2)

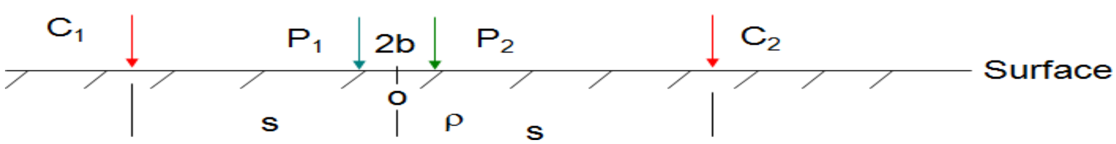

Figure 3.2: Schlumberger array configuration

$$When\ r_1 = s - b, r_2 = s + b, r_3 = s + b, r_4 = s = b \quad [3.19]$$

Equation [3.19] can be used to find the potential difference ΔV if O is the array's center.

$$\Delta V = \frac{I\rho}{2\pi}\left[\left(\frac{1}{s-b} - \frac{1}{s+b}\right) - \left(\frac{1}{s+b} - \frac{1}{s-b}\right)\right] \text{ And}$$

$$\Delta V = \frac{I\rho}{2\pi}\left[\left(\frac{1}{s^2-b^2}\right)\right] \quad (3.20)$$

$$\rho_a = \pi\left(\frac{s^2-b^2}{2b}\right)\left(\frac{\Delta v}{I}\right) \quad (3.21)$$

Next, K's geometric factor is provided by $k = \pi\left(\frac{s^2-b^2}{2b}\right)$ (3.22)

A series of main curves, where layer thickness grows with depth and layer resistivity values are computed assuming several layers in the Earth, can be fitted to estimate layer resistivity values. One plot can represent the two layers and the primary curves.

3.2.4 Apparatus resistivity

The actual resistivity of the regular earth and the symmetrical component determine the measured potential difference if the surface is homogeneous (Gibson & George., 2013). Though, in practice, the earth is locally homogeneous and the potential difference is influenced by the applied current, the mediums of subsurface resistivity and the geometrical factor (k), which is established by the electrode array or configuration types. The resistivity calculated from such non homogeneous term "ground" refers to apparent resistivity ρ_α will be connected to the parameter as

$$\rho_\alpha = \frac{k\Delta v}{I} \qquad [3.23]$$

Curve matching or inversion methods are used to interpret the apparent resistivity in ground surveys. Typical electrode arrangements consist of Wenner, Schlumberger, and Dipole-Dipole designs. The ideal electrode arrangement is determined by the lateral solution power and depth. The variations in geometrical factors cause variations in the apparent resistivity expression. In Schlumberger arrays, the electrode arrangement is symmetric.

3.2.5 Resistivity of some rocks

Three types of electrical conduction can happen in subterranean rocks and earth materials: those are rock type, fluid nature, porosity, pore connectivity, and metallic content of the solid (Kearey et al., 2002). The main geologic factors influencing resistivity are porosity and pore fluid properties. The amount of porosity in a rock is determined by its fault, fissure, fracture, and crack structures. As pore fluid temperature, salinity, and porosity rise, rock resistivity decreases. This is caused by high salinity pore fluids, which contain more ions, conduction pathways provided by interconnected pore fluids, and high temperatures, which increase ion mobility and conductivity.

3.2.6 Basic principles of vertical electrical resistivity for groundwater

Groundwater, with its salts, is ionic conductive, allowing electrical current to movement into the ground. The Extent of soil and resistivity of subsurface helps identify the presence or absence of water. The Rock resistivity depends on water content, water resistivity, clay content, and metallic mineral content. Hard rocks without pores or cracks are highly resistive to electrical current flow, while dry sand is very resistive. Porous or fractured rocks' resistivity depends on water resistivity and rock porosity. Impermeable clay layers may not be suitable for groundwater use. Resistivity measurements are used to determine groundwater presence in hard rock environments, where low resistivity anomalies correspond to groundwater, and high resistivity anomalies correspond to fresh water in conductive clayey or saline environments. Resistivity measurements are influenced by the resistivity of igneous, sedimentary and metamorphic. Igneous rocks have the highest resistivity sedimentary rocks are the most conducive.

3.2.7 Field procedures of resistivity survey

Vertical Electrical Sounding (VES) are the methods used in resistivity surveys by using Wenner or Schlumberger arrays. VES is a 1D resistivity approach that maps the vertical change of subsurface resistivity with depth. It is a reasonably priced method and among the earliest for determining resistivity. In the meantime, by moving the entire electrode array along a profile, lateral in homogeneity.

3.2.8 Dar-Zrrouk parameters

The Dar-Zarrouk parameters are crucial for interpreting geo electric layers in a conceptualized medium, particularly when considering parameters like resistivity (ρ) and thickness (h) for each individual layer (Batte et al., 2010). Within an n-layered, homogeneous, isotropic sequence characterized, transverse resistance (T) and longitudinal conductance (S), which are the Dar-Zarrouk parameters, are defined as follows by resistivity (ρi) and thickness (hi)

$$Lc=\sum_{i}^{n}\frac{h_i}{\rho_i} \qquad (3.24)$$

$$T_R=\sum_{i}^{n}\rho_{ih_i} \qquad (3.25)$$

The relationship between aquifer and Dar-Zarrouk parameters can be expressed mathematically, providing insights into the aquifer's characteristics based on geo electric data.

3.2.8.1 Aquifer parameters

Aquifer properties play a crucial role in determining the groundwater potential of a well (Todd and Mays (2004). The coefficients of transmission, storage, and hydraulic conductivity are key parameters that provide insights into the behavior and capacity of an aquifer system. The storage coefficient quantifies the storage capacity of an aquifer, representing the amount of water discharged per unit area covered by a change in hydraulic head. It is a fundamental parameter for understanding how water is stored and released within the aquifer. Hydraulic conductivity, on the other hand, refers to the ability of the aquifer material to transmit water. It is affected by influences such as grain size, sorting, and shape in the case of alluvial sediment, and by the degree of fractures and pore space connectivity in basement and volcanic rocks. The amount of water that can pass through a unit width under a unit hydraulic gradient is measured by transmissivity, which is closely related to hydraulic conductivity. (Batte et al., 2010). It is calculated as the product of hydraulic conductivity and thickness of aquifer. Mathematically, hydraulic conductivity (K) is determined by dividing the discharge (Q) by the cross-sectional area (A) multiplied by the hydraulic gradient (Δh/Δl).

$$K = \frac{Q}{A\frac{\Delta h}{\Delta l}} \qquad (3.26)$$

Similarly, transmissivity (T) is intended by dividing the discharge (Q) by the width (w) multiplied by the hydraulic gradient (Δh/Δl).

$$T = \frac{Q}{w\frac{\Delta h}{\Delta l}} \qquad (3.27)$$

Additionally, transmissivity (T) is equal to the product of hydraulic conductivity (K) and the aquifer thickness (h).

$$T=Kh \qquad (3.35)$$

And the hydraulic conductivity also given by

$$k=T/h \qquad (3.28)$$

3.3 Magnetic method of prospecting

Those are methods that measure the Earth's magnetic field passively at various locations over its surface using a magnetometer (Alemu., 2020). Anomalies in magnetic data can point to the existence of very magnetically susceptible subterranean regions, which are utilized to describe a site (Benson & Mustoe., 1998). Depending on the size of planet Earth, the primary magnetic fields can change in strength in alteration or anomaly. The impacts of the core magnetic field depend on the shape, location, burial depth, and magnetic properties of object of the direction than the strength of earth-induced field (Benson & Mustoe., 1998). A map of subsurface magnetic anomalies is produced by processing and analyzing data using specialist software after several survey lines are utilized to acquire a thorough subsurface image. Applications for the magnetic maps and models produced include resource assessment, environmental monitoring and mining exploration.

3.3.1 Fundamental concepts and units in geomagnetism

A magnetic flux that extends of the magnet sharp from one end to the other end in the area of the bar magnet. The flow can be followed from the direction indicated by the little compass needle hanging exclusively by the magnets. The magnet's poles are the location inside the magnet where the magnetic flux converges (Stevenson., 2020). The magnet's pole points in the direction of its positive, or north, pole, while its negative, or south, pole, is located at its opposite ends and has the same strength. The magnetic poles are always found in pairs that face each other and form dipoles; however, for a pole to stop affecting the other poles, it must be separated from its partner by a considerable distance.

A. **Magnetic force**

The magnetic force F_M is provided by force between two magnetic poles, P_1 and P_2, with a separation of r. given as

$$Fm = \frac{\mu_0}{4\pi\mu R}\frac{P_1 P_2}{r^2}\bar{r} \qquad (3.29)$$

Where the constants $\mu 0$ and μR correspond to the vacuum's magnetic permeability and the medium separating the poles' relative magnetic permeability (Alemu., 2020). Additionally, the force is repellent when the poles are similar to one another and appealing when they are in opposing signs.

B. **Magnetic field**

The magnetic force on moving charges is described by the vector field called magnetic field B (Alemu., 2020). The force acting on a unit positive pole on a given expanse from the pole is well-defined as the magnetic field B caused by the pole strength of P. From the points, the magnetic field is thus given by:

$$B = \frac{\mu_0}{4\pi\mu R}\frac{P}{r^2} \qquad (3.30)$$

Moreover, just like gravitational fields, the magnetic potential can also be used to define the magnetic field. V represents the magnetic potential at a distance r from the pole then a single pole of strength P is as follows:

$$V = \frac{\mu_0}{4\pi\mu R}\frac{P}{r^2} \qquad (3.31)$$

The potential's partial derivative as expressed in a particular path gives the magnetic field component in that direction. The usual magnetic display known as a dipole consists of two poles. The SI unit is Tesla (T). Next, given the dipole's strength (m) and distance (l) apart the magnetic moment M of the dipole is given by:

$$M = ml \qquad (3.32)$$

The coil's cross-sectional area, number of turns and current magnitude all affect the current's carrying coil and magnetic moment. The SI unit is Am^2 Therefore represents the magnetic moment through dipole moment per unit volume of material, or J_i is the extent of how strongly a particular material is induced to magnetize.

$$J_i = \frac{M}{LA} \qquad (3.33)$$

The variables M, A, and J_i represent the magnetic moment, magnetization, cross-sectional area and sample length, respectively.

C. Magnetic flux

Magnetic flux is the measurement of the total magnetic field that passes through a certain region. Additionally, it is a useful tool for explaining the effects of magnetic force on an object in a specific location (Alemu., 2020). The magnetic flux is determined by:

$$\phi_B = B.A = BA\cos\theta \qquad (3.34)$$

Where A is a real vector, B is the magnetic field, and ϕ_B magnetic flux SI unit is the tesla-square meter (Tm^2).

D. Relationship between relative permeability susceptibility and magnetization

The relationship between magnetic permeability= $\mu_r\mu_0$, relative permeability($\mu_r = 1$) for air and many rocks, and permeability of free space $\mu_0 = \pi \times 10^{-7}$ B magnetic flux density, and H magnetic field may all be inscribed when the medium differs from the vacuum.

$$B = \mu H, B = \mu_r\mu_0 \text{H},$$

$$\text{B} = \mu_0\text{H} + \mu_0\,(\mu_r - 1)\text{H then } B = \mu_0 H + \mu_O kH$$

In terms of both magnetic permeability and permeability of free space, where$k = \mu_r - 1$, that is, $k = \mu_r - 1$ and from the material $M = kH$, the relative permeability is also given by:

$$\mu = \mu_0(1 + \text{k}).$$

The magnetic flux density, which is dependent on the magnetization of the materials, can thus be expressed as

$$B = \mu_0(H + M) \qquad (3.35)$$

The relationship between H&M in non-magnetic substances is represented by the permeability of free space. Magnetic susceptibility and permeability are physical qualities investigated by materials' magnetic characteristics. Most rocks' magnetic characteristics are characterized in terms of κ.

3.3.3 Origin of the earth magnetic field

The earth's outer core is composed of molten iron and nickel (a collection of charge carriers called ions in conductors) (Alemu., 2020). The convention of molten iron or nickel constitutes the motion of the charged particle (ions) resulting in the electric current in the form of loops producing the magnetic fields. The geomagnetic field produced behavior as though the north geomagnetic pole in the Southern Hemisphere and the south geomagnetic pole in the Northern Hemisphere. According to Zhong et al (2002) (magneto-hydrodynamic (MHD) theory) the outer core's intricate flow of highly conductive metallic iron is the primary source of the geomagnetic field, acting as an independent generator through compulsively moving fluid.

3.3.4 Nature of earth magnetic field

The geomagnetic field, also known as the earth's magnetic field, spans millions of kilometers and attracts each other due to its north and south poles (Alemu., 2020).

3.3.5 Component sources of earth total magnetic field

The rotation of the Earth is the source of its magnetic field, and it is connected to the liquid metallic iron within the planet. This spin, referred to as the "geodynamo" or "dynamo effect," is caused by the outer-core fluid rotating about the Earth's magnetic field due to convection. The Earth's magnetic field originates from two sources: electric currents in the ionosphere and magnetosphere, which are exterior sources, fluid motion in the Earth's outer core and magnetized rocks in the lithosphere, which are internal sources.

A. External field

Defines as it having formed from an electric current made up of particles ionized by solar radiation in motion that was flowing through the earth's ionosphere. The magnetic storm is an external magnetic field that is generated by electrical currents in the ionosphere, which is made up of particles ionized by solar radiation. This field is typically varied over hours at tens of nT, but it can sometimes infrequently vary over minutes at hundreds of nT.

B. Main earth magnetic field or dipole field

Large regional fluctuations in strength and direction are explained by the main magnetic field, which is created by electrical currents in the outer core. It is constant on a timescale of days, but varies over years at a rate of about 50,000 nT. A dynamo mechanism in the Earth's fluid outer core is the source of the Main Magnetic Field. With almost 95% of the field strength detected at the Earth's surface, (Kearey et al., 2002).

C. Rock magnetism

Rock magnetism aids in the development of techniques by geomagnetism to measure the Earth's magnetic field and account for metamorphism and compaction of sediment. (Kearey et al., 2002).

D. Total magnetic field: The Earth's total magnetic field is used to locate mineral resources or beneath geological formations (Kearey et al., 2002). It is also expressed by the total of the whole component sources of earth's total fields and denoted by B_T

$$B_T = B_{ex} + B_{rm} + B_D \qquad (3.36)$$

3.3.6 Temporal variations of the earth total magnetic field

The Earth's magnetic field varies with time, called the temporal version. The versions are classified into three classes.

A. Secular variation

It is a sustained alteration in the geomagnetic field brought about by fluid movement in the outer core of the earth. (Alemu., 2020). Earth's geomagnetic field has reversed its polarity multiple times throughout geologic time, with the most recent instance occurring 7-15 years ago (Alemu, 2020). These longer variations are believed to be induced by changes in electric currents.

B. Diurnal variation

Smaller but more frequent variations in the Earth's field occur daily due to external factors like solar radiation. The number of daily diurnal variations, around (20-30) Y (Alemu., 2020).

C. Magnetic storm

Magnetic storms are a rare occurrence of an upsurge in magnetic activity in the ionosphere. During a magnetic storm, an impulsive, unbalanced magnetic field with an amplitude of 1000Y is recorded. In The Solar wind and flares, Earth's magnetic field is disturbed by magnetic storms, which interfere with electrical systems, navigational systems, and communication (Alemu., 2020). Auroras in the polar areas can also be caused by severe storms, as indicated by the K-index. Precautions and observation are essential.

3.3.6 Elements of Earth's Magnetic Field

The earth's magnetic field, also known as the geomagnetic field, is a vector quantity that changes over time and space over the spherical earth's surface in both magnitude and direction. Cartesian components (X, Y and Z) that run parallel to the three orthogonal axes can be used to represent the components of a geomagnetic field (Alemu., 2020). These are the Z-component flowing downhill down the vertical axis, the X-component paralleling the geographic north axis, and the Y-component paralleling the geographic east axis. (Alemu, 2020). Two angles determine the geomagnetic field's orientation. Specifically, the angle is represented by (I) for inclination and (δ) for declination. The angle between the magnetic and geographic north axes is identified as the declination (δ). The angle at which the geomagnetic vector B beads below its horizontal components H performing along the magnetic north axis identified as the inclination I (Alemu., 2020). At an observation place like (Fig 3.3), the earth's magnetic field B is represented by a collection of seven physical parameters. These elements are referred to as geomagnetic elements: B, X, Y, Z, H, δ, and I. (Alemu., 2020).

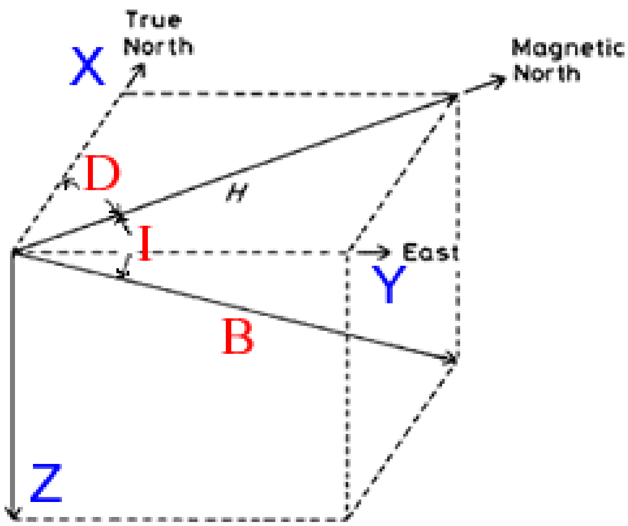

B= total intensity

I= inclination

B_H= horizontal intensity

B_n= North component of the horizontal

B_e= east components of the horizontal

z =vertical components intensity

δ =declination

From the above elements of Earth's magnetic fields we can find the total magnetic field vectors and declination angle as given below:

$$B_H^2 + B_Z^2 = B^2$$

$$B = \sqrt{B_N^2 + B_Z^2} = \sqrt{B_N^2 + B_E^2 + B_Z^2}$$

$$B_H^2 = B_N^2 + B_E^2$$

$$i = \tan^{-1}\left(\frac{B_N}{B_H}\right)$$

$$\delta = \tan^{-1}\left(\frac{B_E}{B_H}\right) \qquad (3.37)$$

Figure 3.3: Earth's magnetic field elements.

3.3.7 Magnetization and Magnetic susceptibility of materials

Magnetism originates from electric charges moving through electrons, with each atom acting like a magnet in two ways with two magnetic dipole moments, influenced by the electron's orbit (Alemu., 2020). An object in an induced magnetic field acquires small magnetization, which is proportional to the dipole moment per unit volume, and the relationship between magnetization and source is given.

$M = KH$ (3.38) Where K is the magnetic susceptibility.

CHAPTER IV

4. DATA ACQUISITION AND PROCESSING

4.1 Introduction

The design and execution of magnetic and vertical electric sounding (VES) lines, positioned perpendicular to regional strike, play a critical role in geological and geophysical investigations. These lines are strategically planned to effectively capture subsurface structures and variations in the geological formations. Essentially, magnetic lines are designed to detect anomalies in the Earth's magnetic field, while VES lines are used to measure the electrical resistivity distribution beneath the surface. In the initial planning phase, factors such as the geological context, target depth and desired resolution determine the design of these lines. Typically, the magnetic and VES lines are spaced at regular intervals to ensure comprehensive coverage of the study area while maintaining an optimal balance between data density and cost efficiency. The total number of VES and magnetic data points collected depends on the scope and objectives of the study, as well as the desired resolution and accuracy of the results. This number is determined by careful consideration of factors such as the size of the study area, the complexity of the geological structures and the available resources. Topographically, the terrain characteristics of the study area significantly influence the conduct of the study. The raw data is processed and analyzed using advanced geophysical techniques to gain insights into subsurface structures and properties.

4.1 VES Data

For the VES survey, four profile lines were utilized in the area: approximately three of them were oriented in a northeast-southwest direction and one was oriented in an N-S direction. Along each profile the separated between sounding points was half a kilometer. The study area characterized by the thick alluvial sediments deposited by Mille River's juxtaposing against basalt flows due to normal faulting. To reach the maximum depth of interest, electrical resistivity measurements were performed using a Schlumberger array along traverse lines with a maximum current electrode of spacing 1000 m (AB/2 =1000 m). In addition to the 10 VES points collected for the present study, 10 data points collected by the Amhara Design and Supervision Corporation as part of the Kobo-Girana Valley Pressurized Irrigation Project, were also interpreted. The maximum AB/2 for the secondary data also is the same to that the primary data the length of the VES profiles is approximately 6 kilometers each lines.

Table 4.1: Location of the VES sounding points along each traverse

Line	Travel VES points	UTM Location			Total line/Profile lengths in meter
		Easting	Northing	Elevation (m)	
1	VES-1	574246	1289489	1544	6 km
	VES-2	575028	1289974	1525	
	VES-3	576088	1290303	1503	
	VES-4	577021	1290684	1489	
	VES-5	577848	1291102	1511	
2	VES-6	575462	1288588	1565	5.4 km
	VES-7	576264	1288425	1532	
	VES-8	577393	1288118	1494	
	VES-9	5822968	1281376	1470	
	VES-10	574217	1289045	1458	
3	MVES-6	574835	1286378	1542	5 km
	MVES-7	573873	1286434	1503	
	MVES-8	575869	1278641	1480	
	MVES-9	577318	1278596	1452	
	MVES-10	578256	1286019	1441	
4	MVES-1	578320	1290789	1538	5.81km
	MVES-2	578513	1289963	1507	
	MVES-3	578819	1289053	1497	
	MVES-4	579135	1288082	1504	
	MVES-5	579582	1286466	1503	

4.1.1 Field procedure and data acquisition

The Schlumberger array arrangement is broadly chosen for its capacity to penetrate greater depths and its reduced sensitivity to lateral heterogeneity, help to fixed potential electrodes. In a VES study comprising four lines, a symmetrical Schlumberger array was employed with a maximum current electrode spacing of 1000 meters, along with potential difference measurements. For electrical resistivity measurements, the points of the VES survey were distributed in both North-South and West-East directions. Measurements were taken at an average distance of 600 meters, utilizing a current electrode spacing configuration ranging from AB/2: 1.5 to 1000.0 meters. The potential electrode gap, denoted as MN/2, varied between 1.0, 12.0, and 90.0 meters during fieldwork.

To minimize ambiguity regarding subsurface in homogeneity, overlap values (AB/2) of 20.0, 30.0, 150.0, and 220.0 meters were incorporated into the data collection strategy. These measures were undertaken during the primary data collection phase conducted donated high quality Earth Resistivity Meter PASI Mod. 16GL-N by the Kobo-Girana Valley Pressure Irrigation project.

4.1.2 Data reduction

The Vertical Electrical Sounding (VES) method involves data reduction to simplify and summarize collected data while retaining essential information. This process involves filtering and smoothing to remove noise, calculating apparent resistivity values, plotting resistivity values against electrode spacing, interpreting the depth sounding curve, and estimating layer thicknesses. The reduced data is then summarized and presented in a clear format, such as depth profiles and geo electric sections by using appropriate software.

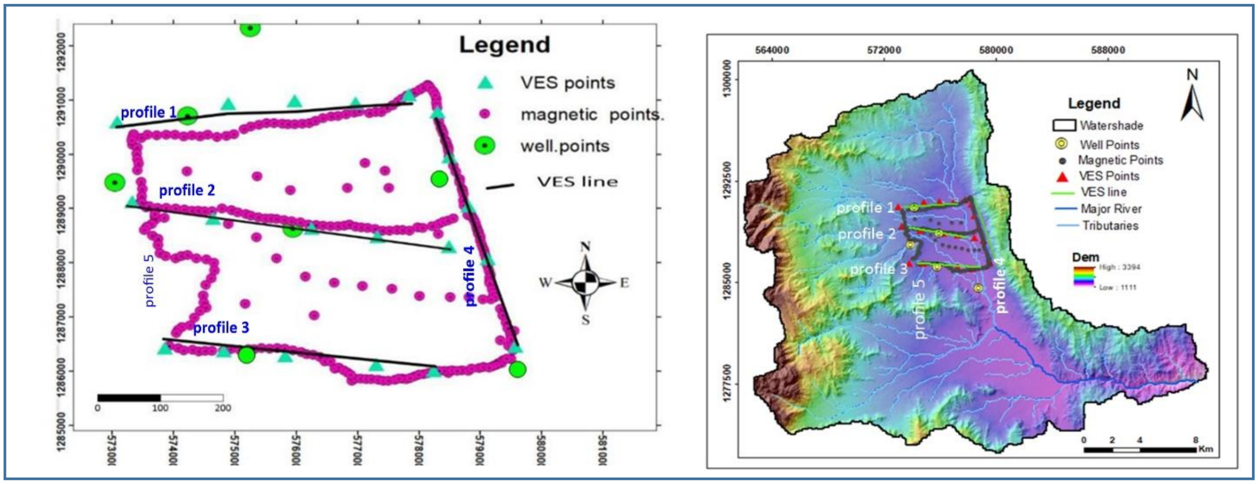

Figure 4.1: VES point and magnetic profile distribution

4.1.3 Data interpretation and Presentation

In processing VES data, inverse modeling techniques are often employed to interpret the measured resistivity values in relation to subsurface geology. Parameters obtained from lithological units from existing wells, serve as model parameters in the initial phase of the inversion process using WIN RESIST software. This involves creating a database of geo electric sections for each VES, illustrating the vertical distribution of different geological units. Geo electric sections are constructed based on traverses and are calibrated using lithologic logs from nearby drill holes. Interpreted VES points at current drill locations are also incorporated as probing points to refine the accuracy of the sections. This approach ensures that the geo electric sections accurately represent the subsurface geology, allowing for a more precise interpretation of VES data and better-informed decision-making in various applications such as groundwater exploration.

4.2 Magnetic methods

The magnetic measurement was conducted along the VES outlines and perpendicular to VES line , taking 293 point data with transect separation ranging from 100 meter .The Magnetic profiles were oriented northwest-southeast and west-east to detect possible geological structures, but few magnetic data were measured close to previously boreholes. Data was recorded from initial morning to 12:30 a.m. and 3:00 p.m. by using Portable Proton Magnetometer and handheld GPS for magnetic survey and time/position measurements.

4.2.1 Field procedures and data acquisition

Data acquisition refers to the procedure for gathering the basic material formed by magnetometer arrangement. These data was collected in hard copy or electronic demonstration, or visually presented for the hand to record. Measurement of TMI was measured along traverse lines successively perpendicular to the subsurface feature that is offered to limit or block the movement of fluids, such as groundwater. In order to create a magnetic contour map that shows the magnetic patterns of geologic relevance, magnetic data were also gathered on all loop dispersed short profiles over the path. The station spacing of 100 meters was selected based on the expected geological structure or barriers approximate geometry, depth, and trend. For the purpose of monitoring and adjusting for diurnal fluctuations, a base station located away from man-made disruptions such electricity lines, railroads, steel fencing, and footings, among other things, is selected. Except for at the start and finish of the survey, readings were taken within the base station nearly every three hours each day.

The study conducted total magnetic field measurements along traverse lines 1, 2, 3, 4, 5, and 6. A base station was chosen for each survey, away from magnetic noise, to facilitate easy reoccupation. Proton magnetometer 600 a portable magnetometer known for its high sensitivity to the overhauled effect. It is versatile and suitable for handheld, towed or base station applications Using Microsoft Excel 2007, the diurnal variation was separated from the measured magnetic field data. Using Geosoft Oasis Montaj mapping software, the magnetic field anomaly map was gridded and contoured. The base station's core magnetic field was received from the (IGRF).

4.2.2 Data processing and presentation

Processing magnetic data includes assessing the quality of the collected data, filtering and smoothing to remove noise, and isolating anomalies using mathematical techniques. Depth estimation techniques are used to estimate the depth and geometry of magnetic sources that contribute to anomalies. Interpretation involves relating anomaly features to known geologic features. Data presentation includes magnetic maps, profile charts and 2D visualization. The study involved conducting three-hour magnetic baseline analyses, which were subsequently modified using Microsoft Excel 2007 and corrected using the International Geomagnetic Reference Field (IGRF 13th Generation). The corrected data was processed using Geosoft Oasis Montaj total magnetic anomaly map. To eliminate unpredictable features, the data was smoothed using a moving average filter. The corrected and smoothed data were then presented in contour map formats.

4.2.3 Magnetic data reduction

Steps are involved in both data reduction and processing aimed at eliminating signals from the data as well as random noise ensuring that only geologically relevant information remains. This procedure makes the dataset for analysis by focusing on the signal pertinent to the task at hand. The key steps involved are as follows:

I. Editing and verifying data:
   This step includes taking out spikes and unnecessary noise caused by external sources, such as high power cables.

II. Diurnal removal: This process modifies for the time-based variation of the Earth's main magnetic field. It is realized by subtracting the time-synchronized signal recorded at a fixed base station from the investigation data.

III. IGRF removal: This step eliminates the strong effect of the Earth's main magnetic field.

CHAPTER V

5. RESULT AND DISCUSSION

5.1 Generals

In this thesis study, interpretations have been made using a combination of magnetic and vertical electrical sounding data, with the results being constrained by lithological log data from a borehole. The electrical resistivity and magnetic data interpretation is completed in the parts that follow. To create distinct sections for the electrical data that illustrate the disparity in resistivity and depth of the subsurface rocks, the apparent resistivity data and the interpreted layer parameters of each sounding curve were employed. The geo electric sections, the outcome of the electrical survey interpretation, are thought to more accurately depict the underlying electrical stratification since they are the product of interpreted real resistivity values of the subsurface. Conversely, from magnetic data residual anomaly plots, magnetic profile plots, and 2D model sections were created and displayed to demonstrate the variance in subsurface lithology and the presence of potential structures throughout the detected area.

5.2 Discussions and interpretation of VES

5.2.1 Interpreted VES curves

Apparent resistivity against electrode space plotted on a bi-log scale is construed utilizing of the Win Resist to obtain the starting model parameters to be further constrained by the existing boreholes and input into the inversion program (RESIST). The interpreted field curves demonstrate that, for each of the five VES locations, there is a very strong correlation between the field data and the interpreted model sections. An RMS error of 2.5 to 4.5% derived from the sounding data supports this claim. Five interpreted VES curves, one from each survey trip, are used to create an example. These are provided in (Fig 5.1). Using an AB/2 of 1000 meters for the survey, four underlying layers are seen in the four sounding curves, making them too well representative of the subsurface. Annex1 lays out the remainder of the VES curve interpretation. From the (tab 5.1) the HA curve types dominant, their resistivity ranges, depth ranges.

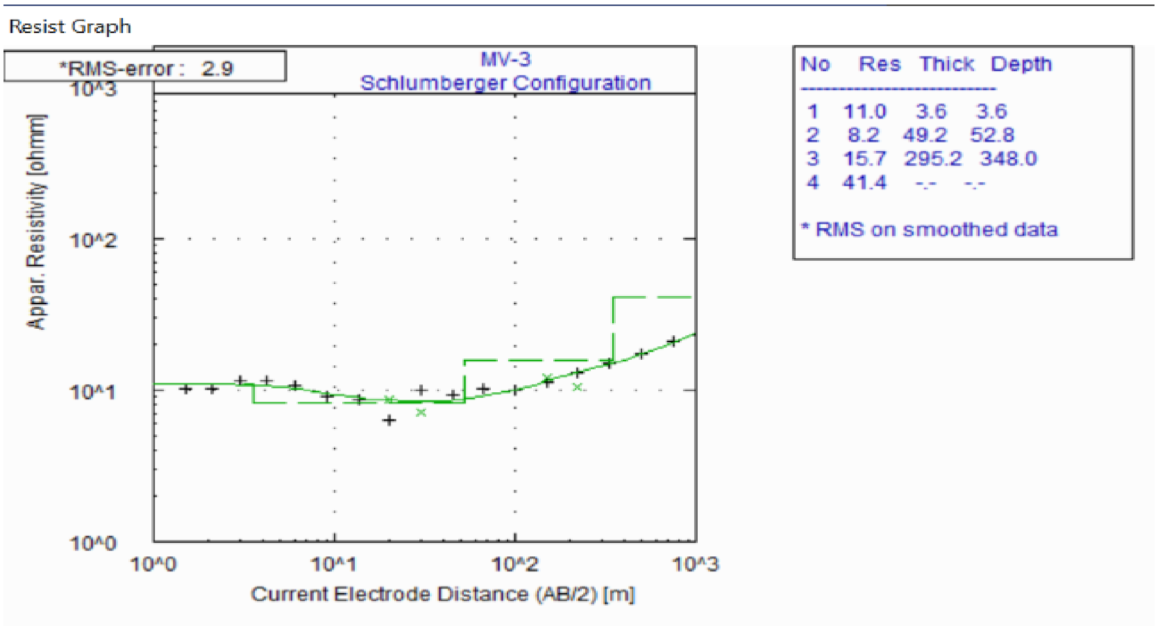

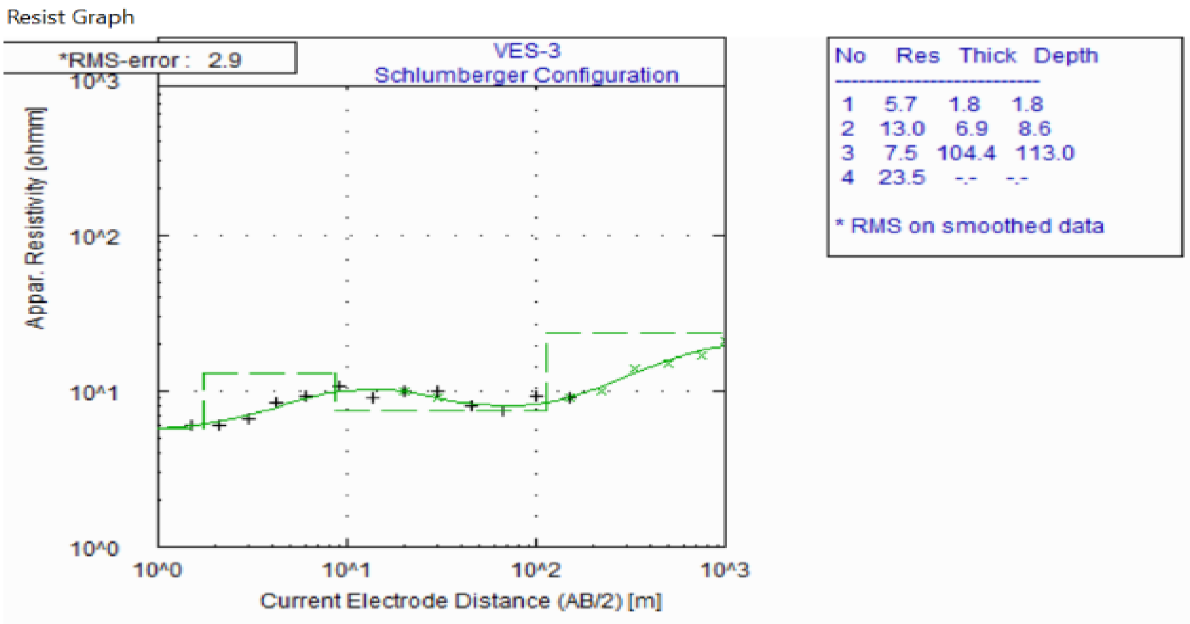

Figure 5.1: Interpreted sounding curves (VES)

Table 5.1 Interpreted sounding curves based on layer resistivity and layer thickness

VES	Layer Resistivity (Ω.m)	Layer thickness (m)	No of Layer	Resistivity Pattern	Carve type
`V-1	12.2,11.5,21.9,48.9	1, 9.2,99 ….	4	ρ1> ρ2< ρ3< ρ4	HA
V-2	10,17.9,32.2,36.9	1.4,14.8,188.2	4	ρ_1< ρ_2< ρ_3< ρ_4	AA
V-3	5.7,13,7.6,23.5	1.4,6.9,104.4	4	ρ_1> ρ_2< ρ_3> ρ_4	KH
V-4	5.6,5.7,15,22.5	4.4,14.4,260.6	4	ρ_1< ρ_2< ρ_3< ρ_4	AA
V-5	27.2,18.8,25.8,56.1	4,10.4,63.5	4	ρ1> ρ2< ρ3< ρ4	HA
V-6	16.6,8.7,34.1,55.6	5.6,28,101.2	4	ρ1> ρ2< ρ3< ρ4	HA
V-7	5.7,4.7,9.9,83.6	3.6,3.4,90.9	4	ρ1> ρ2< ρ3< ρ4	HA
V-8	6.4,14.5,14.8,38	1.7,20,185.1	4	ρ1< ρ2< ρ3< ρ4	AA
V-9	9.8,14.8,36,46	1.4,5.6,182	4	ρ1< ρ2< ρ3< ρ4	AA
V-10	6.4,18.4,26.8,70.3	1.6,8.4,343	4	ρ1< ρ2< ρ3< ρ4	AA
MV-6	14.8,10.1,24,63.9	5.4,15.7,43.8	4	ρ1> ρ2< ρ3< ρ4	HA
MV-7	26.2,32.4,40,45.5	6.4,32.7,85.1	4	ρ1< ρ2< ρ3< ρ4	AA
MV-8	5.4,14.2,14.8,18.3	1.2,48.4,210.2	4	ρ1< ρ2< ρ3< ρ4	AA
MV-9	13.2,11.9,15.3,29	5.7,43.9,101.9	4	ρ1> ρ2< ρ3< ρ4	HA
MV-10	5.1,15.3,11.4,30.8	0.8,5,259.3	4	ρ1> ρ2< ρ3>ρ4	KH
MV-1	27.5,5.9,7.4,51.2	4,151,389	4	ρ1> ρ2< ρ3< ρ4	HA
MV-2	6,5.4,11,38	5.1,45.7,458.3	4	ρ1> ρ2< ρ3< ρ4	HA
MV-3	11,8.2,15.7,41.4	3.6,49,259	4	ρ1> ρ2< ρ3< ρ4	HA
MV-4	13.8,5.5,9,59	2.7,127,348	4	ρ1> ρ2< ρ3< ρ4	HA
MV-5	7.7,2.4,26.6,44.6	6.4,18.3,337.6	4	ρ1> ρ2< ρ3< ρ4	HA

From the above table the dominant cave type is HA and AA

5.2.2 1D Inverse model correlation with lithology

In 1D inverse modeling, an iterative inversion process is employed to minimize the misfit between field curves and model curves, thereby deriving a representative resistivity versus depth model. Initially, a model is specified based on the desired number of layers, with resistivity values estimated for each layer using IPWIN software. Subsequently, the final model is inverted using Win Resist, with the root mean square (RMS) error measuring at 4.4%. In the VES 1D inverse modeling results, correlations were drawn for VES points where nearby boreholes (BH2) were available. These findings revealed a strong correlation between lithology and resistivity values in the geo electric sections depicted. The result shows the top layer from the well correlates with top soil, the second layer from the well correlates with clay sediments, the third layer from the well correlates with Alluvial sediments and the fourth layer from the well correlates with Bedrocks with their resistivity and lithology (Fig 5.2).

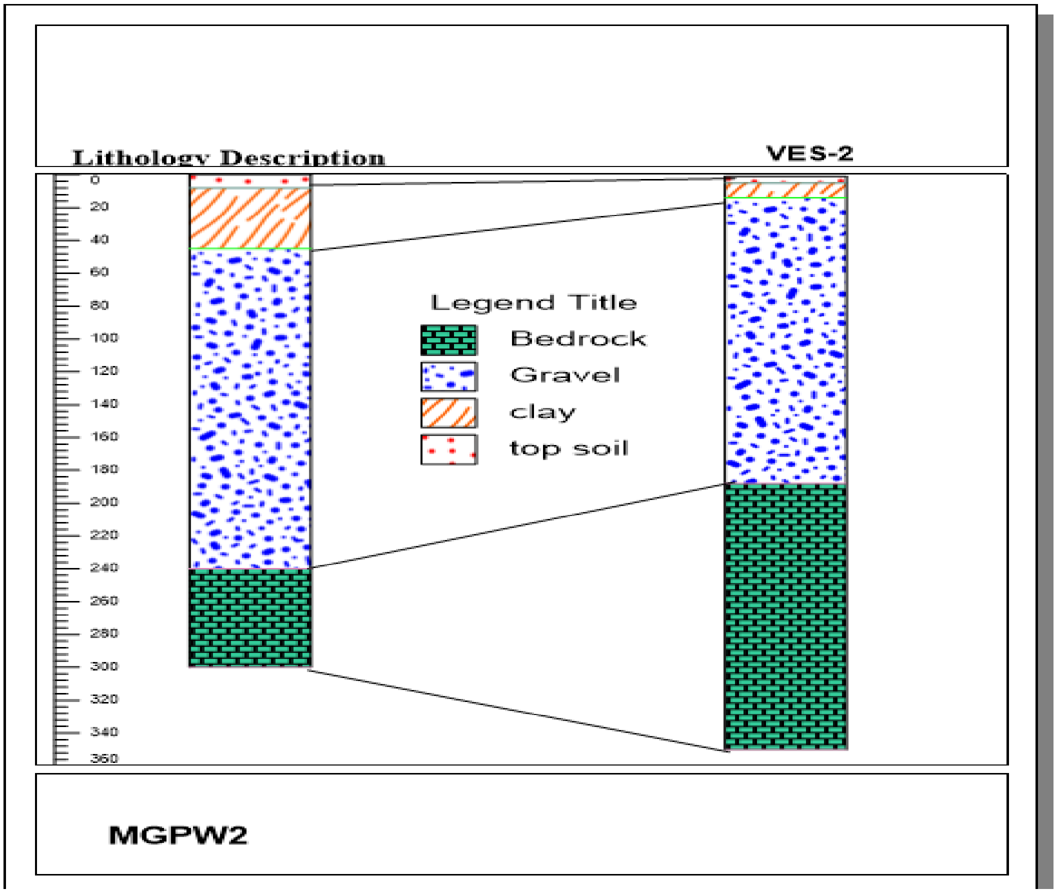

Figure 5.2 Correlation of lithology and resistivity's values

5.2.3 Sliced-stacked section

It is promising to create the Sliced-sectional pseudo-depth map (Fig 5.3) by overlaying the 2D Sliced-Stacked plan maps for the chosen AB/2 values of 1.5, 100, 330, 500 and 1000. To qualitatively evaluate the electrical properties of the geological medium, all VES points are used. The sounding points are believed to provide a fairly accurate overall picture of the soil because they are almost evenly distributed.

5.2.3.1 Sliced-stacked for different AB/2

The visualization and analysis of resistivity data along multiple electrode configurations in geophysical surveys, particularly electrical resistivity measurements using the Schlumberger configuration, is stated as in (Fig 5.3) sliced-stacked for different AB/2 involves dividing resistivity data along the survey profile into vertical slices or sections that are stacked horizontally to allow thorough visualization and interpretation.

Accepting of hydrogeological features, aquifers and structural components of the study area is supported by the ability to perform variation analysis, depth profiles and interpretation of resistivity variations. The separation between the electrodes which are potential and current, is indicated by the value AB/2. This method allows geologists to map underground structures, assess groundwater potential at various depths, analyze the distribution of geo-electric units, and identify potential aquifers. The stacked target cards for AB/2=1.5, 100, 330, 500 and 1000 meters are shown in (Fig 5.2). The changeability b/n them and the desire to display the sideways of resistivity fluctuations at diverse pseudo depths influence the choice of such a distance. In particular, the map illustrates between the current electrode spacing, the apparent resistivity of the entire region varies at different depths in a vertical and lateral direction.

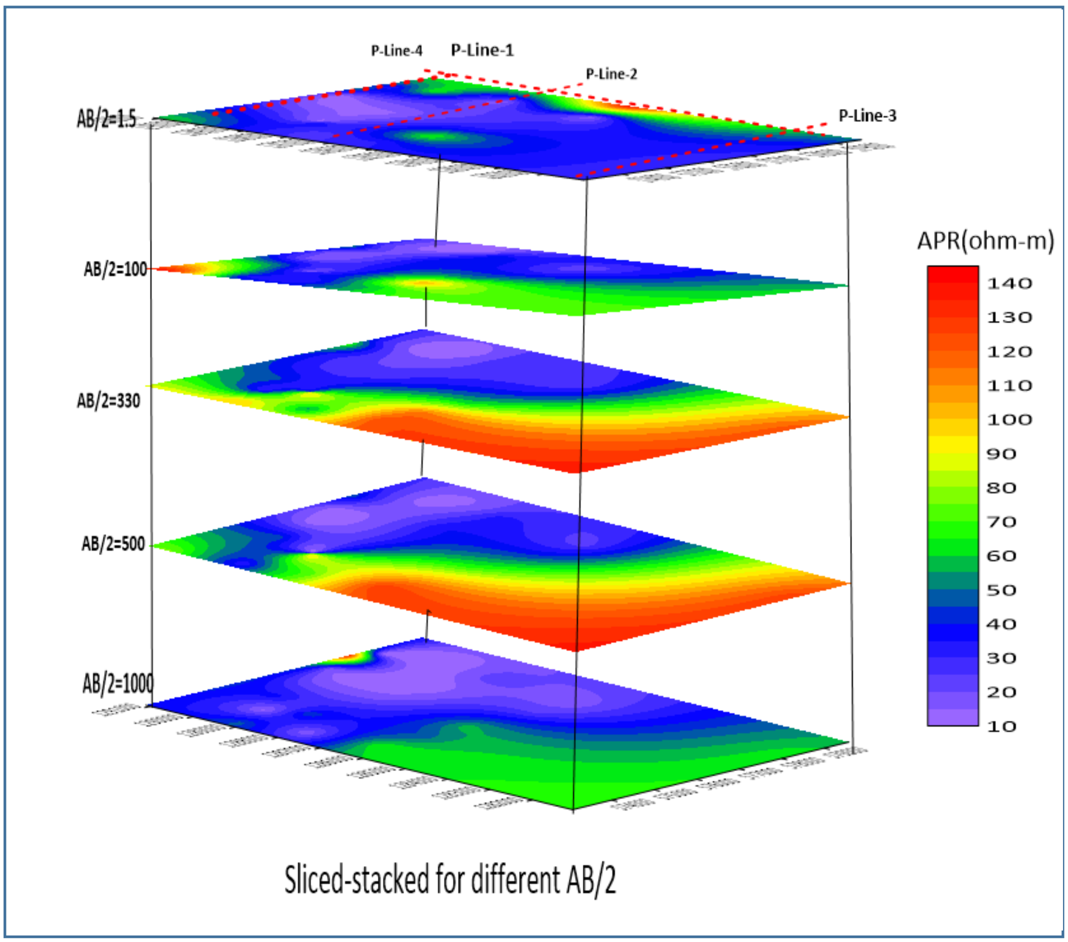

Figure 5.3: Sliced-stacked for different AB/2

5.2.4 Pseudo depth section and Geo-electric Section of all Profiles

Utilizing the 20 VES, Pseudo depth and geo-electric sections plotted along the profile lines one to four lines are made by Surfer 20 software on average each VES point distance is within 0.6 km and the total distance of all VES 40 km^2 out of 503 km^2 is used to represent the area. In the descriptions on every line, VES is present and its UTM location is specified in (Tab 4.1)

5.3.2 Pseudo depth section and geo-electric section of the profiles one

A. Pseudo depth section of traverse Line one

Profile 1 is constructed from VES-1, 2, 3, 4 and 5 with an east-west azimuth. It has a total length of 6000m plotted as a function of AB/2 to 1000m. The resistivity along this profile range between 5-135 ohm-m and from the pseudo-depth section shown in (Fig 5.4), it can be seen that almost all the section has resistivity values below 45 ohm-m; at the location of VES- 3 and VES-4 the range of resistivity goes below 25 ohm-m. The highest resistivity value of 135 ohm-m is measured under VES-5 and the vertical nature of the contact may be attributed to faulting.

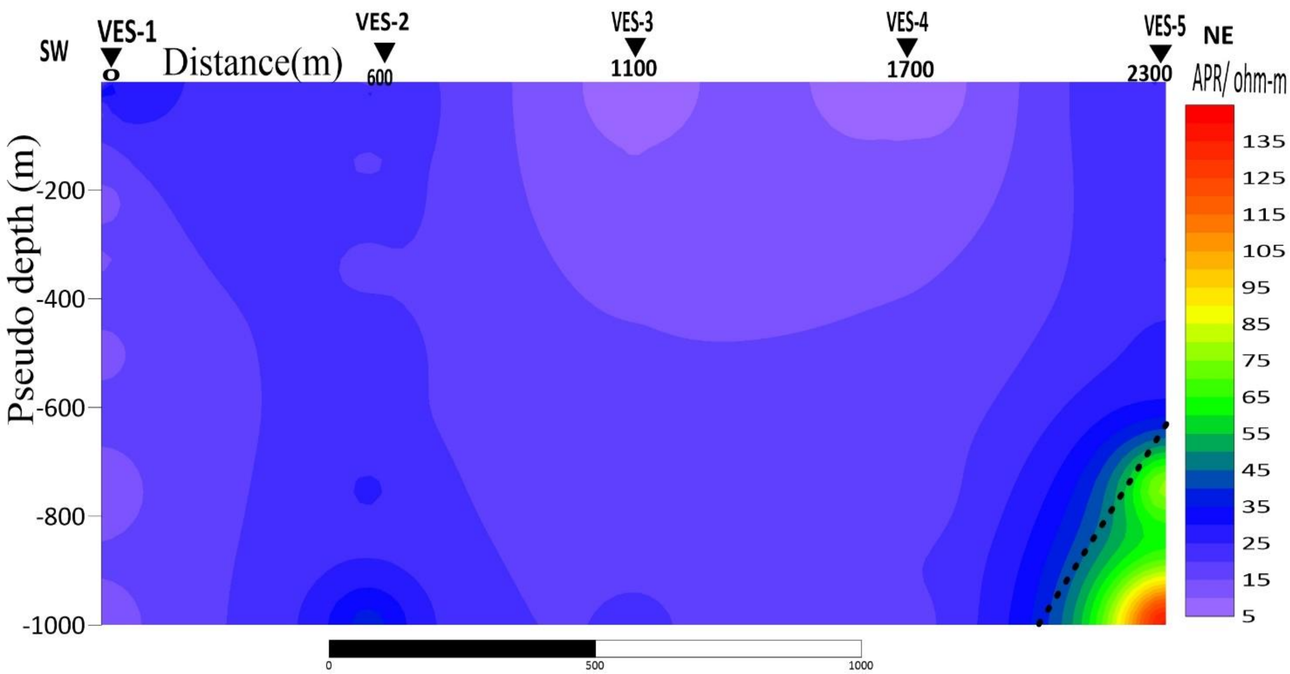

Figure 5.4: Apparent resistivity pseudo depth section along traverse Line one

A. Geo electric section along traverse Line one

Geo electric section was constructed in (Fig 5.5) using the interpreted layer characteristics identified from the five VES locations along this trip. The depth and lithological units beneath these VES locations were determined throughout the modeling procedure were determined using a drill hole designated BHP2 (574158, 1290510 UTM) located near Profile-1, specifically between VES-2 and VES-3. To create a comprehensive geo-electric section, the lithological descriptions from the borehole depth section (in Appendix 2A) were used along with resistivity constraints obtained from each stated VES point. The near-surface geo-electric layer has fluctuating resistivity within approximately 3 to 60 ohm-m. The top layer involved of dry topsoil, which has a relatively high resistivity compared to the underlying clay sediment layer and varies in thickness between 1 and 4.4 meters. The second layer was clay sediment with the resistivity values fluctuating from 5 to 12 ohm-m, through thickness variations ranging from 6 to 15 meters.

The third layer, interpreted as sand dominated, has an average thickness variation of 100 to 300 meters with 13 to 35 ohm-m resistivity and the effects of geological structure or weak zone shows are NW-SE direction in (Fig 5.5) and it is the Main aquifer of the sections. The fourth layer was beneath bedrock identified by resistivity of 40-60 ohm-m and infinite thickness, indicating its presence at all VES points.

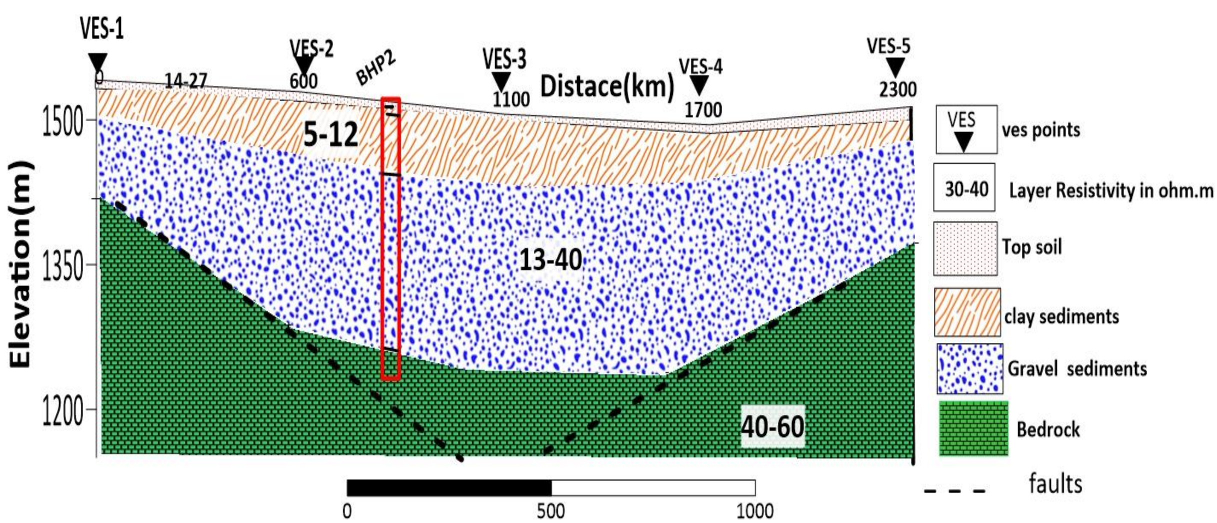

Figure 5. 5: Geo-electric section along traverse Line one

5.3.3 Pseudo depth section and geo-electric section of the profiles traverse line two

The traverse line two oriented on NE-SW direction that measures over all distance of 5.40 km. This line involves of five VES points that were situated within a typical VES point average distance was1.08 km.

A. Pseudo depth section of profile two

Profile 2 is constructed from VES-6, 7, 8, 9 and 10 with an east -west azimuth. It has a total length of 5400 m. and is plotted as a function of AB/2 to 1000m. The resistivity along this profile range between 4- 48 ohm-m and from the pseudo-depth section shown in (Fig 5.6), it can be seen that almost all the section has resistivity values below 35 ohm-m; at the location of VES- 8 and VES-9 the range of resistivity goes below 15 ohm-m. The highest resistivity value of 48 ohm-m is measured under VES-6 and the vertical nature of the contact may be attributed to faulting.

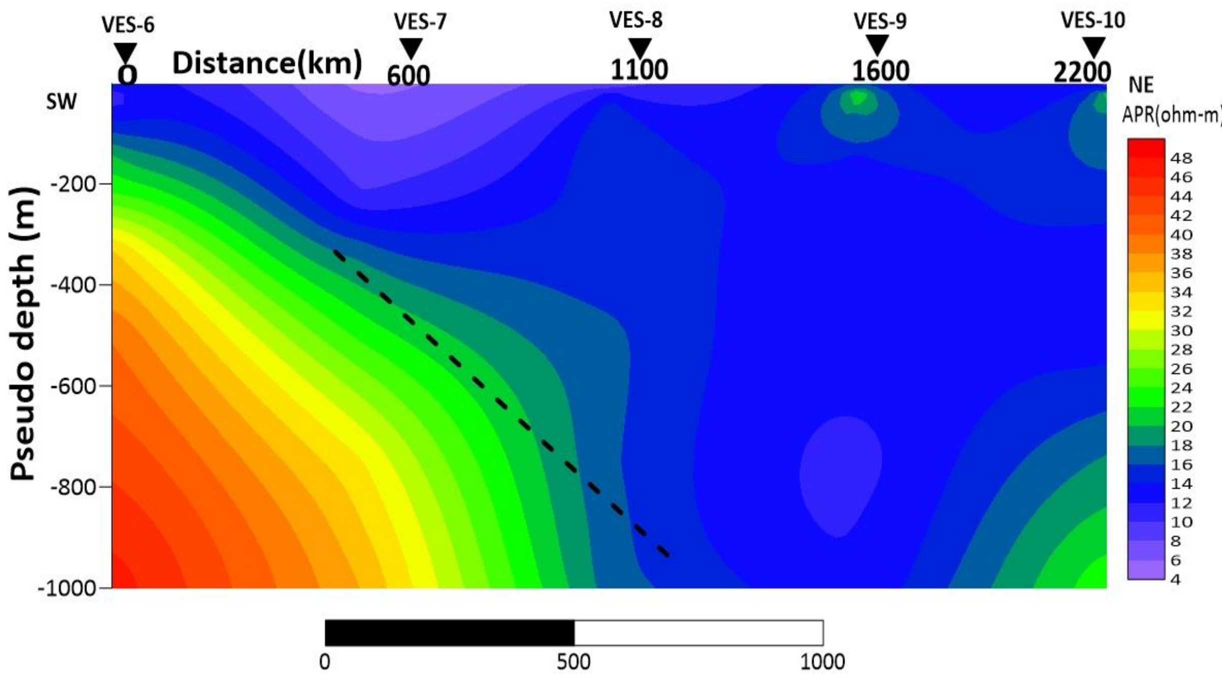

Figure 5.6: Pseudo depth sections along traverse line two

B. Geo-electric section

The geoelectric section along profile line two (VES-6 to VES-10), extending from UTM coordinates 574132 mE, 1289447 mN to 578211 mE, 1287217 mN, extends for approximately 6000 km and shows the presence of four main geoelectric layers (Fig 5.7). Using the interpreted layer parameters obtained from the five VES points adjacent to the traverse, a geoelectric section was developed as shown in (Fig 5.7). During the modeling process, depth conditions and lithological units were determined beneath these VES locations using a well named BH2 (576148, 1288640 UTM), located near profile two, specifically between VES-7 and VES-8.

To create a comprehensive geoelectric section, the lithological descriptions from the borehole depth section (see Appendix 2B) were included along with their respective resistivity parameters from each explained VES. The near-surface geoelectric layer had a varying resistivity ranging from about 4 to 70 ohm-m. The top layer consisted of dry topsoil with a relatively high resistivity value compared to the underlying clay sediment layer and a thickness of between 1.5 and 6 meters. Beneath the topsoil, a thick clay sediment layer was identified throughout the VES of the section, extending between VES-5 and VES-10 and characterized by resistivity values between 4 and 15 ohm-m. The clay sediment layer varied in thickness from 5 to 48 meters, probably due to alluvial deposition of sand, clay and silt. The third layer, interpreted as sand dominated, had resistivity values ranging from 15 to 40 ohm-m, with varying thicknesses observed at the VES points. Notably, the thicknesses ranged from 65 to 343 meters, reflecting the spatial variability of sediment deposition and the effects of the geological structure or weak zone in the NW-SE direction (Fig 5.7). The aquifer zone of the section is identified by alluvial sediments (gravel sediments). A fourth layer, identified as bedrock, had resistivity values of 41 to 66 ohm-m with infinite thicknesses varying from VES-6 to VES-10, indicating changing lithological features throughout the section.

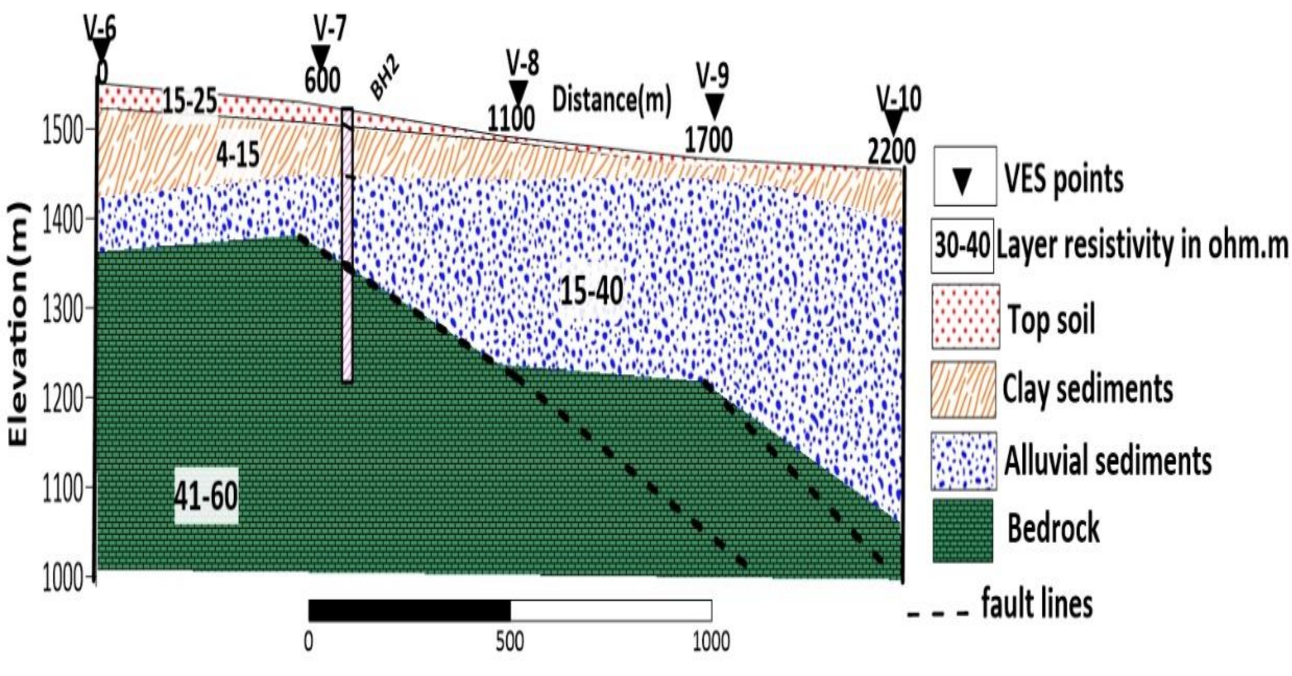

Figure 5.7: Geo-electric section along traverse Line two

5.3.4 Pseudo depth and geo-electric section along profiles three

This line, which extends for 5 km and is oriented northwest to southeast in (Fig 5.8), is distinguished by five VES points: MVES-6, MVES-7, MVES-8, MVES-9 and MVES-10. The average distance between the individual VES locations is almost exactly 0.934 kilometers.

A. Pseudo depth section along traverse line three

Profile 3 is constructed from MVES-6, 7, 8, 9 and 10 with an east – west azimuth. It has a total length of 5000 m. and is plotted as a function of AB/2 to 1000m. The resistivity along this profile range between 6- 66 ohm-m and from the pseudo-depth section shown in (Fig 5.8), it can be seen that almost all the section has resistivity values below 35 ohm-m; at the location of MVES- 9 and MVES-10 the range of resistivity goes below 22 ohm-m. The highest resistivity value of 66 ohm-m is measured under MVES-6 and MVES-7 and the vertical nature of the contact may be attributed to faulting.

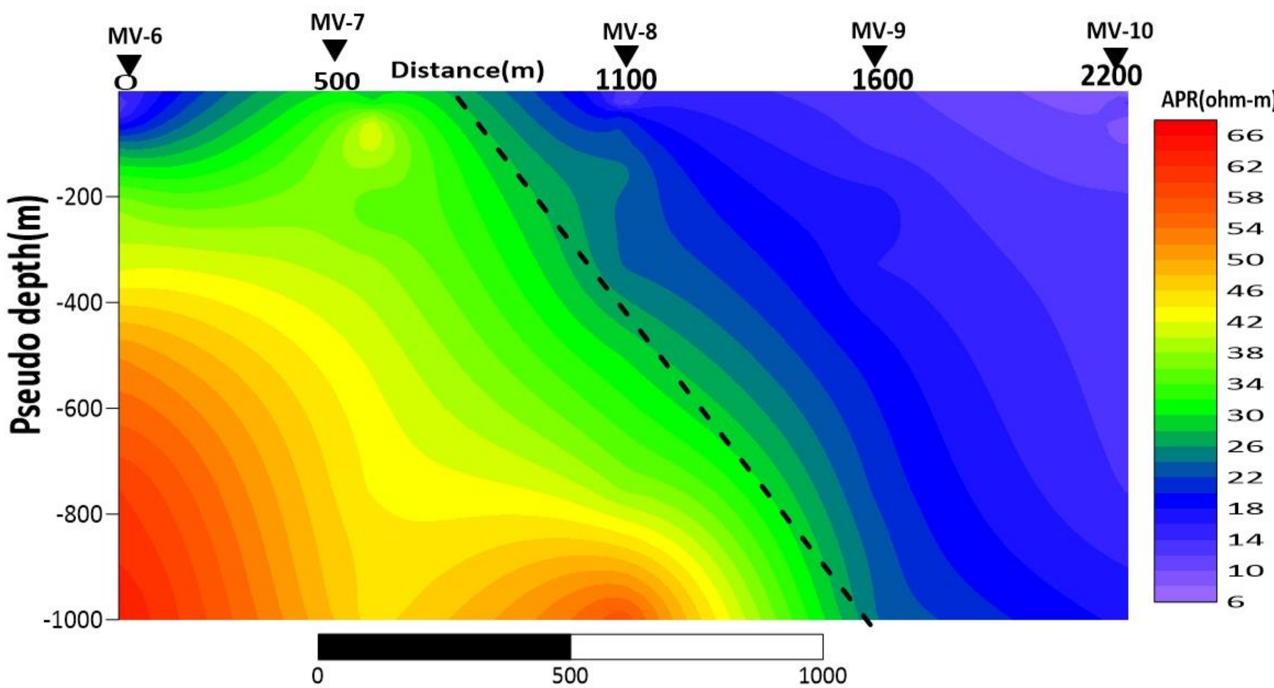

Figure 5.8: Apparent resistivity pseudo depth section along traverse Line three

A. Geo-electric section along traverse Line three

The geoelectric section along profile line three (MVES-6 to MVES-10) extends a distance of approximately 5 kilometers from UTM coordinates 574835 mE, 1286378 mN to 578256 mE, 1286019 mN and shows the presence of four distinct geoelectric layers (Fig 5.9). A comprehensive geoelectric section was constructed using five VES locations along the interpreted layer parameters of this traverse, as shown in (Fig 5.9). The depth and lithologic units beneath these VES points were determined from a drill hole named BH1 (576148, 1288640 UTM), which is located near profile two but some distance from MVES-8. To briefly summarize, the resulting geoelectric section (Fig 5.9) included data from the borehole depth unit lithology report (in Appendix 2B) as well as resistivity parameters from each resolved VES. The near-surface geoelectric layer had a resistivity that varied between about 6 and 70 ohm-m. The top layer is described by dry topsoil and had a higher resistance value compared to the underlying clay layer, with thickness variations ranging between 1 and 6 meters. And the second layer, a clay-sediment layer characterized by resistivity values of 7 to 15 ohm-m, was identified beneath the topsoil. This clay sediment layer had an average thickness of about 43 meters. The third layer, interpreted as sand dominated, had resistivity values varying between 15 and 32 ohm-m, with varying thicknesses observed throughout the section: 43 to 259 meters. This indicates an alluvial cover of sand, clay and silt and possibly the largest aquifer area as well as the effects of the geological structure or weak zone shown in the NW-SE direction in (Fig 5.9). A fourth layer was then identified, which was due to bedrock and had resistivity values of 40 to 68 ohm-m. The infinite thickness provides insight into the geologic composition and resistivity distribution along profile line three.

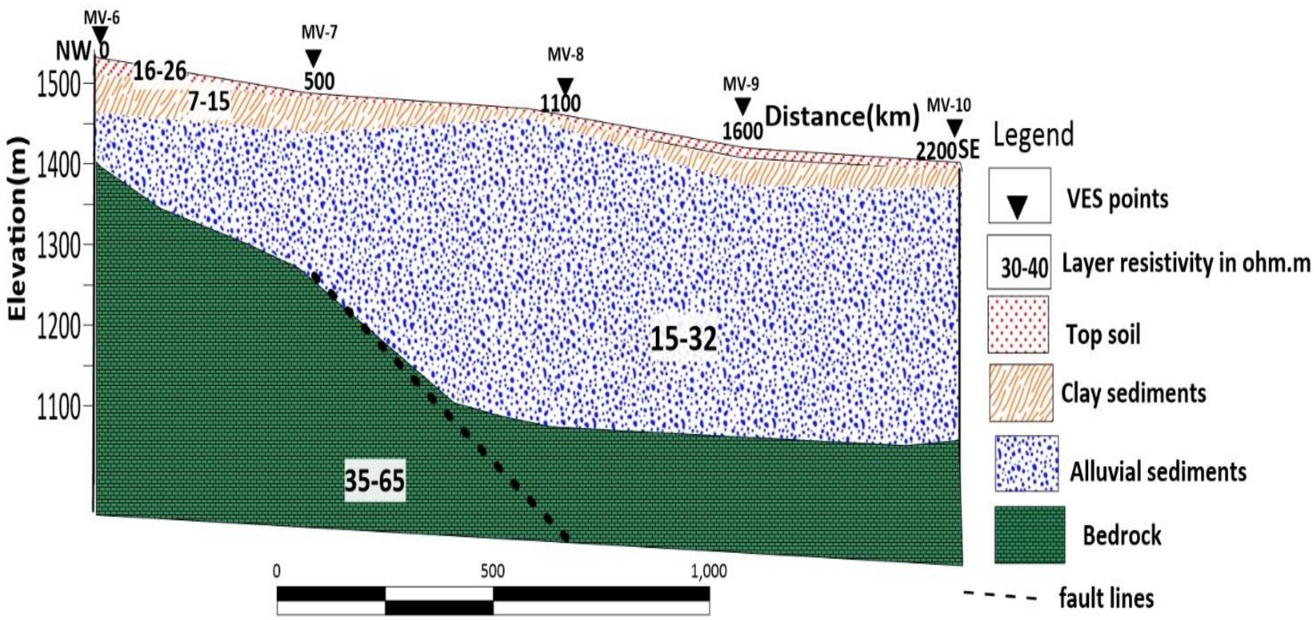

Figure 5.9: Geo-electric section along traverse Line three

5.3.5 Pseudo depth section and geo-electric section of the profiles line four

The direction of this line is from southwest to northeast, is about 5.81 kilometers long and has five VES points: MVES-1, MVES-2, MVES-3, MVES-4 and MVES-5. On average there are almost exactly 0.962 kilometers between the individual VES locations.

A. Pseudo depth section along Line four

Profile 4 is constructed from MVES-1, 2, 3, 4 and 5 with north – south azimuth. It has a total length of 5.81m.and is plotted as a function of AB/2 to 1000m. The resistivity along this profile range between 5-68 ohm-m and from the pseudo-depth section shown in (Fig 5.10), it can be seen that almost all the section has resistivity values below 45 ohm-m; at the location of MVES- 3 and MVES-4 the range of resistivity goes below 20 ohm-m. The highest resistivity value of 64 ohm-m is measured under MVES-5 and the vertical nature of the contact may be attributed to faulting.

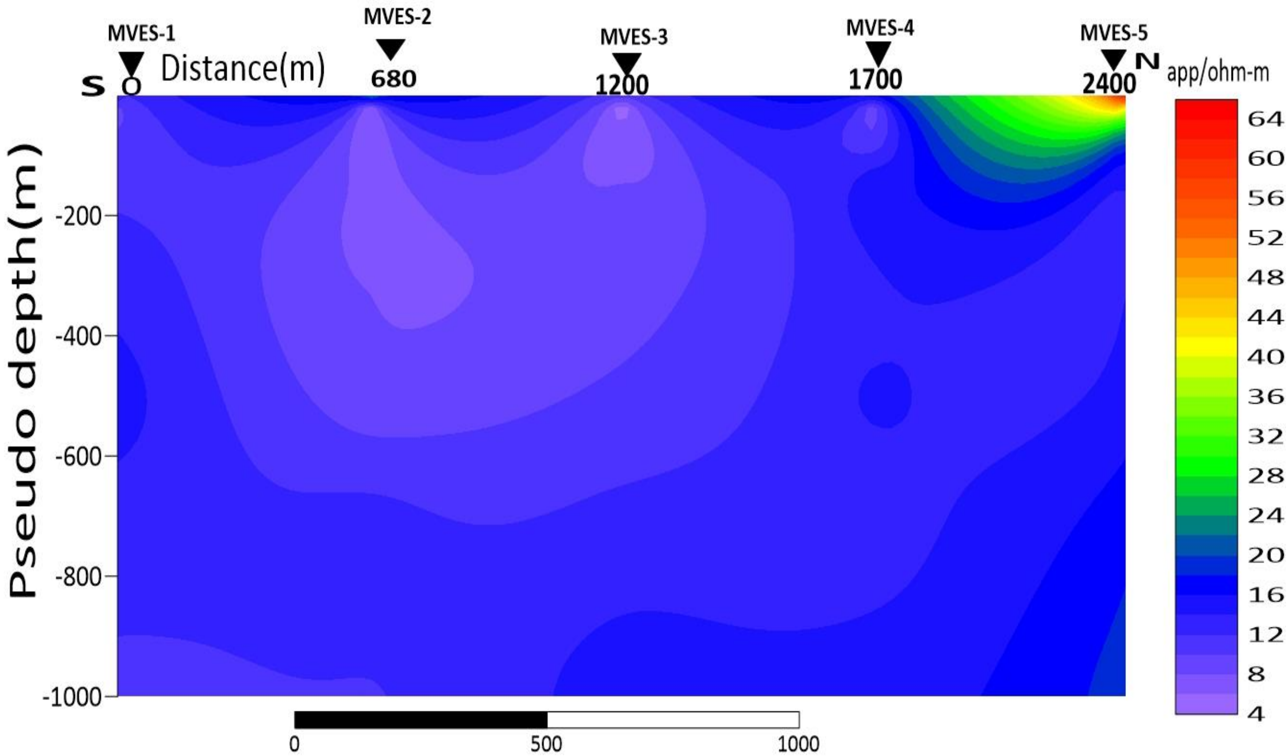

Figure 5. 10: Pseudo depth sections along traverse Line four

B. Geo electric section along traverse line four

The geoelectric section along profile four from MVES-1 to MVES-5 covers a distance of approximately 5.81 kilometers and extends from UTM coordinates 578320 mE, 1290789 mN to 579582 mE, 1286466 mN, indicating the presence of four different geoelectric layers revealed (Fig. 5.11). The identified layers and their properties are summarized as follows: The geoelectric section result (Fig 5.11) includes data from lithological well descriptions (Appendix 2B) and resistivity parameters obtained from each resolved vertical electrical sounding (VES). The near-surface layer had a resistivity in the range of 6 to 27 ohm-m, with the dry topsoil being characterized by a higher resistivity compared to the underlying clay layer and the thickness varying between 2 and 6.4 m. The second layer, identified as clay sediment, had resistivity values varying between 2 and 9 ohm-m, with an average thickness of 28 to 151 meters. Below this, the third layer, identified as sand dominated, had resistivity values varying between 11 and 40 ohm-m, with thickness varying between 295 and 458 meters. This layer may indicate a significant aquifer area covered by clayey sediments. The effects of geological structures or weak zones oriented in a north-south direction can be seen on both sides of the study area. In addition, the fourth layer, which corresponds to the bedrock, is categorized by resistivity values between 40 and 60 ohm-m and an infinite thickness. This layer provides insight into the geologic composition and resistivity distribution along sketch line four.

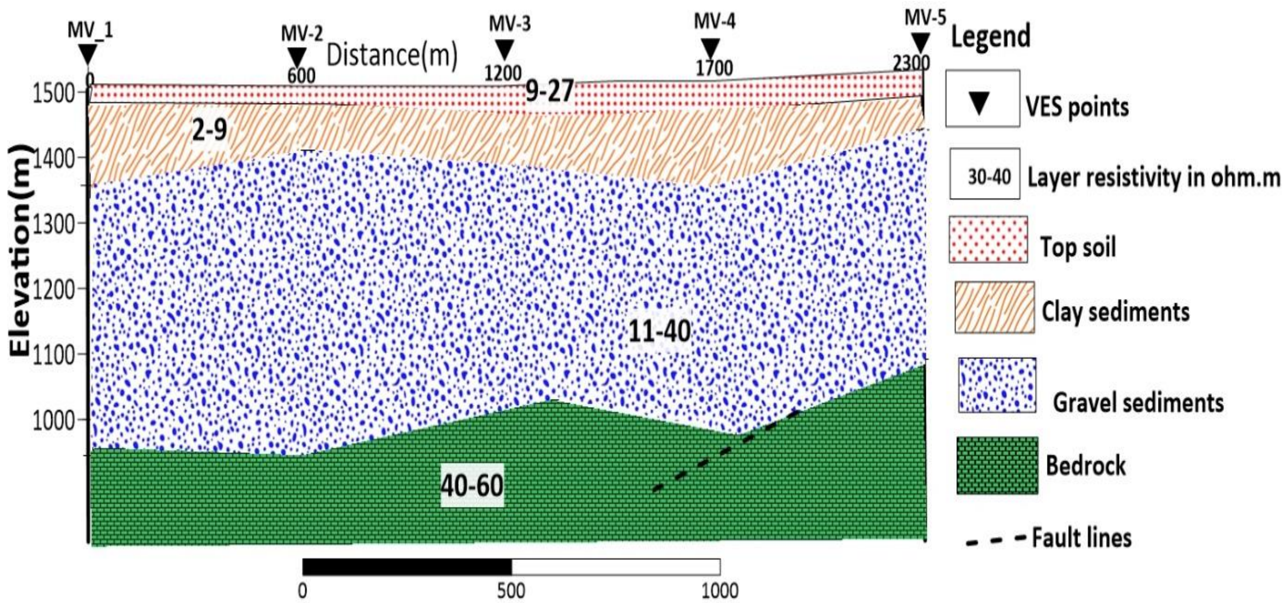

Figure 5.11: Geo-electric section along traverse Line four.

5.4 Results and discussions of aquifer parameters

Aquifer characterization assesses physical, hydraulic, and geological characteristics determining water storage and transmission capabilities (Sylvia et al., 2022). But the estimation of transmissivity and hydraulic conductivity using conventional method is time consuming and cost. Therefore, by integrating the vertical electrical sounding data and some reference pumping test data, the regression equation established. In order to integrate a geophysical data with pumping test data, the VES parameter like thickness, depth from surface and resistivity of each layer are very crucial (Babatunde et al., 2021). Using the regression equation the hydraulic conductivity and transmissivity of each VES point were estimated (tab 5.2). In this study to construct the regression equation, the five borehole data and the five VES those are measure near to wells were used (tab 5.3).

Table 5.2 pumping test data and VES parameters in study area.

VES	Well Name	Total Thickness (m)	Total Transfers Resistance	Well Log Transmissivity	Estimated Transmissivity (m^2/d)	Well Log Hydraulic Conductivity	Estimated Hydraulic Conductiv
V2	MGPW2	231.2	4276.7	263.87	238.1942	2.6	1.030252
V8	MGTW2	482.1	14571	1021.72	818.7899	1.39	1.698382
MV7	MT3	109.1	746.24	32.06	39.07344	0.314	0.358143
MV3	MGPW1	419.3	5962.5	389.78	333.2722	1.22	0.79483
MV5	MT1	450	15150	921.72	851.4545	2.01	1.892121

From the above (tab 5.2) this typically involves fitting a line or curve to the data points to find the relationship between transverse unit resistance and transmissivity. The regression equation can be of the form $T=a \cdot T_R-b$, where a, and b are the regression coefficients. As X-axis: Plot the transverse unit resistance (T_R) for each well and Y-Axis: Plot the estimated transmissivity (T) for each well.

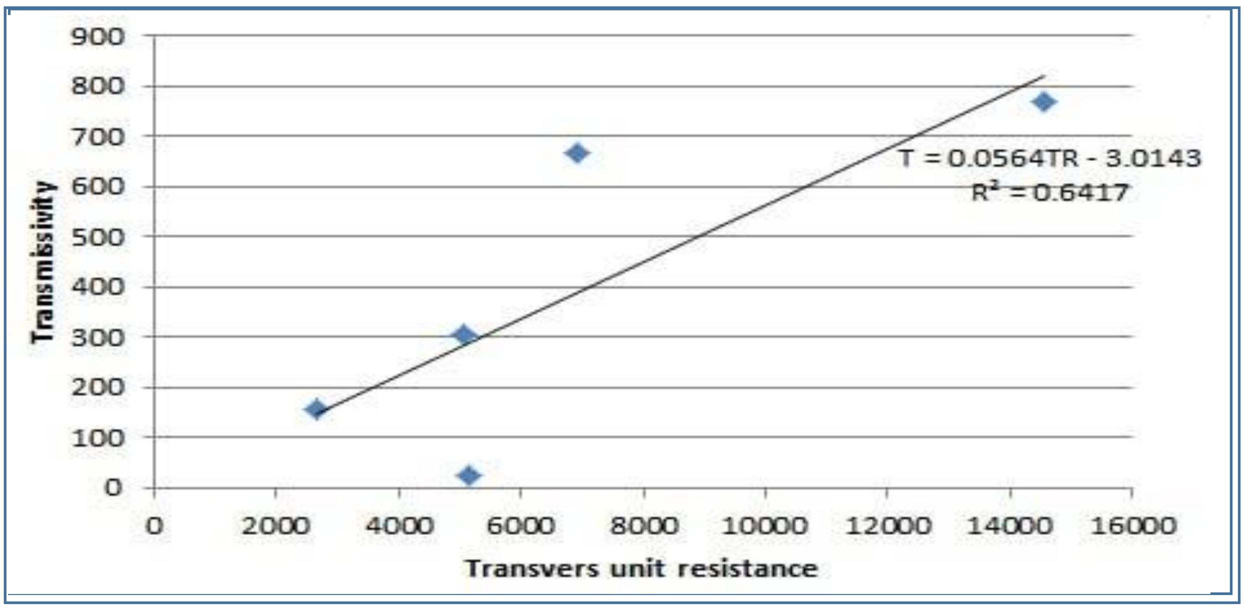

Figure 5.12: Relationship between Transmissivity and Transverse Resistance.

5.4.1 Aquifer parameters (Transmissivity, Hydraulic Conductivity)

In order to show the variation of hydraulic conductivity and transmissivity of the study area, the contour map were made. According to the result, the estimated hydraulic conductivity and transmissivity values are notably high in the central and eastern region of the research area.

Conversely, the northeaster and southwestern sections show lower values (Fig 5.13 and 5.14). This suggests that the southern part of the research area holds promising potential for supplying a significant amount of groundwater to wells. According to Türk et al (2021), Aquifers can be classified based on Transmissivity values, with transmissivity values greater than 500 m²/day are considered to have high productivity. Those with values between 50 and 500 m²/day are classified as having moderate productivity. Aquifers with transmissivity values between 5 and 50 m²/day are categorized as low productivity, and those with values between 0.5 and 5 m²/day are considered very low productivity. In the research area, it was found that 35% of the aquifers exhibit high productivity, while 65% of the aquifers demonstrate moderate productivity (Fig 5.14).

Table 5.3: transmissivity, hydraulic conductivity and longitudinal conductance

VES	Total Thickness	Total transfers resistance	Well log transmissivity	Estimated Transmissivity(m^2/d)	Well log Hydraulic Conductivity	Estimated Hydraulic Conductivity
`V-1	186.7	2649.09		146.39		0.7841
V-2	231.2	4276.75		282.94		1.2238
V-3	298.2	10211.87	363.87	398.19	1.66	1.3353
V-4	194.9	2771.2		353.28		1.8126
V-5	164.5	2208		221.52		1.3466
V-6	64.9	1286.99	93.72	63.79	1.39	0.9829
V-7	124.2	4242.73		106.28		0.8557
V-8	482.1	14571		813.57		1.6876
V-9	151.5	2226.93		302.58		1.9973
V-10	265.1	3036.6		268.25		1.0119
MV-6	162.8	5059.38	121.72	123.45	1.01	0.7583
MV-7	109.1	746.24		87.56		0.8026
MV-8	252.1	4600.06		297.85		1.1815
MV-9	238.7	3561.39	302.06	305.07	0.914	1.2781
MV-10	410.8	5131.68		496.41		1.2084
MV-1	414.9	6936.43	389.78	488.20	1.22	1.1767
MV-2	509.3	5046.54		581.61		1.1420
MV-3	419.3	5962.53		833.27		1.9873
MV-4	439.6	4180.77		732.78		1.6669
MV-5	450	15150.16		482.33		1.0719

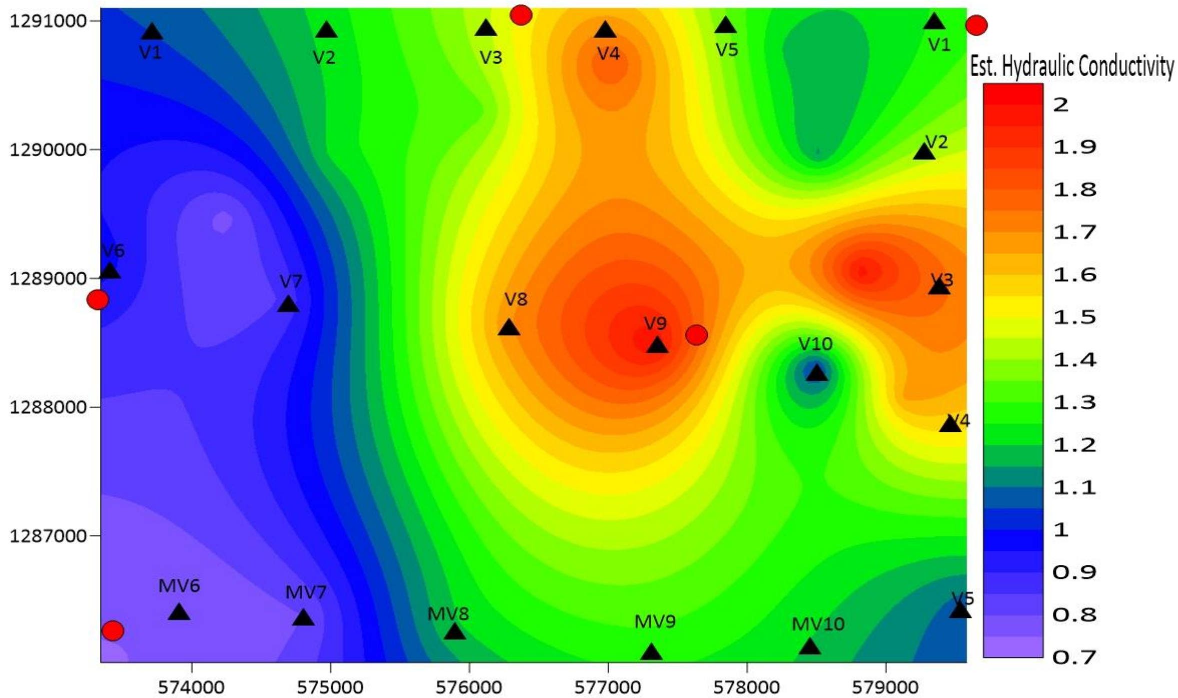

Figure 5.13: estimated hydraulic conductivity

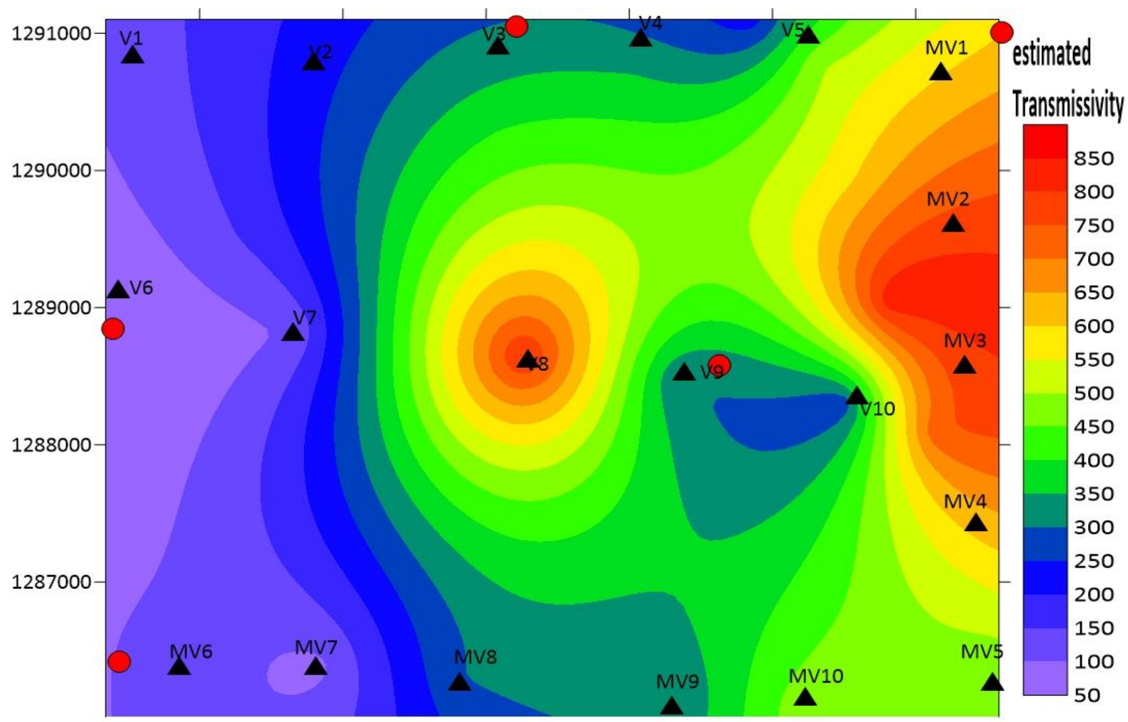

Figure 5.14: Transmissivity distribution in the study area.

5.4.2 Correlationof aquifer parameters.

Correlation of aquifer parameters refers to the statistical relationship between different characteristics or properties of an aquifer system. Aquifer parameters may include hydraulic conductivity (K) and permeability

Table 5.4: Correlation of pumped and the estimated transmissivity

VES points	Well Name	Pumped T(m^2/day)	Estimated T'(m^2/day)
VES-3	BH-3	398.2	363.8
VES-6	BH-4	93.7	63.79
MVES-1	BH-5	123.45	121.7
MVES-9	BH-6	305	302.06
MVES-6	BH-7	488	389.8

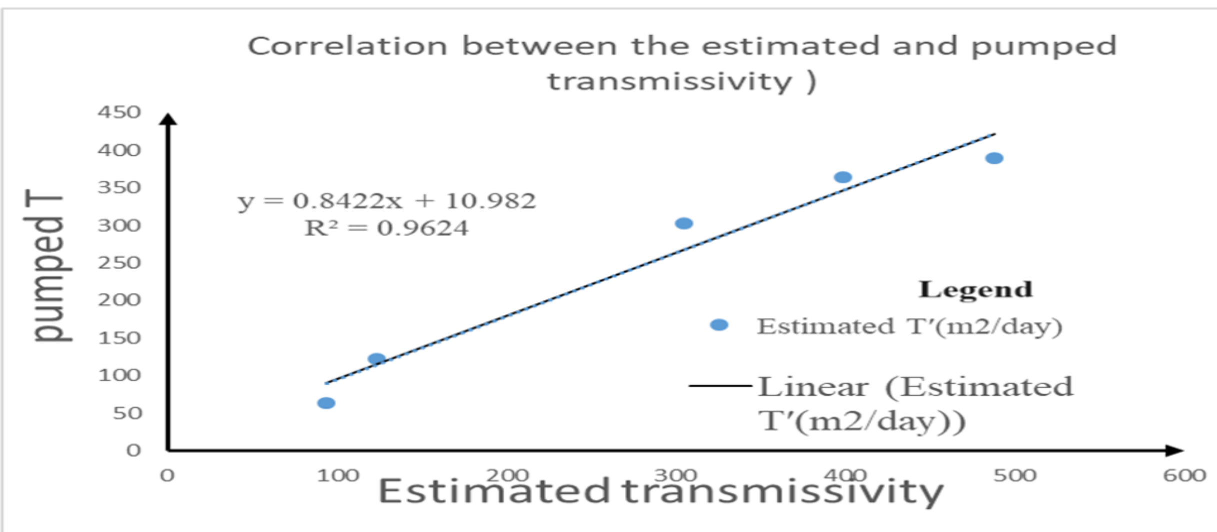

Figure 5.15: Correlation between estimated and pumped transmissivity

By using the linear relation y=0.8422x+10.982 formula from the VES points with the well data Pumped T, Estimated T'. The correlation coefficient of 0.97 indicates a strong positive linear relationship between the estimated and pumped transmittance values. This means that as one variable increases, the other tends to increase proportionally. The high correlation coefficient indicates a strong relationship between the estimated and actual transmission measurements carried out in the study area. This result underlines the reliability of the estimation methods used, as they correspond closely to the values obtained through direct pumping tests.

Table 5.5: correlation of pumped and the estimated Transmissivity

VES POINTS	Well name	pumped T(m/day)	estimated T′(m/day)
VES-3	BH-3	1.66	1.33
VES-6	BH-4	1.39	0.99
MVES-1	BH-5	1.01	0.76
MVES-9	BH-6	1.32	1.28
MVES-6	BH-7	1.22	1.18

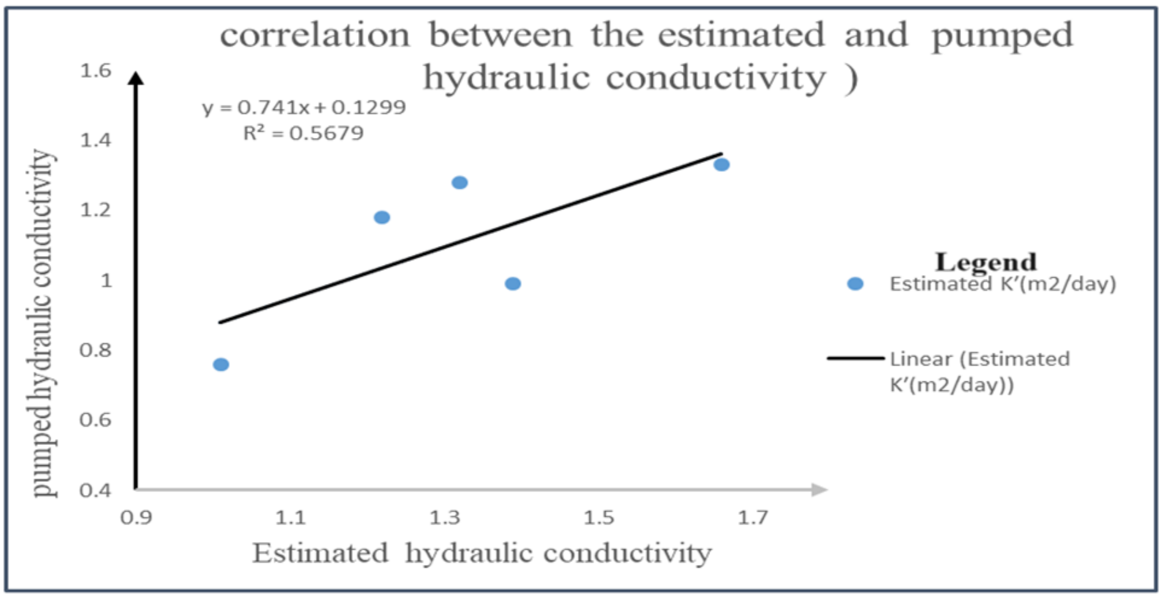

Figure 5.16: correlation between estimated and pumped hydraulic conductivity

A correlation coefficient (r) of pumped and estimated hydraulic conductivity is 0.573591. This correlation indicates a moderate positive correlation between pumped and estimated hydraulic conductivity. This means that there is a tendency for the variables to move in the same direction: as one variable increases, the other tends to increase as well, although not in a perfectly consistent manner. The positive sign of the correlation coefficient confirms this positive relationship, highlighting that higher values of one variable are generally associated with higher values of the other variable

.5.5 Interpretations of Magnetics Data

5.5.1 General

Interpretation of magnetic data involves identifying and characterizing magnetic anomalies in field surveys to infer subsurface geological structures and properties (Salawu et al., 2019). This includes depth estimation, source characterization, structural mapping and correlation with geology. Anomalies represent changes in the magnetic field of Earth brought on by subsurface geological features, while depth estimation helps estimate the depth of magnetic sources. Understanding these structures aids in geologic mapping and resource exploration. The study processed magnetic anomalies after accounting for noise and surface features, applying diurnal and IGRF correction, to analyze the data using Geo-soft v 8.4.2. Conversions such as RTE and tilt angle derivative improved the interpretation, anomaly maps that depict differences in the susceptibility, magnetization direction, and remanence of the basement rocks are briefly discussed and examined individually.

5.5.2 Total Magnetic Field Anomaly (TMA) map

The total magnetic anomaly of the region has been calculated by subtracting IGRF from the total magnetic intensity. The IGRF value for the area was obtained from the IGRF model (13th Generation). In this study, the Total Magnetic Anomaly map was generated following the exclusion of diurnal variation and IGRF or main field influences from field-collected data. The Total Magnetic Field Anomaly (TMA) map is a representation of the total intensity magnetic anomalies across a study area. The calculated value of TMA is plotted on a map to visualize difference in the Earth's magnetic field over the surveyed area. Contour lines or color gradients are commonly used to represent different levels of magnetic anomaly intensity, with anomalies typically categorized as positive (high) or negative (low) relative to the regional magnetic field (Hilemichaeil et al., 2024). Total magnetic field anomaly maps are interpreted to identify and delineate magnetic anomalies of geological significance. Positive anomalies indicate the presence of geological structures with enhanced magnetization, such as sediment, faults, or igneous intrusions. Negative anomalies suggest areas where non-magnetic materials dominate, such as low magnetic anomaly on the other hand high magnetic susceptibilities.

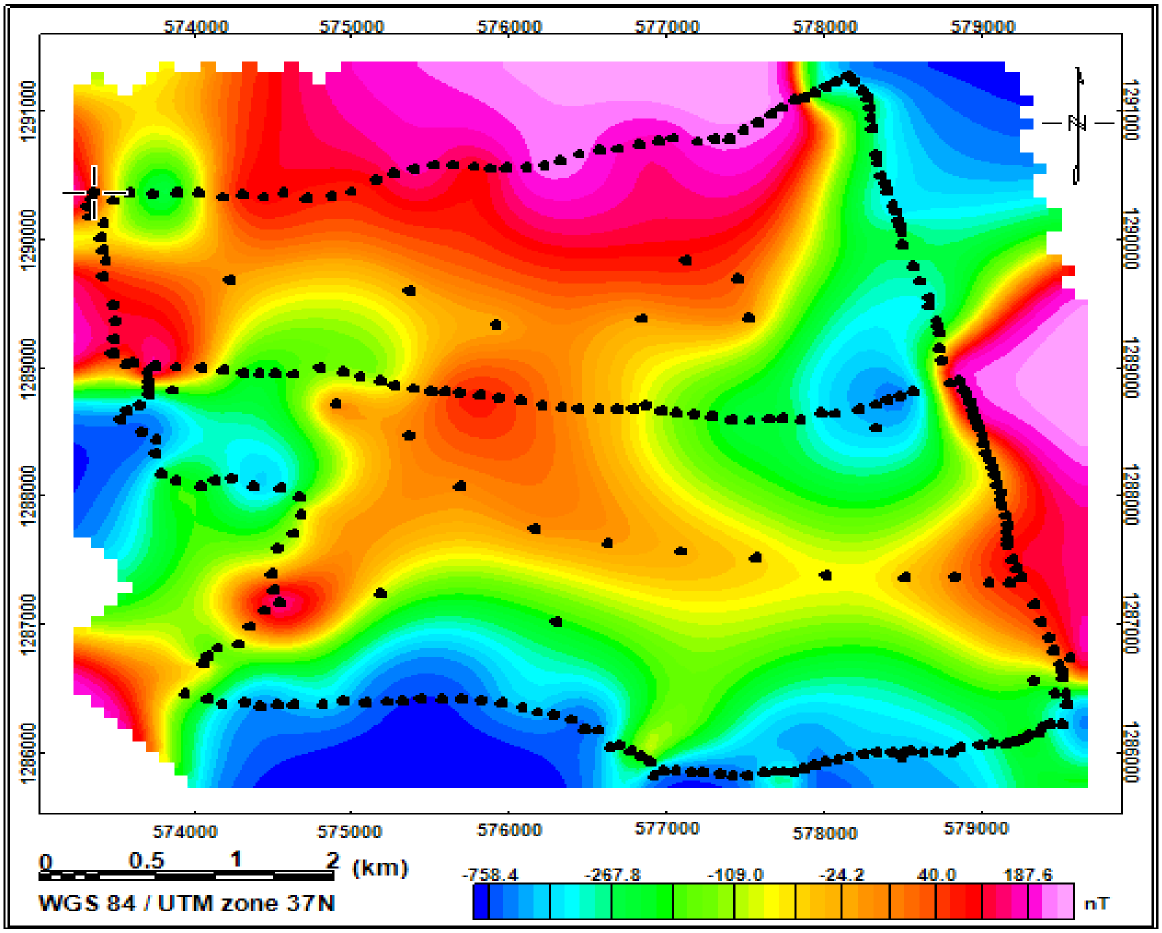

Figure 5.17: Total magnetic anomaly map

The (Fig 5.17) depicts the magnetic anomaly map of the study area, displaying the total magnetic anomaly (TMA). The magnetic anomaly values range from -1213 to 550 nT. On the total magnetic anomaly (TMA) map, larger low magnetic anomalies are observed, exhibiting northeast and west trends in (Fig 5.17). These anomalies appear in both circular and elongated shapes, primarily situated in the southern central area and northeast regions of the study area.

5.5.3 Separation of regional and residual magnetic anomaly

An essential aspect of magnetic data processing and interpretation involves discerning between residual and regional magnetic anomalies. One popular method for achieving this distinction is through upward continuation at depth of interest. This technique starts with the acquisition of magnetic data, usually in the form of total magnetic anomaly (TMA), across the study area.

5.5.3.1 Regional magnetic anomaly

The term "regional anomaly" denotes large-scale fluctuations in the magnetic field, influenced primarily by deep-seated geological formations and significant magnetic sources like basement rocks and major tectonic features. Techniques such as upward continuation at 800 meters are commonly employed to estimate this anomaly. This approach aids in identifying and analyzing broad magnetic patterns linked to deep geological structures such as basement rocks, major fault zones, and tectonic boundaries. Regional Magnetic Anomaly Maps provide a visualization of the magnetic field distribution across a study area before localized anomalies are filtered out. By interpreting these maps, researchers can glean insights into the regional geological framework and structural characteristics that impact the magnetic field, especially those associated with deep-seated geological formations.

5.5.3.2 Residual magnetic anomaly

To display the local magnetic field, a smooth surface must be adapted to the magnetic data during channel math expression builder (Hilemichaeil et al., 2024). The residual anomaly is the short-wavelength or small-scale variations in the magnetic field. It reflects the effects of near-surface geological features, mineralization, and local anomalies that are superimposed on the regional field. The residual anomaly is obtained by subtracting the estimated regional field (obtained through upward continuation at 400 m) from the observed total magnetic anomaly. The residual field represents the short-wavelength variations in the magnetic field, which are attributed to near-surface geological features and anomalies the result illustrates a higher anomaly signature corresponding to the central part of the study area. This may be due to the presence of a weak zone or alluvial sediment. Additionally, the anomaly trend in a northeast-southwest direction is high. This may be due to the presence of an elongated, low magnetized body in the central part of the research area.

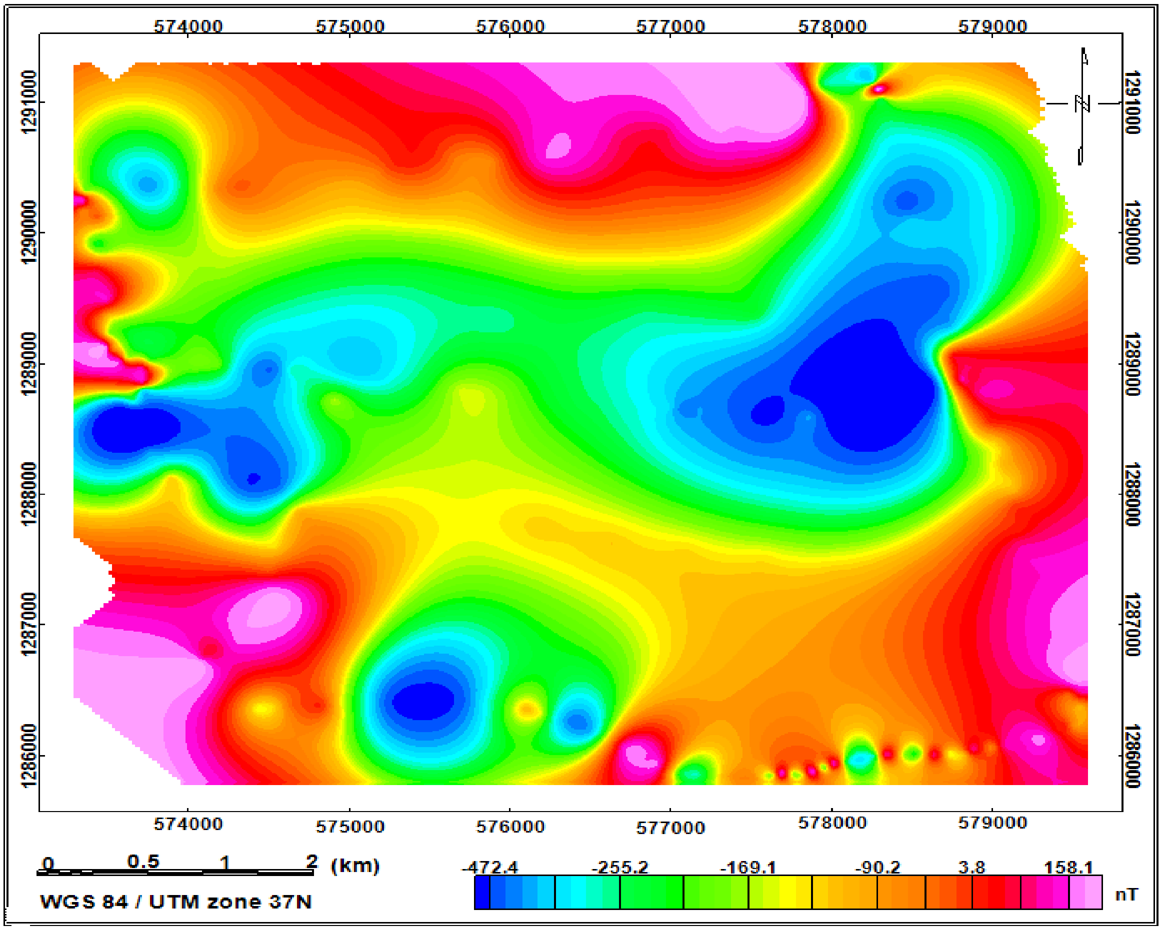

Figure 5.18: Map of Residual magnetic anomalies.

5.5.4 Magnetic analytical signal map (MAS)

To define the edges of magnetic source figures and estimate their depths, the analytical signal is obtained from the entire magnetic intensity data. To calculate the analytical signal, use the formula $AS=\sqrt{(\frac{\partial M}{\partial x})^2+(\frac{\partial M}{\partial y})^2+(\frac{\partial M}{\partial z})^2}$, where M is the total magnetic intensity at a given place. The partial derivatives in x, y and z directions of the magnetic field are $\partial M/\partial x$, $\partial M/\partial y$ and $\partial M/\partial z$, respectively. The map of analytical signal created by processing the map of magnetic anomaly shows anomalies caused by both vertical and horizontal changes in geological formations. This map covers a wide area that stands out from the surrounding sediments and areas of low magnetic susceptibility. The highest peaks on the analytical signal map coincide with the most significant magnetic anomalies in the northern, northwest, southern and southwest of the research area.

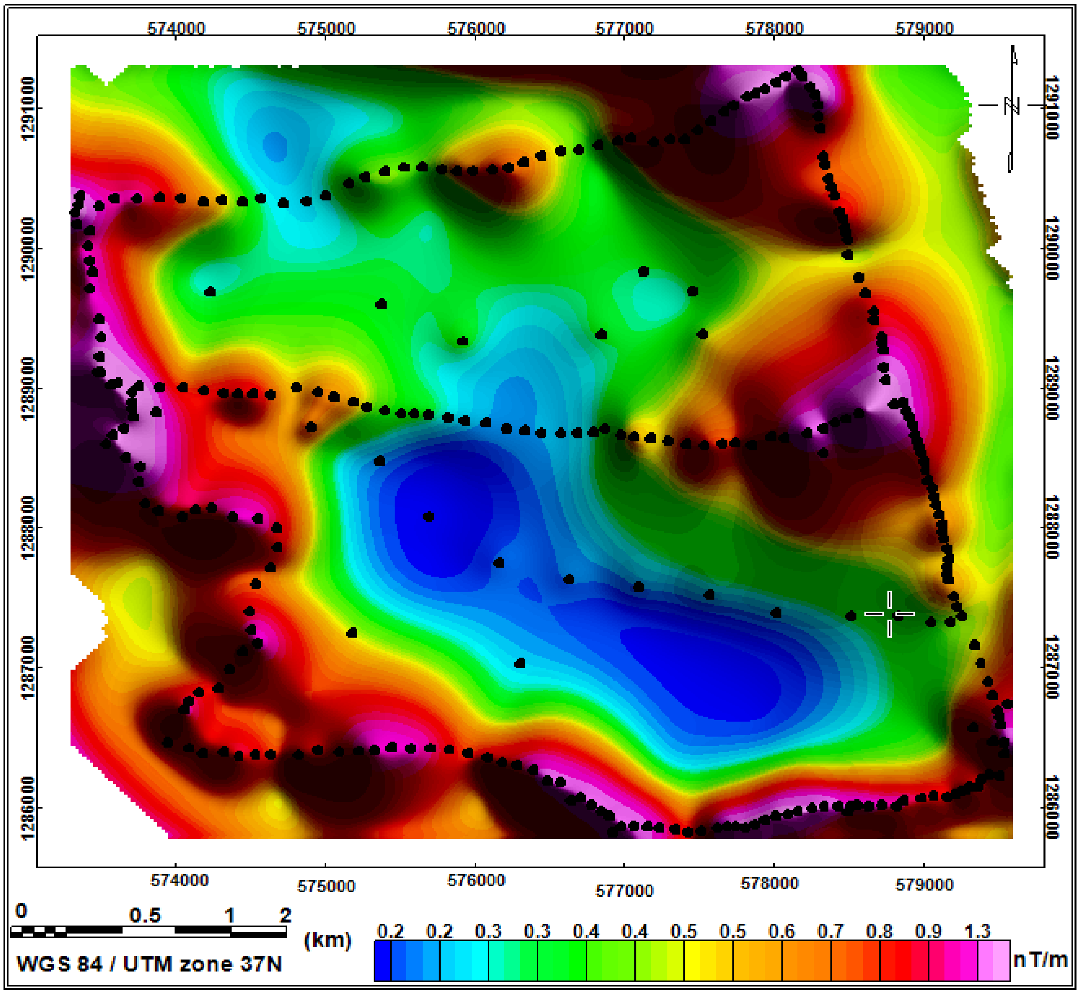

Figure 5.19: Analytic signal (AS) map

In (Fig 5.19) shows the results of entire magnetic anomaly map with in analytical signal algorithm. A picture of near-surface conditions is helpful as the analytical signal map shows the response of the anomalous bodies from their upper parts. The high amplitude is also precisely sited via a magnetic interaction, which depends on the depth and horizontal coordinates of the body, but not on the magnetization inclinations. NE-SW and NW-SE are the two primary vertical structures that dominate the study area. The NE-SW and NWSE bodies that cause the relatively strong magnetic anomalies are shown in (Fig 5.19). The high amplitude of the analysis signal in the northeastern, eastern, western and southern regions has discontinuities moving from south to north that may be caused by shear. The study area is part of the western margin of The Ethiopian Rift and is characterized by extensive volcanic activity. High MAS values in this region likely indicate basaltic flows, which are common in the rift margins. The rift margins are zones of intense tectonic activity, and high MAS values could highlight areas with significant tectonic uplift or volcanic intrusions. The low value of ASM is related to Sedimentary Basins. The Ethiopian Rift includes several sedimentary basins which are low MAS values in these areas indicating thick accumulations of sediments.

5.5.5 Tilt Derivative (TDR)

Magnetic anomaly maps serve as valuable tools for identifying areas with significant magnetic variations and for depicting structural features like faults and dikes in the Mersa area. These geological structures are highlighted using edge detection techniques, with total horizontal gradient (THG) and vertical derivative (VD) methods being among the most commonly employed techniques (Salawu et al., 2019). The tilt derivative ratio (TDR) is a formulated utilized in this context, calculated as the arctangent of the ratio of vertical derivative to horizontal derivative (TDR = arc tan (VD/HD)). TDR values typically range from -90° to +90° (-π/2 to +π/2 radians), regardless of the amplitude of VD or the absolute value of THG. The TDR varies significantly with slope; however, at inclinations of 0° and 90°, its zero crossing closely aligns with the edges of 2D magnetic source bodies such as dikes and blocks (Salawu et al., 2019).

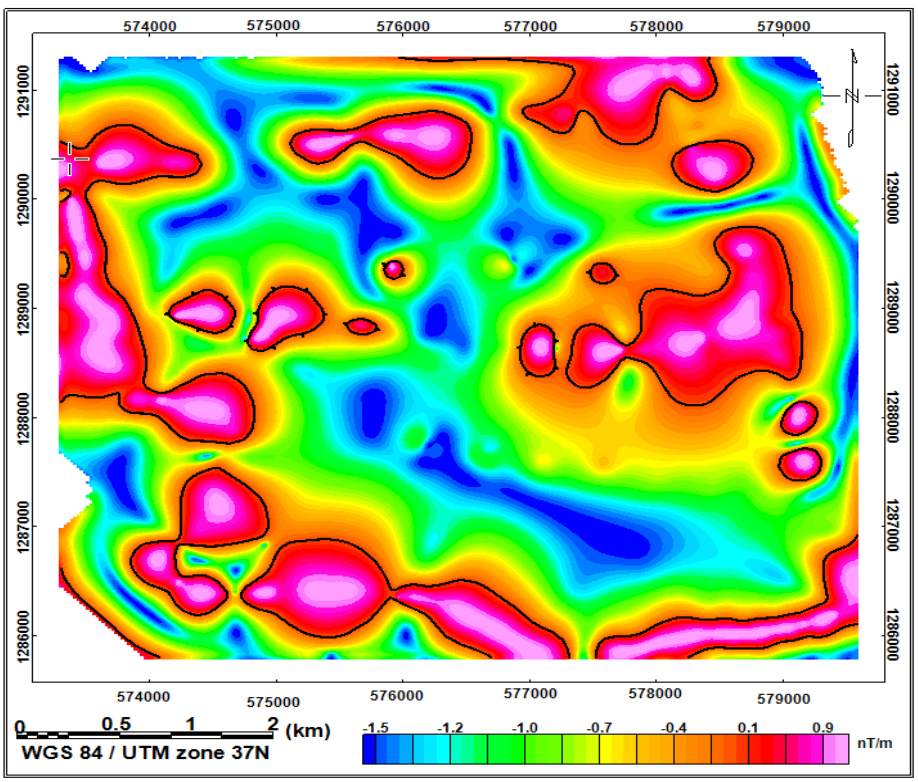

Figure 5.20: Tilt derivative magnetic map of study area

As a result, the Tilt derivative map (Fig 5.20) identifies and interprets subsurface geological structures, The output is easily identified location of fault /contacts and geological boundary and the zero crossing lines closely aligns with edges of 2D magnetic sources body. The TDR is identify subsurface structure and it shows more detailed structural contacts the major trends in NW-SE and N-S direction. Understanding the relationship between TDR values and magnetic anomalies helps identify fault lines, volcanic intrusion, and alluvial sediment deposits. The major trends in this case northwest- southeast direction.

5.5.6 Euler deconvolution Map

The depth and location of magnetic sources within the study area are estimated using the Euler deconvolution technique applied to the total magnetic anomaly data. Each model resulting from Euler deconvolution corresponds to a specific structural type, identified by a structural index (SI). Structural index values of 1, 2, and 3 represent horizontal cylinders/vertical pipes, spheres, and contact geological features, respectively. In (Fig 5.21), the SI is 1 for the Euler deconvolution magnetic map is presented, utilizing variously colored symbols to indicate magnetic sources at different depths. Pink, radish, and yellow circles in (Fig 5.21) represent magnetic sources less than 65 meters deep, while Green circles denote sources within the depth range of 65 to 149 meters. Red circles indicate magnetic sources deeper than 149 to 245 meters, whereas blue circles represent sources within the depth range of 245 to 405 meters. Yellow circles depict magnetic sources exceeding 405 to 588 meters in depth. The map highlights the presence of structures, particularly weak zones, in the southeast flank of the study area, housing highly magnetized bodies. Additionally, it suggests that the southwest flank of the region may exhibit a higher bearing capacity compared to the northeast, which holds significance for groundwater considerations. The interpretation of (Fig 5.21) focusing on structural indices, depth estimates, clusters of solutions, anomaly boundaries, and geological lineaments, enables a comprehensive understanding of the subsurface geological framework. The depths in the study area are determined using Euler deconvolution analysis, which estimates the depths of magnetic sources based on surface anomalies. A structural index (SI=1) indicates linear features where eastern and western parts of the area meet. On the map (Fig 5.21), different colored symbols represent magnetic sources at depths ranging from 65 to 588 meters. These results highlight linear features predominantly along the edges of magnetic sources, consistent with analytic signal and tilt derivative analyses. The southeast portion of the study area exhibits deeper depths and more pronounced linear features (Fig 5.21).

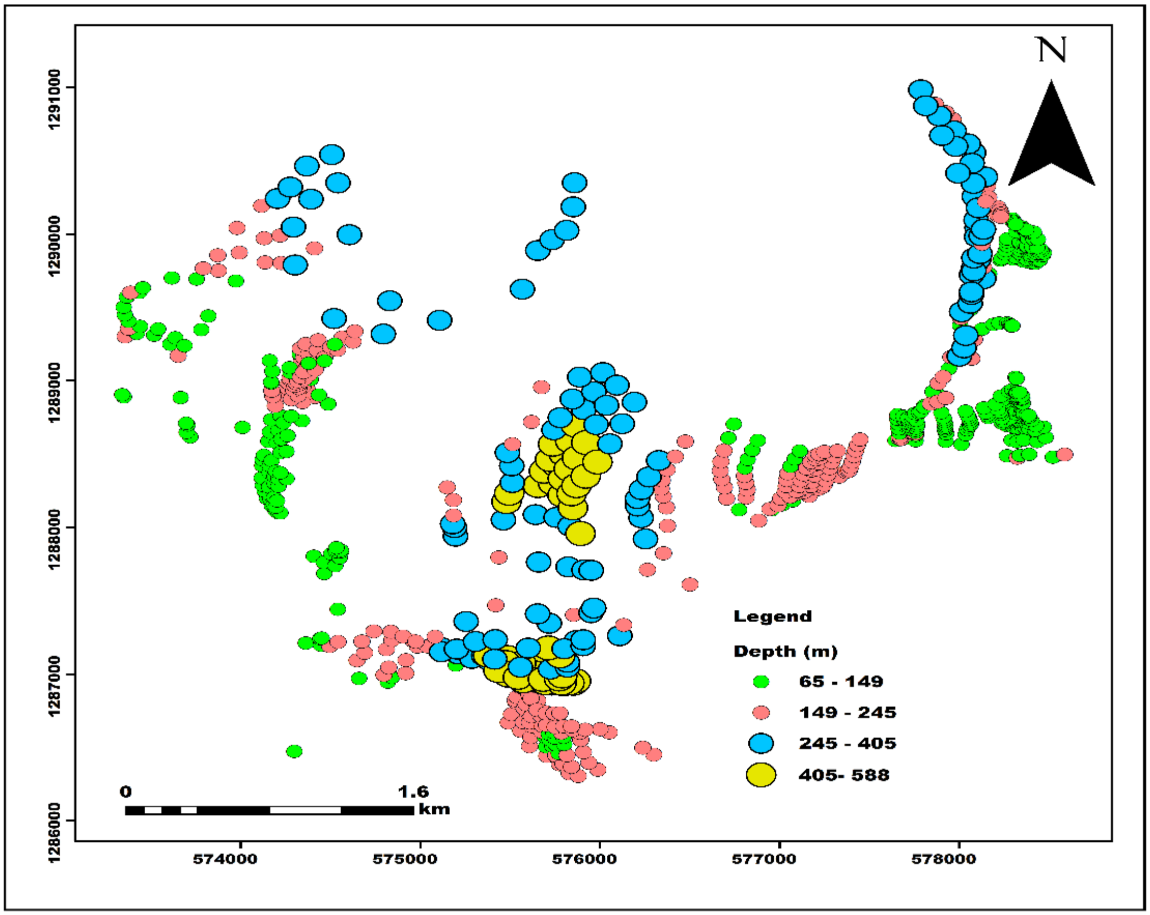

Figure 5.21: The Euler deconvolution magnetic map (SI =1).

5.6. 2D modelling

Using GM-SYS software, 2D modeling entails an interactive forward modeling process in which user-defined geological models are used to determine the magnetic response. The model structure is refined iteratively to reduce discrepancies between the modeled response and real magnetic field measurements (Salawu et al., 2019). It is notable to acknowledge the non-uniqueness of magnetic models, as varying geological compositions can produce comparable magnetic responses, and susceptibility properties can be used to infer distinct lithologies. It is crucial to integrate numerous data sources to increase model accuracy. GM-SYS usually produces 2D models that change beside of profile (X direction, perpendicular to strike) and in depth (Z direction) down to a maximum of 6 km. Therefore, spatial variations along the profile are taken into consideration during 2D magnetic modeling. Making use of the comparison map between the detailed studies of magnetic anomalies is carried out, providing important insights about subsurface geological formations, residual and its upward continuation at 800 m. This method facilitates the interpretation of the magnetic data and improves knowledge of the existing geological features.

5.6.1 Profile-one

The 2D magnetic profile model for Profile One is shown in (Fig 5.22) and is based on interpreted layer characteristics from Vertical Electrical Soundings (VES), geological cross-sections, and borehole data (particularly, BHP2, described in Annex 2A). The model shows geological contacts that are situated below 180 meters and that go vertically up to 500 meters next to a basaltic intrusion. The geo-electric section analysis shows that the basalts have different levels of weathering and fracture intensity. Additionally, there is diversity in the remanence of basalt layers among various strata. Profile-one's 2D magnetic modeling, shown in (Fig 5.22), offers important insights into subsurface geological formations and advances our understanding of the local geological setting. The magnetic anomaly maps can be used to determine the thickness and distribution of alluvial sediments. River valleys, floodplains, and coastal regions are frequently linked to alluvial deposits, which build up over time as a result of sediment transport and deposition processes. These sedimentary structures can show up in 2D modeling as large areas of muted magnetic anomalies over the floodplain or as elongated low-magnetic anomaly zones along basaltic. The geological contacts (fault lines) were observed in the NW-SE direction and the N-S direction along the river channel.

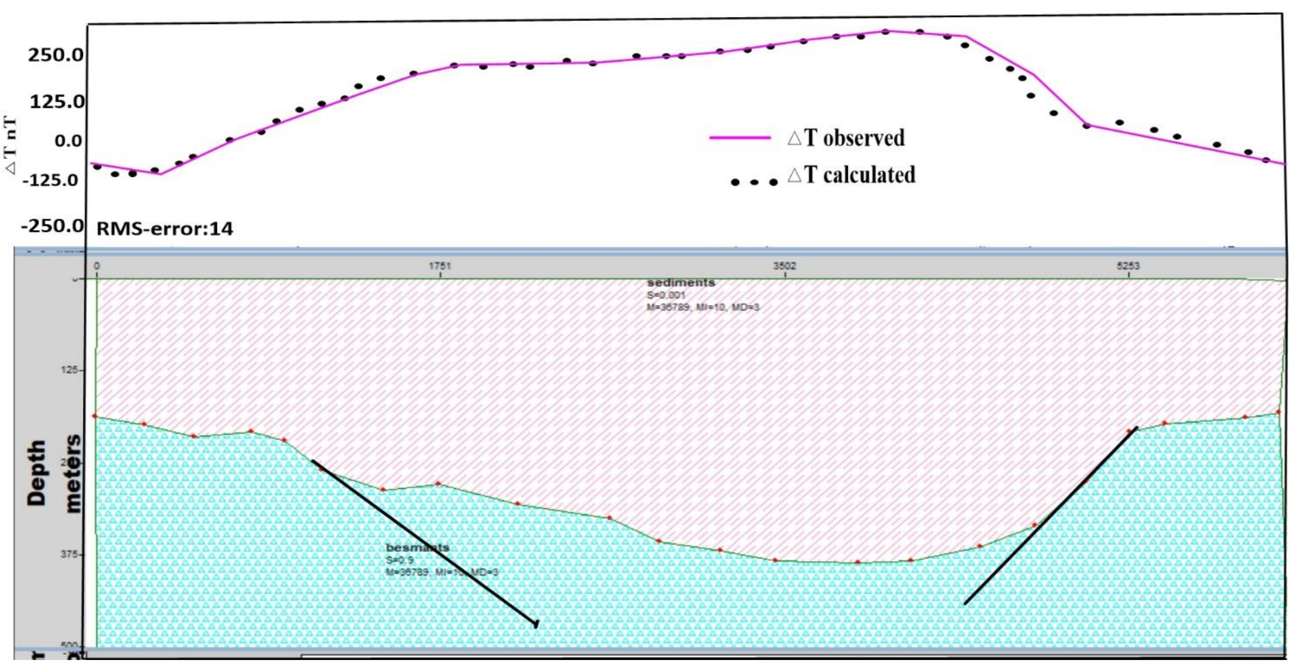

Figure 5.22: 2D modelling along profile one

To ensure coherence between the results obtained from magnetic and geoelectric data, it's crucial that the depth of the magnetic basement corresponds to the depth of the bedrock as identified in the geoelectric section along the same profile. This alignment between magnetic and geoelectric findings enhances the accuracy and reliability of the subsurface characterization. (Fig 5.5 and fig 5.22) provide visual representations of this alignment, showcasing the parallel depths of the magnetic basement and the bedrock across the respective profiles. This congruence strengthens the overall interpretation of the geological structure and facilitates a more comprehensive understanding of the subsurface conditions in the study area.

5.6.2 Profile-two

The 2D magnetic profile model for Profile Two is shown in (Fig 5.23) and is based on interpreted layer characteristics from Vertical Electrical Soundings (VES), geological cross-sections, and borehole data (particularly, BH2, described in Annex 2B). The model shows geological contacts that are situated below 125 meters and that go vertically up to 500 meters next to a basaltic intrusion. The geo-electric section analysis shows that the bedrock has different levels of weathering and fracture intensity. Additionally, there is diversity in the remanence of bedrock layers among various strata. Profile-two's 2D magnetic modeling, shown in (Fig 5.23), offers important insights into subsurface geological formations and advances our understanding of the local geological setting. The magnetic anomaly maps can be used to determine the thickness and distribution of alluvial sediments. River valleys, floodplains, and coastal regions are frequently linked to alluvial deposits, which build up over time as a result of sediment transport and deposition processes. These sedimentary structures can show up in 2D modeling as large areas of muted magnetic anomalies over the floodplain or as elongated low-magnetic anomaly zones along basaltic zones and high magnetic anomalies along river channels. Magnetic 2D modeling reveals distinct magnetic patterns in basement deposits, indicating the presence of dense magnetic materials in crystalline rocks like granite, gneiss, and basalt. These anomalies can help in identifying the depth and amount of basement deposits, with larger anomalies indicating deeper structures.

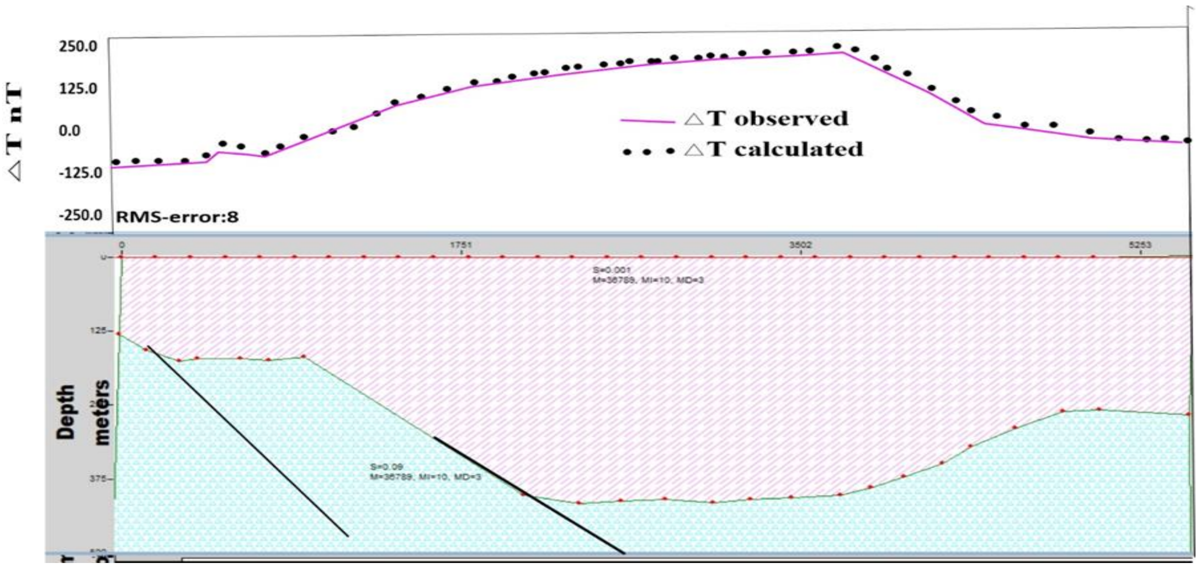

Figure 5.23: 2D modelling along profile two

To ensure coherence between the results obtained from magnetic and geoelectric data, it's crucial that the depth of the magnetic basement corresponds to the depth of the bedrock as identified in the geoelectric section along the same profile. This alignment between magnetic and geoelectric findings enhances the accuracy and reliability of the subsurface characterization. (Fig 5.6 and fig 5.23) provide visual representations of this alignment, showcasing the parallel depths of the magnetic basement and the bedrock across the respective profiles. This congruence strengthens the overall interpretation of the geological structure and facilitates a more comprehensive understanding of the subsurface conditions in the study area.

5.6.2 Profile-three

The 2D magnetic profile model for Profile three, depicted in (Fig 5.24), was constructed based on interpreted layer parameters derived from Vertical Electrical Soundings (VES), geological cross-sections, and borehole data detailed in Annex-2B. This model reveals geological contacts situated at depths ranging from below 180 m to 500m, as well as the presence of basaltic intrusions. Variations in the degree of weathering and fracture intensity by analysis of the geo-electric section. The 2D magnetic modeling of Profile-three, shown in (Fig 5.24), improves significantly our knowledge of the geological composition of this area by shedding light on subsurface geological formations. Magnetic 2D modeling distinguishes alluvial sediments from other geological formations due to their low magnetic susceptibility and high magnetic anomaly. These sediments can be found in river valleys, floodplains, and coastal regions. Basement deposits, which contain crystalline rocks like granite, gneiss, and basalt, show distinct magnetic patterns. High positive magnetic anomalies associated with sediment deposits indicate dense magnetic materials. These maps can help in identifying the amount and depth of sediment deposits, with larger anomalies arising from deeper structures and weaker ones from shallow or discontinuous features.

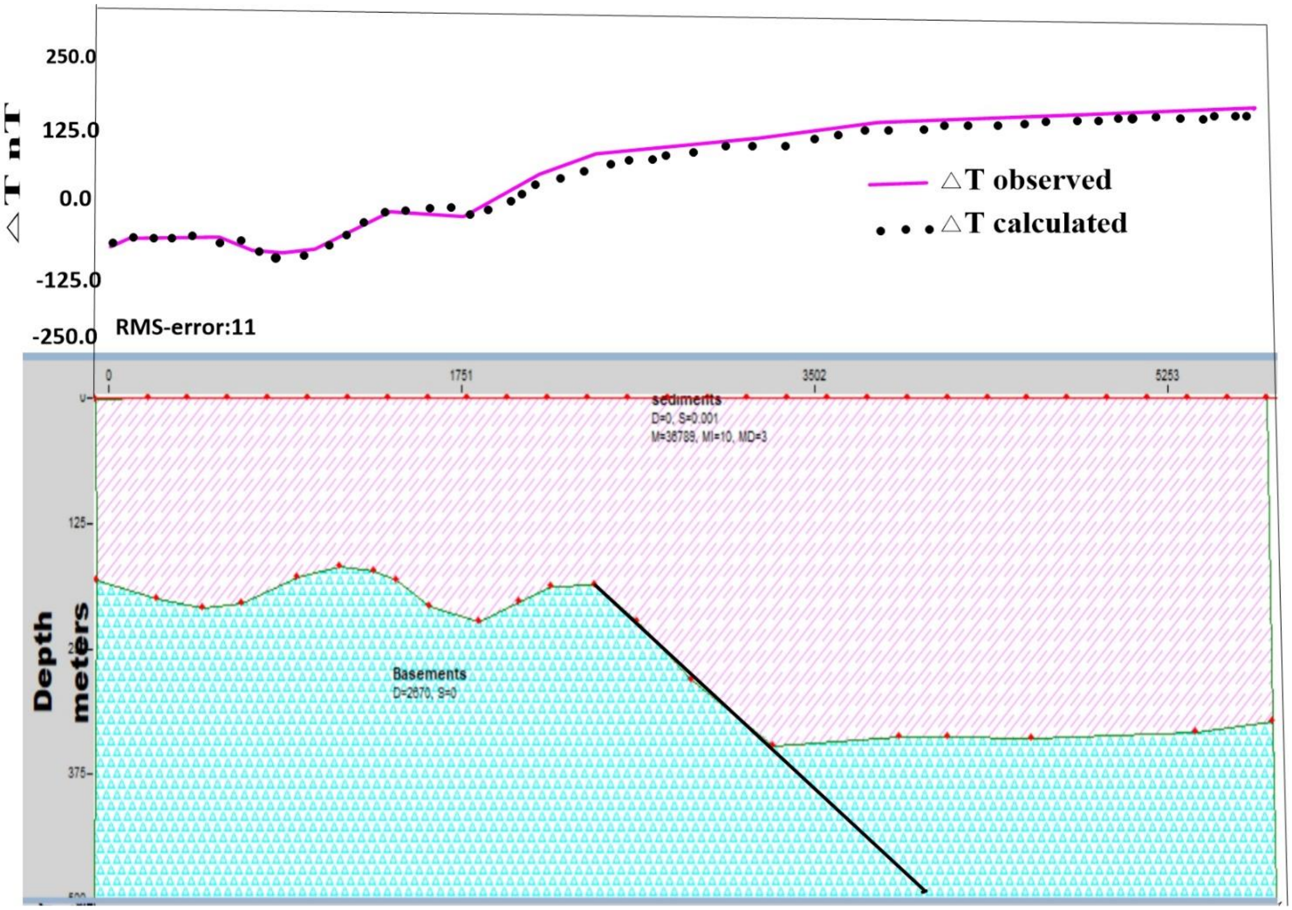

Figure 5.24: Magnetic data modelling in 2D along line three.

To ensure coherence between the results obtained from magnetic and geoelectric data, it's crucial that the depth of the magnetic basement corresponds to the depth of the bedrock as identified in the geoelectric section along the same profile. This alignment between magnetic and geoelectric findings enhances the accuracy and reliability of the subsurface characterization. (Fig 5.9 and 5.24) provide visual representations of this alignment, showcasing the parallel depths of the magnetic basement and the bedrock across the respective profiles. This congruence strengthens the overall interpretation of the geological structure and facilitates a more comprehensive understanding of the subsurface conditions in the study area.

5.7 The integrated results of magnetic and VES data

The integration of the results mainly focused on Correlation between magnetic anomalies and VES findings, identification of groundwater potential zones and implications of structural and lithological variations. The measurements of Vertical Electrical Sounding (VES) surveys, land magnetic data, and information from available drill holes, were employed to assess groundwater potential and identify suitable drilling locations in the study area.

Among the VES results in geo electric section identified four different geo-electric layers, representing various deposits such as topsoil, clay sediments intercalations, gravel sediments (Alluvial sediments) and bedrock defines the geological zone. The 2D magnetic modeling also identified the sediment deposit and basements with appropriate depths. The results of geo electric section and 2D modeling shows the best correlations identification of sediments and basements in the study areas.

The lithological and hydrogeological characteristics of each geological unit are considered to establish a connection between VES results and the aquifer system. This connection of aquifer depend on the aquifer parameters. This aquifer parameters are transmissivity and hydraulically conductivity’s the high value of transmissivity were found at the center and eastern part of the study area (the faults are older in age, they do not affect transmissivity of the quaternary sediments. The high value of transmissivity shows the fault lines and fracture zones of the area. This fault zones also identify by 2D magnetic modeling in (Fig 5.22). In areas with a high density of faulting, the bottom volcanic layer can indeed become an aquifer zone. This occurs due to the fractured nature of the rock caused by faulting. Faulting creates cracks and fractures in the rock layers, allowing water to infiltrate and accumulate within the spaces. The volcanic layers, often composed of porous materials like basalt, can act as reservoirs for groundwater. The fractures and pores within these layers allow water to move through them, creating underground water storage areas known as aquifers. These aquifers can be significant sources of water for wells and springs in regions with active faulting and volcanic activity. The research used tilt derivative and analytic signal approaches to identify discrete geologic trends in a specific area. Tilt derivative helps detect lateral variations of the magnetic field and output is easily identified location of fault /contacts and geological boundary which shows more than detailed structural contacts boundary than analytical signals identifying potential subsurface magnetic source bodies. It also identifies discontinuities perpendicular to the direction of derivation that characterize the edges of geological structures. High magnetic anomalies can indicate geological structures that influence groundwater movement and deposition. Geo-electric section and 2D magnetic modeling results show similar trends in geological contacts and lithological units. The basement was identified at depths ranging from 125 meters to 359 meters in the geo-electric section along profile line one. Similarly, the 2D magnetic section revealed the basement at depths between 180 meters and 380 meters. These results indicate that both the geo-electric and magnetic surveys provide consistent findings regarding the depth of the basement.

Generally, Correlation between Magnetic Anomalies and VES Findings: Geo-electric Sections: VES identified four distinct geo-electric layers, including topsoil, clay sediments, gravel (alluvial) sediments, and bedrock, defining geological zones and their resistivity characteristics. 2D Magnetic Modeling: Magnetic data identified sediment deposits and basement rocks at various depths, showing consistency with VES findings, indicating a strong correlation between these methods. Depth Correlation: Comparison between geo-electric sections and 2D magnetic sections showed close alignment in basement depths, reinforcing the reliability of the integrated geophysical methods.

CHAPTER VI

6. CONCLUSIONS AND RECOMMENDATIONS

6.1 Conclusions

The geophysical data were analysis using Surfer, IPI2WIN, WINRESIST and Oasis Montaj (Geo soft v 8.4.2) software. According to the magnetic result, the subsurface geological structures or contact in the study area are north-south trending. These faults were observed to be interconnected, with the ascending fault from the Mersa aquifer serving as a conduit for groundwater flow. These fault and fracture systems play a critical role in facilitating the movement, recharge, and diversion of groundwater resources.

The geoelectric results show a four geological units such as topsoil, clay sediments, gravel sediments, and bedrock. The pseudo depth section results insight as the central and eastern part of study area are characterized by low apparent resistivity. There are both shallow and deeper low-resistivity horizons that could be areas of groundwater saturation, as indicated by pseudo-depth sections of apparent resistivity and the geo-electric sections of true resistivity. The thickest thickness and low resistance of these horizons are a sign of the high potential of groundwater in the study area.

The results of electrical resistivity and magnetic measurements also show that the region is strongly influenced by tectonic forces, which have caused local faults and fractures of the rock units at different depths. Groundwater movement is believed to be regulated by these fractures and faults (contacts). The main barriers that prevent groundwater from flowing across the region are fractures and weak points. A comparison of the well-log results and the geophysical interpretations shows a strong correlation between the geophysical survey results and the drill hole lithological logging results.

Gravel (Alluvial) sediments and fractured basalt are the major geological units throughout the study area that are likely to contain groundwater depending on the extent to which they are weathered and fractured. In the research area, it was found that 35% of the aquifers exhibit high productivity, while 65% of the aquifers demonstrate moderate productivity. The estimated hydraulic conductivity and transmissivity values are high in the central and eastern region of the research area. Conversely, the northeastern and southwestern sections exhibit lower values. This suggests that the central part of the research area holds promising potential for supplying a significant amount of groundwater potentials.

6.2 Recommendation

Based on the result of the study the following recommendation are proposed.

- Traverse line one's 63-260 meters thick aquifer offers significant water storage capacity, making it a promising site for future drilling(UTM: 574246-1289489 to 577848-1291102).
- To obtain sufficient groundwater in small depths, it is recommended to locate VES 8 and 9 along traverse line two (UTM: 577393-1288118 and 582296-1281376).
- According to the result of 2D magnetic section and geoelectric section result, the central part of the study area is a good groundwater potential zone. Therefore for the feature well drilling to extract groundwater, the central part is recommended.
- According to VES and magnetic results, the eastern and central parts of the study area are characterized by a weak zone and thick sediment. Therefore, drilling there is recommended to obtain a good yield of groundwater.
- The significant aquifer thickness and low resistivity observed in the profile line four indicate a high potential for groundwater. Therefore, it is recommended to establish future well sites in this region (UTM: 578320,129789 to 579582, 1286466).

References

Abbate, E., Bruni, P., & Sagri, M. (2015). Geology of Ethiopia: a review and geomorphological perspectives. Landscapes and landforms of Ethiopia, 33-64.

Abera Alemu. (2020). Geophysics: Principles, Practices and Applications of Geophysical Methods to Resource Exploration and Geohazard Studies``.

Ali, H. Y., Priju, C., & Prasad, N. N. (2015). Delineation of groundwater potential zones in deep midland aquifers along Bharathapuzha river basin, Kerala using geophysical methods. Aquatic Procedia, 4, 1039-1046.

Ayenew, T., Demlie, M., & Wohnlich, S. (2008). Hydrogeological framework and occurrence of groundwater in the Ethiopian aquifers. Journal of African Earth Sciences, 52(3), 97-113.

Benson, A. K., & Mustoe, N. B. (1998). Integration of electrical resistivity, ground-penetrating radar, and very low-frequency electromagnetic induction surveys to help map groundwater contamination produced by hydrocarbons leaking from underground storage tanks. Environmental Geosciences, 5(2), 61-67.

Chorowicz, J., Collet, B., Bonavia, F., Mohr, P., Parrot, J., & Korme, T. (1998). The Tana basin, Ethiopia: intra-plateau uplift, rifting and subsidence. Tectonophysics, 295(3-4), 351-367.

Dereje Ayalew, Barbey, P., Marty, B., Reisberg, L., Yirgu, G., & Pik, R. (2002). Source, genesis, and timing of giant ignimbrite deposits associated with Ethiopian continental flood basalts. Geochimica et Cosmochimica Acta, 66(8), 1429-1448.

Dereje Ayalew, Ukstins, I. A., Renne, P. R., Wolfenden, E., Baker, J., & Menzies, M. (2002). Matching conjugate volcanic rifted margins: 40Ar/39Ar chrono-stratigraphy of pre-and syn-rift bimodal flood volcanism in Ethiopia and Yemen. Earth and planetary science letters, 198(3-4), 289-306.

Diga, G. M. (2005). Using seasonal climate outlook to advise on sorghum production in the Central Rift Valley of Ethiopia University of the Free State].

Ebrahim Asqual. (2021). Groundwater and Surface Water Interactions in Hayk and Ardibo Lake, Sustainability Challenge, Northern Ethiopia.

Endayen Belay. (2020). Volcanic-stratigraphy and petrography of flood volcanics along Jita River in north-central Ethiopia.

Ghinassi, M., D'Oriano, F., Benvenuti, M., Awramik, S., Bartolini, C., Fedi, M., Ferrari, G., Papini, M., Sagri, M., & Talbot, M. (2012). Shoreline fluctuations of Lake Hayk (northern Ethiopia) during the last 3500 years: geomorphological, sedimentary, and isotope records. Palaeogeography, Palaeoclimatology, Palaeoecology, 365, 209-226.

Gibson, P. J., & George, D. M. (2013). Environmental applications of geophysical surveying techniques: 2nd edition.

Hofmann, A. W. (1997). Mantle geochemistry: the message from oceanic volcanism. Nature, 385(6613), 219-229.

Holden, J., Burt, T., & Vilas, M. (2002). Application of ground-penetrating radar to the identification of subsurface piping in blanket peat. Earth Surface Processes and Landforms, 27(3), 235-249.

Kazmin, V. (1979). Stratigraphy and correlation of Cenozoic volcanic rocks in Ethiopia. Reports of Ethiopian Institute of Geological Survey, 106, 1-26.

Igor S. Zektser and Lome G. Everett, (2004). Groundwater resources of the worldand their use, UN. pp:20

Kearey, P., Brooks, M., & Hill, I. (2002). An introduction to geophysical exploration (Vol. 4). John Wiley & Sons.

Kieffer, B., Arndt, N., Lapierre, H., Bastien, F., Bosch, D., Pecher, A., Yirgu, G., Ayalew, D., Weis, D., & Jerram, D. A. (2004). Flood and shield basalts from Ethiopia: magmas from the African superswell. Journal of Petrology, 45(4), 793-834.

Babatunde R. Onawola1, Saminu Olatunji2, Ologe3*and, O., & Jimoh4, R. O. (2021). Determination of Aquifer Parameters from Resistivity Data: A Case of University of Ilorin Campus, NorthcentralNigeria.TanzaniaJournalofScience47(1):,91-103. https://doi.org/10.4314/tjs.v47i1.9

Batte, A., Barifaijo, E., Kiberu, J., Kawule, W., Muwanga, A., Owor, M., & Kisekulo, J. (2010). Correlation of geoelectric data with aquifer parameters to delineate the groundwater potential of hard rock terrain in Central Uganda. Pure and applied geophysics, 167, 1549-1559.

Hilemichaeil, S., Haile, T., & Yirgu, G. (2024). Integrated geophysical methods to constrain subsurface structures of Tulu Moye-Bora-Berecha axial volcanic complex, main Ethiopia rift: Implicationsforgeothermalresources.Heliyon,10(7).https://doi.org/10.1016/j.heliyon.2024.e28499

Hinze WJ, von Frese RRB, & AH., S. (2013). The gravity method. In: Gravity and Magnetic Exploration: Principles, Practices, and Applications. . Cambridge: Cambridge University Press; : .

Hussein, Mohamed, Jama, Karakilçik, & Hatice. (2023). Investigating Groundwater Resources in Somaliland's Sool and Gebiley Regions Using the Vertical Electrical Sounding (VES) Method. Geosound, 58(1), 20-39.

Kobo-Girana Project report. (2009). Existing groundwater development situation in girana.

Moussa , , M. K., Mathieu Le Coz 2, 1, O. R. Y., Cheick Oumar Zouré 3, and, M. D. F., & 1, B. L. (2021). Use of Multidisciplinary Approaches for Groundwater Recharge Mechanism Characterization in Basement Aquifers: Case of Sanon Experimental Catchment in Burkina Faso. MDPI stays neutral with regard to jurisdictional claims in published maps and institutional affiliations., 13, 3216. . https://doi.org/10.3390/w13223216

Oteri, A. (1981). Geoelectric investigation of saline contamination of a chalk aquifer by mine drainage water at Tilmanstone, England. Geoexploration, 19(3), 179-192.

Refsgaard, Christian, J., Christensen, Steen, Sonnenborg, O, T., Seifert, Dorte, Højberg, Lajer, A., & Troldborg, L. (2012). Review of strategies for handling geological uncertainty in groundwater flow and transport modeling. Advances in Water Resources, 36, 36-50.

Salawu, N. B., Olatunji, S., Adebiyi, L. S., Olasunkanmi, N. K., & Dada, S. S. (2019). Edge detection and magnetic basement depth of Danko area, northwestern Nigeria, from low-latitude aeromagnetic anomaly data. SN Applied Sciences, 1(9). https://doi.org/10.1007/s42452-019-1090-3

Sylvia S. Simon1, M., J., Ishaku1, Ahmed Buba Seli2, & Boniface1*, F. (2022). Evaluation of Groundwater Potentials Using Dar Zarrouk Parameters in Mapeo and Environs, North-Eastern Nigeria. Dutse Journal of Pure and Applied Sciences (DUJOPAS), 8, 124-135,. https://doi.org/10.4314/dujopas.v8i3b.13

Todd, D. K., & Mays, L. W. (2004). Groundwater hydrology. John Wiley & Sons. (Vol.).

Türk, k. B., baran, m. F., aslam, z., & seydoşoğlu, s. (2021). Proceedings book.

Lillie, R. J. (1999). Whole earth geophysics. An Introductory Textbook for Geologists.

M.H., L. (2004). Tutorial : 2-D and 3-D electrical imaging surveys2004.

Mohr, P., & Zanettin, B. (1988). The Ethiopian flood basalt province. Continental flood basalts, 63-110.

Niwas S and Singhal DC 1981 Estimation of aquifer transmissivity from Dar-Zarrouk parameters in porous media. J. Hydrol. 50: 393-399.

Philip Kearey, Michael Brooks, & Ian Hill. (2002). An Introduction to Geophysical Exploration.

Raymond, M. (1947). The fundamental equations of electrical prospecting. Geophysics, 12(4), 529-556.

Shepherd, R. G. (1989). Correlations of permeability and grain size. Groundwater, 27(5), 633-638.

Stevenson, D. J. (2020). Jupiter's interior as revealed by Juno. Annual Review of Earth and Planetary Sciences, 48, 465-489.

Syed Muzyan Shahzad, Liu Jianxin, Asim Shahzad, Muhammad Sharjeel Raza, Sun Ya, & Fanidi Meryem. (2018). Groundwater Potential Zone Identification in Unconsolidated Aquifer Using Geophysical Techniques around Tarbela Ghazi, District Haripur, Pakistan. World Academy of Science, Engineering and Technology International Journal of Geological and Environmental Engineering , , 12, 7.

Telford, W. M., Geldart, L. P., & Sheriff, R. E. (1990). Applied geophysics. Cambridge university press.

Tesfaye Kidane, Otofuji, Y.-I., Komatsu, Y., Shibasaki, H., & Yokoyama, M. (2010). Structural and geochronological implications of the Fentale Volcanics at a nascent passive margin of the Main Ethiopian Rift: Constraints from magnetostratigraphy study at the Kereyou Lodge, Ethiopia. Tectonophysics, 495(3-4), 159-170.

Ukstins, I. A., Renne, P. R., Wolfenden, E., Baker, J., Ayalew, D., & Menzies, M. (2002). Matching conjugate volcanic rifted margins: 40Ar/39Ar chrono-stratigraphy of pre-and syn-rift bimodal flood volcanism in Ethiopia and Yemen. Earth and planetary science letters, 198(3-4), 289-306.

Watchorn, F., Nichols, G., & Bosence, D. (1998). Rift-related sedimentation and stratigraphy, southern Yemen (Gulf of Aden). In Sedimentation and Tectonics in Rift Basins Red Sea:-Gulf of Aden (pp. 165-189). Springer.

Williams, D. R., & Collins, C. (2016). Racial residential segregation: a fundamental cause of racial disparities in health. Public health reports.

Zanettin, B. (1978). The evolution of the Chencha escarpment and the Ganjuli graben (lake Abaya) in southern Ethiopian rift. Neues Jahrb. Geol. Paleontol. Monatshefte, 8, 473-490.

Zanettin, B., & Justin-Visentin, E. (1975). Tectonical and volcanological evolution of the western Afar margin (Ethiopia). E. Schweizerb. Verlag.

Zhong, J., Yi, M., & Bau, H. H. (2002). Magneto hydrodynamic (MHD) pump fabricated with ceramic tapes. Sensors and Actuators A: Physical, 96(1), 59-66.

Appendix I VES curve

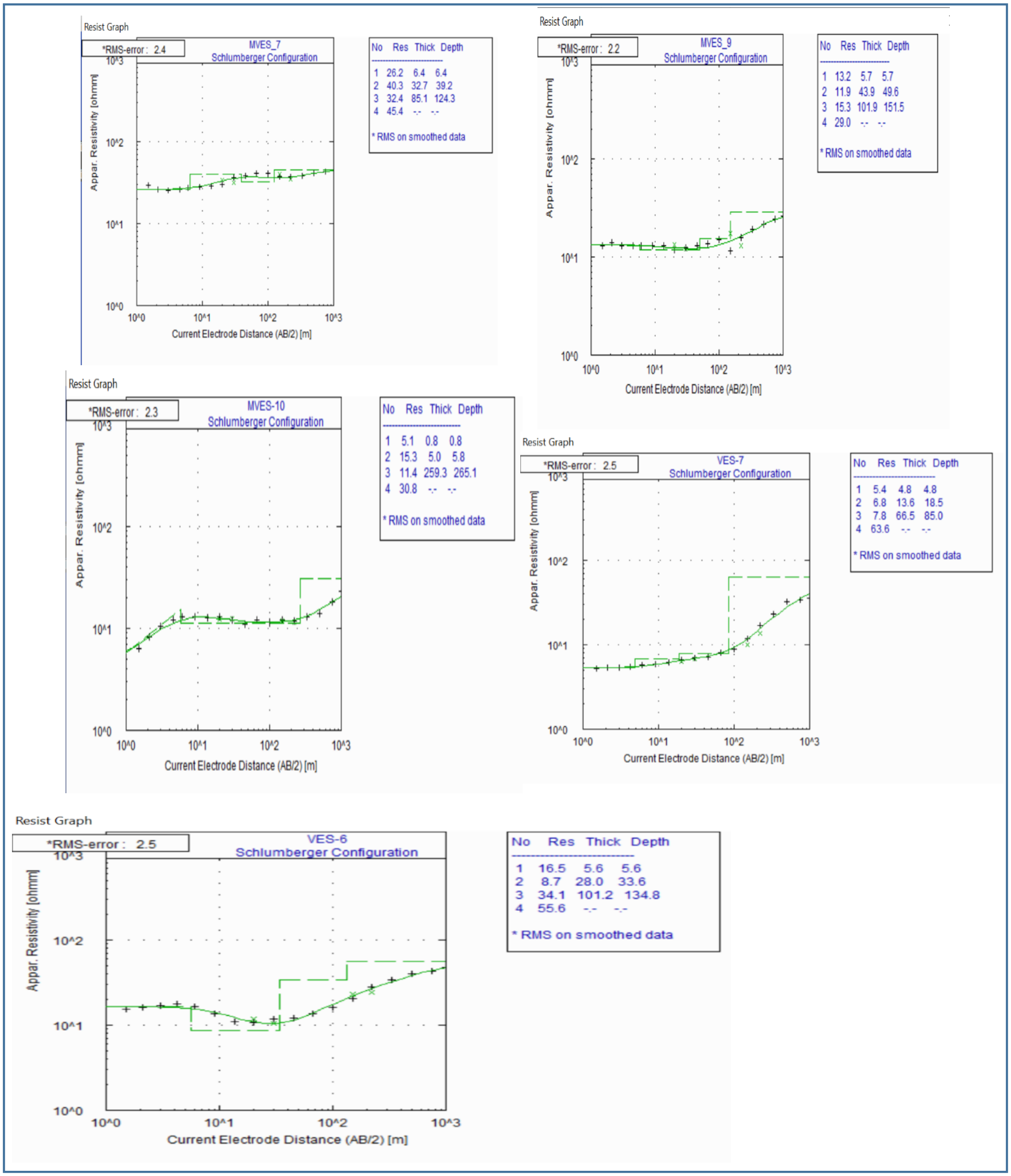

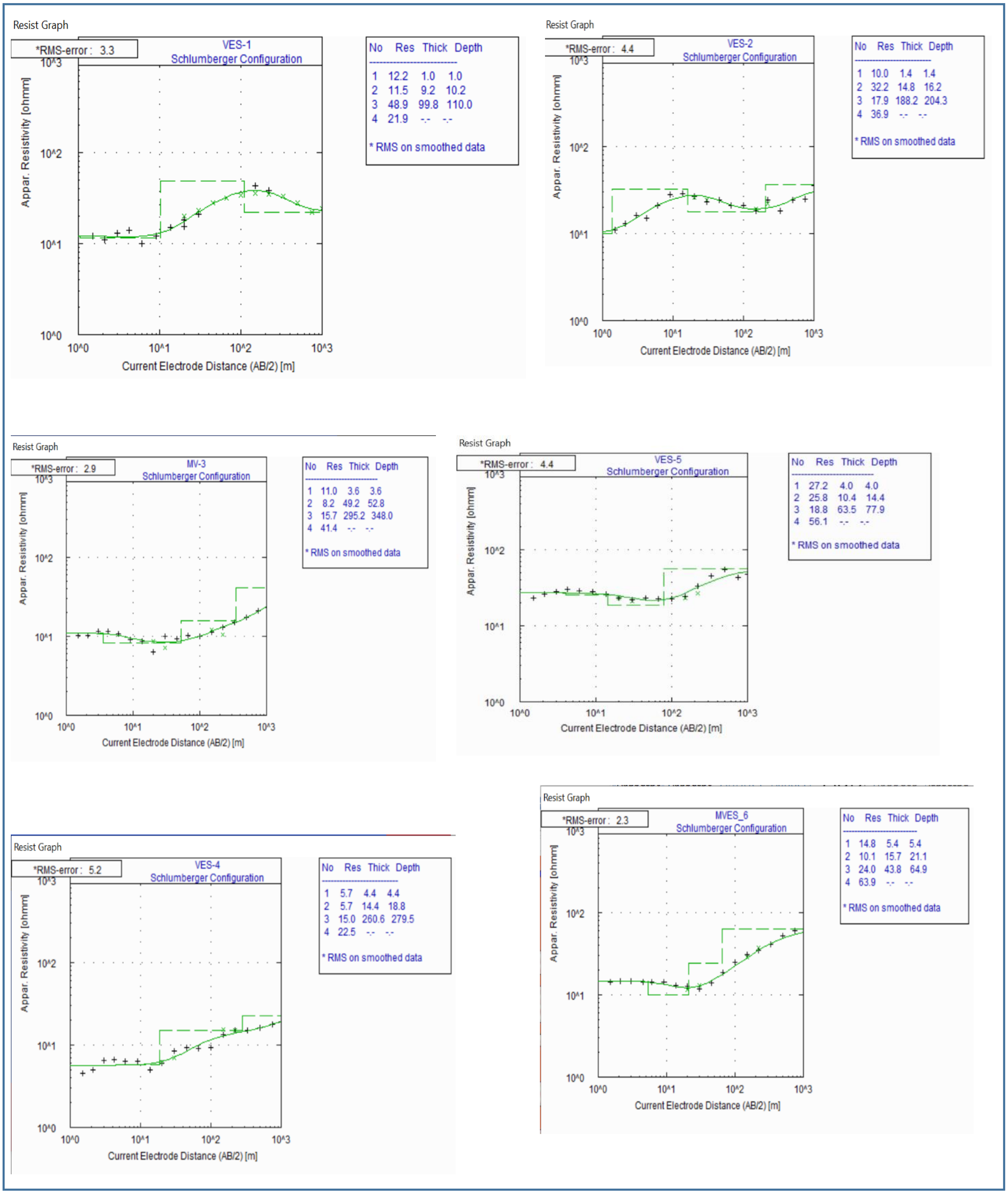
Resist Graph
*RMS-error : 3.3
VES-1
Schlumberger Configuration
Appar. Resistivity [ohmm]
Current Electrode Distance (AB/2) [m]
No Res Thick Depth
1 12.2 1.0 1.0
2 11.5 9.2 10.2
3 48.9 99.8 110.0
4 21.9 -.- -.-
* RMS on smoothed data
Resist Graph
*RMS-error : 4.4
VES-2
Schlumberger Configuration
No Res Thick Depth
1 10.0 1.4 1.4
2 32.2 14.8 16.2
3 17.9 188.2 204.3
4 36.9 -.- -.-
* RMS on smoothed data
Resist Graph
*RMS-error : 2.9
MV-3
Schlumberger Configuration
No Res Thick Depth
1 11.0 3.6 3.6
2 8.2 49.2 52.8
3 15.7 295.2 348.0
4 41.4 -.- -.-
* RMS on smoothed data
Resist Graph
*RMS-error : 4.4
VES-5
Schlumberger Configuration
No Res Thick Depth
1 27.2 4.0 4.0
2 25.8 10.4 14.4
3 18.8 63.5 77.9
4 56.1 -.- -.-
* RMS on smoothed data
Resist Graph
*RMS-error : 2.3
MVES_6
Schlumberger Configuration
No Res Thick Depth
1 14.8 5.4 5.4
2 10.1 15.7 21.1
3 24.0 43.8 64.9
4 63.9 -.- -.-
* RMS on smoothed data
Resist Graph
*RMS-error : 5.2
VES-4
Schlumberger Configuration
No Res Thick Depth
1 5.7 4.4 4.4
2 5.7 14.4 18.8
3 15.0 260.6 279.5
4 22.5 -.- -.-
* RMS on smoothed data

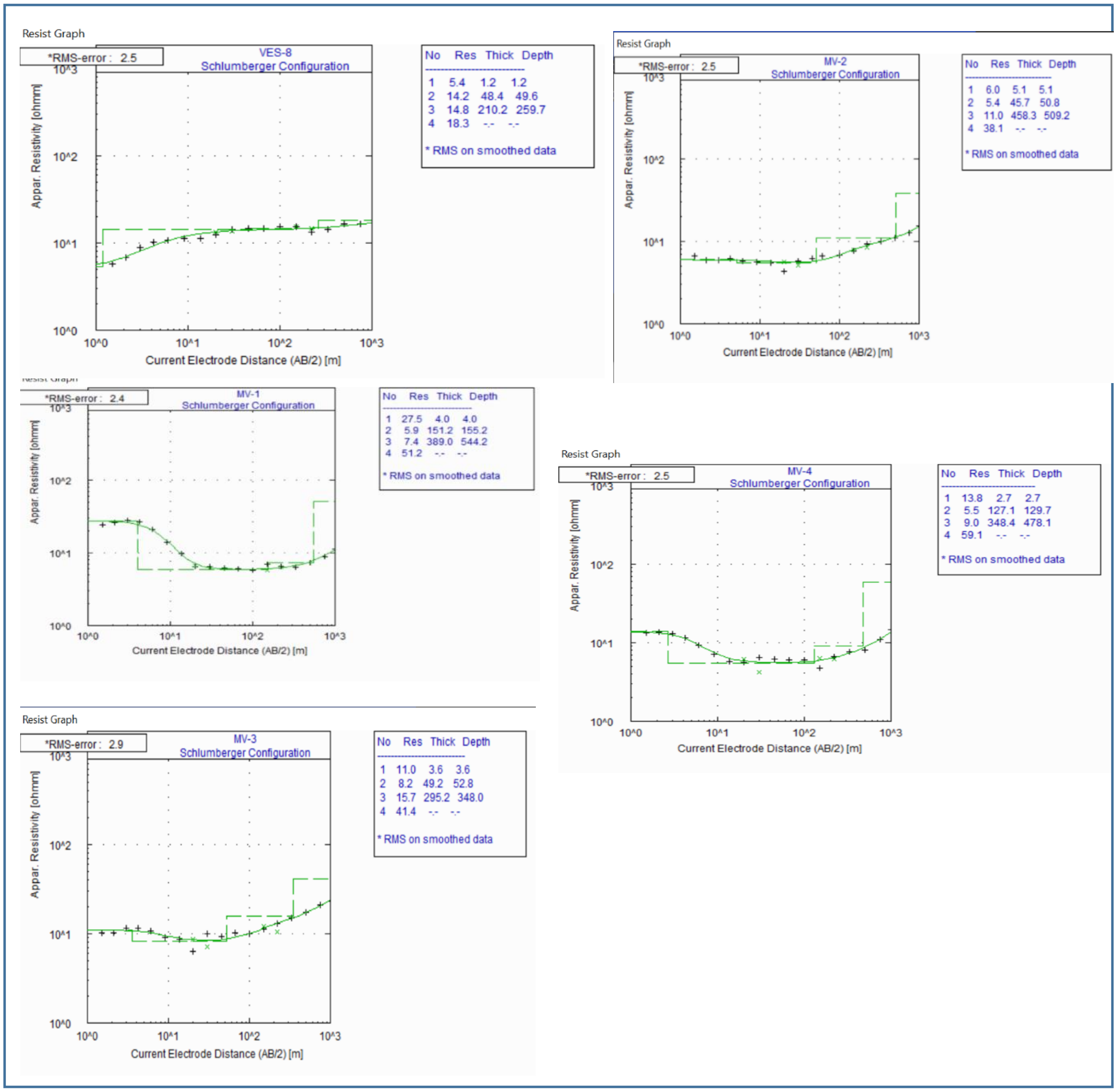
Resist Graph
*RMS-error : 2.5
VES-8
Schlumberger Configuration
Appar. Resistivity [ohmm]
Current Electrode Distance (AB/2) [m]
No Res Thick Depth
1 5.4 1.2 1.2
2 14.2 48.4 49.6
3 14.8 210.2 259.7
4 18.3 -.- -.-
* RMS on smoothed data
Resist Graph
*RMS-error : 2.5
MV-2
Schlumberger Configuration
Appar. Resistivity [ohmm]
Current Electrode Distance (AB/2) [m]
No Res Thick Depth
1 6.0 5.1 5.1
2 5.4 45.7 50.8
3 11.0 458.3 509.2
4 38.1 -.- -.-
* RMS on smoothed data
*RMS-error : 2.4
MV-1
Schlumberger Configuration
Appar. Resistivity [ohmm]
Current Electrode Distance (AB/2) [m]
No Res Thick Depth
1 27.5 4.0 4.0
2 5.9 151.2 155.2
3 7.4 389.0 544.2
4 51.2 -.- -.-
* RMS on smoothed data
Resist Graph
*RMS-error : 2.5
MV-4
Schlumberger Configuration
Appar. Resistivity [ohmm]
Current Electrode Distance (AB/2) [m]
No Res Thick Depth
1 13.8 2.7 2.7
2 5.5 127.1 129.7
3 9.0 348.4 478.1
4 59.1 -.- -.-
* RMS on smoothed data
Resist Graph
*RMS-error : 2.9
MV-3
Schlumberger Configuration
Appar. Resistivity [ohmm]
Current Electrode Distance (AB/2) [m]
No Res Thick Depth
1 11.0 3.6 3.6
2 8.2 49.2 52.8
3 15.7 295.2 348.0
4 41.4 -.- -.-
* RMS on smoothed data

Appendix II well log data